UNIVERSIDAD AUTÓNOMA DE MADRID

Facultad de Medicina

Departamento de Bioquímica

Doctoral Thesis

Molecular mechanisms underlying radiation resistance in brain metastasis

Cátia Patrícia Domingues Monteiro

Madrid, 2020

UNIVERSIDAD AUTÓNOMA DE MADRID

Facultad de Medicina

Departamento de Bioquímica

Doctoral Thesis

Molecular mechanisms underlying radiation resistance in brain metastasis

Cátia Patrícia Domingues Monteiro

Thesis Director

Dr. Manuel Valiente. Cortés

Spanish National Cancer Research Center

Madrid, 2020

Dr. Manuel Valiente Cortés, Head of the Brain Metastasis Group at the Molecular Oncology Programme of the Spanish National Cancer Research Center (CNIO)

CERTIFIES:

That the study “Molecular mechanisms underlying radiation resistance in brain metastasis” developed by Cátia Patrícia Domingues Monteiro meets the necessary requirements to obtain the PhD Degree and, to this purpose, will be presented at the Universidad Autónoma de Madrid. This work has been carried out under my direction and hereby I authorize its defence to a specific PhD Committee assembled for this purpose.

I hereby issue this certification in Madrid on January 15th, 2020.

Manuel Valiente Cortés

PhD, Thesis Director

The work in this doctoral thesis was carried out in the Brain Metastasis Group at the Spanish National Cancer Research Centre (CNIO) from March 2015 to April 2019 under the supervision of Manuel Valiente Cortés.

This work has been supported by the following fellowship and grant:

"Bolsa individual de Douturamento" from Foundation for Science and Technology, FCT, from March 2015 to April 2019

Acknowledgements

Acknowledgements

My journey as a PhD student is ending, after 5 years of hard work is time to close this chapter of my life and move forward to new adventures and challenges. In science as in life we never walk alone and, in my PhD, I had the privileged to know, work and share amazing scientific and personal moments with amazing people. I would like to thank all the people that day after day teach, support and advise me during all of my PhD.

First of all, I would like to thank my thesis director, Dr. Manuel Valiente for the great opportunity that he gave me when he accepted me as part of his team. I had the honour to start the lab with him, to see the lab grow and achieve the great prestige that has today. I am really thankful for the opportunity of working in this lab. I wish all the best to you and to the lab in the future. I would like to thank also my thesis committee: Dr. Massimo Squatrito, Dr. Óscar-Capetillo and Dr. Sebastián Cerdán (Tutor of this thesis) for being a part of my thesis and being available when I needed you. Thank you all for your advice, it's an honour to have you in my thesis committee.

This PhD thesis would never be carried out without the support and the help of the Brain Metastasis Group. I would like to express my sincere and special thanks to all the current and past members of the lab. Specially to Marta, Miguel, David, Manon, Laura, Lucia and Wendy a sincere thank you for all the moments of sharing, help and companionship. I am feeling really honour of having you not only as colleagues but also as friends. Thank you so much you are the best and I wish you all the best for you guys.

I would like to thank all the contributions of the CNIO Units that made their best and always were here to contribute and solve all the pending questions and problems that I had to face. Thanks a lot, to all the people from Histopathology Unit, Bionformatic Unit, Imaging Unit, Confocal Unit, Biosafety Unit, and to the animal facility Unit.

Everything wouldn't be possible if I did not have my family, my relatives and my friends surrounding me with support and love during all these years. The support of my friends has always been fundamental and so here I leave you my

most sincere thanks. Mariana B., Tiago, Mariana G., Márcio, Joana and Daniela thank you for being so patience, for the endless conversations about rats and experiments and for the constant sharing smiles and tears. Thank you! Obrigada!

To all my family, especially my parents and my sisters, I want to leave a very special thank you for all the strength and help you have always given me throughout my life, for teaching me to be the person I am today and for always believing in me. Thank you!

Finally, I would like to thank you Diego. I am really grateful for having you with me, thank you for your help, presence and love. You shared with me the hardest moments of this long road and you never gave up cheering me up and you always believed on me. With you everything was easier. Thank you!

With all my heart,

Thank you!

¡Muchas Gracias!

Bem-haja!

Contents

Contents

Abbreviations

Abbreviations

Abbreviation	Definition
ALK	Anaplastic lymphoma kinase
BBB	Blood Brain Barrier
BLI	Bioluminescence imaging
BrdU	5-bromo-2'-deoxyuridine
BrM	Brain metastasis
BSA	Bovine serum albumin
CDK4	Cyclin-dependent kinase 4
CDK6	Cyclin-dependent kinase 6
cDNA	Complementary DNA
CNIO	Centro Nacional de Investigaciones Oncológicas
CT	Computed tomography
CTL4	Cytotoxic T-Lymphocyte Antigen 4
DAB	3,3'-diaminobenzidine
DMSO	Dimethyl sulfoxide
DNA	Deoxyribonucleic acid
EGFR	Epidermal growth factor receptor
ER	Estrogen receptor
FBS	Foetal bovine serum
FDR	False discovery rate

Abbreviation	Definition
GFP	Green Fluorescence protein
GSEA	Gene set enrichment analysis
HER2+	Human epidermal growth factor receptor 2
IC	Intracardiac injection
IF	Immunofluorescence
KEGG	Kyoto Encyclopedia of genes and genomes
MRI	Magnetic resonance imaging
NFkβ	Nuclear factor kappa-light-chain-enhancer of activated B cells
NGS	Normal goat serum
NSCLC	Non-small cell lung cancer
P	Parental
PBS	Phosphate-buffered saline
PCR	Polymerase chain reaction
PD1	Programmed cell death protein 1
PET	Positron emission tomography
PFA	Paraformaldehyde
PR	Progesterone receptor
qRT-PCR	Real-time quantitative polymerase chain reaction
RAGE	Receptor for advanced glycation endproducts

Abbreviation	Definition
ROI	Regions of interest
RT	Room temperature
S100A9	S100 Calcium Binding Protein A9
SEM	Standard error of the mean
SRS	Stereotactic radiosurgery
Tfm	Transfection media
TKIs	Tyrosine kinase inhibitors
TLR4	Toll-like receptor 4
TMZ	Temozolomide
TNFα	Tumor necrosis factor alpha
WBRT	Whole brain radiotherapy
γ-IR	Gama radiation

Abstract /Resumen

Abstract

Brain metastasis affects 10-30% of cancer patients. Treatments such as surgery, chemotherapy, and radiation are mainly palliative and ineffective. In order to study resistance to radiotherapy, we have developed a model of brain metastasis receiving whole brain radiation therapy (WBRT). We aim to identify mediators of radiation resistance to develop new strategies to sensitize brain metastasis. Several clinically relevant WBRT protocols were applied to lung and breast adenocarcinoma models of brain metastasis that were highly sensitive to radiation *in vitro*. However, none of them impaired the growth rate of metastases or increased mice survival *in vivo*, mimicking the outcomes of recent clinical trials using WBRT in patients with brain metastases. Based on the different sensitivity comparing *in vitro* versus *in vivo* we hypothesized that resistance to radiation could be modulated. Indeed, brain metastatic (BrM) cells grown in organotypic cultures dramatically decreased their sensitivity to radiation. Transcriptomic analysis of a BrM cell line under culture conditions correlating with low or high sensitivity to radiation was performed. The top candidate S100A9, as well as a known receptor and downstream signalling pathway, were all upregulated in conditions involving resistance to radiation.

Although targeting S100A9 in BrM models did not impair the ability to generate brain metastasis, when combined with WBRT a significant reduction in tumour burden was evident. Similarly, an inhibitor blocking S100A9 mediated activation of NFκβ reproduced this finding suggesting a potential therapeutic implication. Analysis of S100A9 levels in human samples reflected inter-patient heterogeneity, suggesting its potential as a biomarker to personalize the use of radiation therapy in patients.

Resumen

La metástasis cerebral afecta a entre el 10 y el 30% de los pacientes con cáncer. Los tratamientos como la cirugía, la quimioterapia y la radiación son principalmente paliativos e ineficaces. Para estudiar la resistencia a la radioterapia, hemos desarrollado un modelo para el estudio de metástasis cerebrales tratadas con radioterapia total del cerebro (WBRT). Nuestro objetivo es identificar mediadores de la resistencia a la radiación y desarrollar nuevas estrategias para sensibilizar la metástasis cerebral. Hemos aplicado, a los modelos de metástasis cerebrales de adenocarcinoma de pulmón y mama que eran altamente sensibles a la radiación *in vitro*, varios protocolos WBRT clínicamente relevantes. Sin embargo, ninguno de ellos redujo la tasa de crecimiento de metástasis, o aumentó la supervivencia de los ratones *in vivo*. Nuestros resultados fueron similares a los obtenidos en ensayos clínicos recientes que utilizan WBRT en pacientes con metástasis cerebrales. En base a la diferente sensibilidad comparando experimentos *in vitro* versus *in vivo*, planteamos la hipótesis de que la resistencia a la radiación podría ser modulada. De hecho, las células metastásicas cerebrales (BrM) que crecen en cultivos organotípicos disminuyeron drásticamente su sensibilidad a la radiación. Se realizó un análisis transcriptómico de una línea celular BrM en condiciones de cultivo que se correlacionan con baja o alta sensibilidad a la radiación. El potencial mediador de la resistencia a la radiación, S100A9, así como uno de sus receptores conocidos, RAGE, y una de sus rutas de señalización, S100A9/RAGE/NFκβ, estaban todos upregulados en condiciones que implican resistencia a la radiación.

Aunque al disminuir la expresión de S100A9 en los modelos BrM no perjudicaba la capacidad de generar metástasis cerebrales, cuando se combinaba con WBRT era evidente una reducción significativa en la carga tumoral. De manera similar, un inhibidor que bloquea la activación de NFκβ mediada por S100A9 reprodujo este hallazgo sugiriendo una posible implicación terapéutica. El análisis de los niveles de S100A9 en muestras humanas reflejó la heterogeneidad entre pacientes, lo que sugiere su potencial como biomarcador para personalizar el uso de radioterapia.

Introduction

Introduction

Cancer is considered to be the epidemic disease of the XXI century, as the number of people affected is on the rise and advanced-stage disease has become more common in recent years (Kaidar-Person, Bar-Sela and Person, 2011). Early in the disease process, various factors, including genetic as well as environmental factors, contribute to the accumulation of genetic damage and errors over time, particularly in dividing cells (Hanahan and Weinberg, 2000). Accumulation of somatic mutations is believed to influence a vast majority of cellular programs at various levels including the transcriptome, epigenome, and proteome, that favour an altered cellular state which is characterized by the aggressive phenotype defining cancerous cells (Hanahan and Weinberg, 2000).

Some classical characteristics of this aggressive phenotype have been extensively reviewed and proposed to consist of uncontrolled growth and spread of these “immortal cells” that alter the normal function of the organs affected. Sometimes, these cells also have the ability to escape the primary organ and colonize a secondary site, resulting in a metastatic tumour.

1. Metastatic disease

Metastatic disease is the last stage of progression of a malignant tumour and the result of a complex and multi-step process (Massague, Batlle and Gomis, 2017). Importantly, metastases are a significant source of morbidity and mortality for most cancer patients (Ferlay *et al.*, 2015).It is estimated that approximately 90% of deaths related to cancer are linked to metastatic disease, due to metastatic spread, cachexia and organ dysfunction and other comorbidities (Seyfried and Huysentruyt, 2013).

Metastatic disease imposes several challenges in terms of treatment. Certainly, a main challenge is to determine what kind of treatment will be the best one for metastases. Clinical observations and previous results available in the literature, suggest that the response of metastases to different treatment regimens may differ from the response to the very same treatment observed in the context of a primary tumour (Klein, 2009; Brastianos, Cahill and Brastianos, 2015; Lambert,

Pattabiraman and Weinberg, 2017). During the metastatic cascade, cancer cells are exposed to and experience a variety of different stressors that depend on the context and localization (e.g. when in transit in blood circulation or after successful dissemination when they colonize a new tissue environment present in another tissue/organ). As a consequence of these stressors and the selection process, cancer cell clones with mutations that favour their viability under such conditions will preferentially survive. Thus, the metastatic tumour can differ genetically from the primary tumour (Brastianos *et al.*, 2015). It is also evident based on clinical observations that different primary tumours present specific tropisms to different metastatic sites (Bos *et al.*, 2009; Nguyen, Bos and Massague, 2009). It is also observed in the clinic that different types of cancer, despite having the same metastatic tropism, develop differences in the kinetics of colonizing secondary organs (Klein, 2009). For instance, breast cancer patients typically experience disease recurrence years or decades after initial treatment (Harbeck *et al.*, 2019). Conversely, lung cancer metastasis usually appears a few weeks or months after diagnosis (Cho *et al.*, 2019).

In summary, cancer cell specific properties (genetic, tropism and kinetics) will influence many aspects of metastatic progression. Therefore, a deeper understanding of the underlying biology of metastasis is of outmost importance in order to develop novel and more effective therapies.

2. **Brain metastasis**

Brain metastasis is an important cause of loss of quality of life and death in patients afflicted with different cancer types. Although our understanding of the biology underlying brain metastasis is improving, we are still far from understanding the underlying mechanisms in their entirety, and there is an urgent need to develop improved therapies to treat and prevent brain metastases.

It has been shown in multiple tumour types that brain metastases are molecularly distinct from both the primary tumour and extracranial metastases (Brastianos *et al.*, 2015). Moreover, it is now understood that the microenvironment plays a significant role in metastases; the “seed and soil” hypothesis suggests that the relationship between specific organ microenvironment and tumour cells affects

the outcome of the metastasis (Psaila and Lyden, 2009; Liu *et al.*, 2017; Peinado *et al.*, 2017).

2.1. Epidemiology of brain metastasis

Brain metastases (BrM) are the most commonly diagnosed central nervous system tumour in the United States (Kaal et al., 2005; Nayak et al., 2012). The global incidence of brain metastasis is unknown, however the estimated range is 7-14 per 100,000 (Fox *et al.*, 2011). These tumours are believed to occur as much as 10 times more frequently than primary malignant brain tumours. (Gavrilovic and Posner, 2005; Kaal et al., 2005; Nathoo et al., 2005; Fox et al., 2011; Davis et al., 2012; Nayak et al., 2012; Feng et al., 2015; Villano et al., 2015).

Among cancer patients, estimates for the frequency of these tumours vary significantly, however, previous studies have reported that they occur in 8,5–10% of all cancer diagnoses (Schouten et al., 2002; Barnholtz-Sloan et al., 2004). These estimates are likely low, due to the date in which these studies were published. Imaging and histology technologies were incomplete, and cerebral disease was not considered in patients with symptomatic advanced cancer, which could cause the difference between the incidence of brain metastasis in the past and nowadays.

Over the last decade, metastatic brain cancer represents an increasing neurological problem among cancer patients. This trend may be explained by the increased incidence of cancer associated with a decline of mortality in cancer patients. This fact is explained by an improvement of diagnostic techniques (e.g. MRI, TC, PET), and more effective treatment of the primary tumour and extracranial metastasis. Consequently, there has been an increase in patient survival, which generates a longer period of time for cancer to get the chance to colonize the brain. Since brain metastasis is associated with later stages of the disease in cancer patients, it is expected to observe an increase on brain metastasis incidence as more patients survive into later phases of the disease (Yamanaka, 2009; Steeg, Camphausen and Smith, 2011).

Between 10% to 30% of patients with cancer with eventually present with brain metastasis, whether at diagnosis or throughout the course of the disease

(Barnholtz-Sloan *et al.*, 2004; Nayak, Lee and Wen, 2012; Tabouret *et al.*, 2012). Brain metastasis diagnose is *per se* a poor survival prognostic factor, independent of primary tumour type (Hall *et al.*, 2000). Most of the patients will develop severe neurological deficits and will eventually die as the disease progresses. It is known that brain metastasis is the cause of death of 52% of patients with neurological disease (Neal *et al.*, 2014; McTyre *et al.*, 2017).

In terms of survival, prognostic factors for patients with brain metastases include age (patients ≥ 65years present a poorer disease outcome), functional status at diagnosis (Karnofsky Performance Score (KPS) <70 is a poor prognostic factor), number of metastatic lesions (more lesions correlates with worse prognosis), and primary disease outcome (uncontrol primary disease is a signal of worse prognosis), among others.(Nieder *et al.*, 2011; Soffietti *et al.*, 2017). Outcome also varies among cancer types; patients with brain metastases secondary to prostate cancer, bronchioloalveolar carcinoma, and breast cancer displayed the longest median survival with 12, 10, and 10 months, respectively (Nieder *et al.*, 2011).

2.2. Main sources of brain metastasis

Theoretically, any type of cancer can spread to the brain and generate a brain metastasis. However, as explained above, cancer cells vary in their tropism to metastasize to various sites (Obenauf and Massagué, 2015).

The brain as a metastatic site is not an exception to this rule, and we know that some types of cancer intrinsically display a higher tropism to the brain than other types of cancer (Obenauf and Massagué, 2015; Chen *et al.*, 2018; Yuzhalin and Yu, 2019). Clinical evidence shows that brain metastases are more frequent in patients with lung (20-56% of the patients), breast (5-20% of the patients) and melanoma primary tumours (7-16% of the patients) (Barnholtz-Sloan *et al.*, 2004; Sperduto *et al.*, 2010; Nayak, Lee and Wen, 2012; Berghoff *et al.*, 2016).

The risk of developing brain metastasis depends on various characteristics of the primary tumour, such as molecular subtype of the tumours and the stage of the development of the disease. Some literature report that patients that present ALK-rearranged non-small cell lung cancer (NSCLC) (Toyokawa *et al.*, 2015),

HER2+ breast cancer and triple negative breast cancer present higher incidence and risk of developing brain metastasis (Martin *et al.*, 2017). Additionally, advanced primary tumours present higher risk to develop brain metastasis. At the following table we can find some of the main sources of brain metastasis and its characteristics in terms of incidence, time of diagnostic and clinical presentation.

Table 1: Most common types of cancer that form brain metastasis

Lung cancer

- Represents the most common type of brain metastases in both men and women
- The brain tumour is often found before, or at the same time, or soon after the primary tumour (average 6 to 9 months)
- Multiple brains metastases are common

Breast cancer

- Represents the second most common type of brain metastases in women
- Metastases tend to occur a few years after the diagnosis (average 2 -2.5 years), but metastases at 5- or 10-years post treatment are not unusual
- They are generally found in younger and premenopausal women
- They are more common in women with triple negative or HER2/Neu+ breast cancer
- Two or more metastatic brain tumours are common

Melanoma

- Represents the second most common type of brain metastases in men
- These cancers may metastasize to the brain and/or the meninges
- Metastases tend to occur several years after the primary melanoma
- Multiple brain metastases are common
- Metastatic melanoma tumours are rich with blood vessels that have a high tendency to bleed

2.3. Mechanisms of brain colonization by metastatic cells

The pathophysiology of metastasis involves a multi-step process where cancer cells must survive severe environmental challenges in order to colonize distant sites (Obenauf and Massagué, 2015). When considering metastatic colonization of the brain, the process is even more selective due to the blood brain barrier and

the various different elements of the microenvironment of the brain (Er *et al.*, 2018; Valiente *et al.*, 2018).

2.3.1. **Extravasation of cancer cells.**

In order to colonize new organs, cancer cells must first travel through the blood flow from primary tumour to distant organ sites. Cancer cells need to extravasate from capillaries into the tissue interstice.

The most common areas of extravasation in the brain are zones of narrowing cerebral microvasculature. Because of the vasculature distribution in the brain, previous studies have shown that 80% of brain metastases occur in the hemispheres, 15% in the cerebellum, and 5% in the brainstem (Patchell, 1995; Saha *et al.*, 2013). After extravasating, cancer cells will remain in close contact with the blood vessels.

In the specific case of the brain, cancer cells will be physically trapped in small capillaries with low perfusion where they require between 3 to 7 days to be able to successfully cross the blood brain barrier (BBB). Previous work showed that the process of extravasation in the brain, requires more time than in other organs colonized by the same cancer cells. To cross the BBB, it is necessary to combine several molecular mediators of extravasation (i.e. HBEGF, COX2) with proteases, cells surface modifications, extracellular vesicles and secreted growth factors. All these conditions will be a requirement to a succeed in extravasation into the brain tissue (Valiente *et al.*, 2018; Arvanitis, Ferraro and Jain, 2019).

2.3.2. **Brain metastasis initiation**

Cancer cells that have completed extravasation into the brain, can experience three possible fates. They can reach the brain tissue and die due to the microenvironment selective pressure, immune surveillance, among other pressures (Lambert, Pattabiraman and Weinberg, 2017). Another scenario is that after extravasation, the cells become rounded and less proliferative initiating a quiescent state termed dormancy (Wells *et al.*, 2013). Finally, after a complete extravasation, cancer cells can remain located at the perivascular niche and begin to adapt to their new microenvironment resuming proliferation (Valiente *et*

al., 2014, 2018; Wingrove *et al.*, 2019). Previous studies on brain metastasis have shown that after arriving to the brain, cancer cells start to become more elongated and engage in a cell-cell interaction with brain capillaries in a process called vascular co-option. This behaviour of the cancer cells does not involve neo-angiogenesis and mimics at the molecular and cellular levels the behaviour of pericytes.

Vascular co-option has been observed in metastasis of multiple different cancer origins, such as lung cancer, breast cancer, melanoma, colorectal cancer and renal cancer. This process is not exclusive of brain metastasis since it has been observed in multiple secondary organs (i.e. lung) (Er *et al.*, 2018). Cancer cells engaging in vascular co-option have preferential access to oxygen, nutrients and angiocrine factors produced by endothelial cells (Chen *et al.*, 2016; Er *et al.*, 2018), which gives these cells a survival advantage in a new, hostile microenvironment. Only cells which engage in co-option will be able to proliferate and form an established brain metastasis (Valiente *et al.*, 2014).

3. Therapeutic options for brain metastasis

Nowadays, with the increasing knowledge and new therapies to treat systemic disease and with more aggressive treatments and better symptom control, more patients have the time to develop brain metastases. Currently, available therapies to patients with brain metastasis are very limited and can be divided into local and systemic. Local options include surgery and radiotherapy, and systemic therapies include chemotherapy, targeted therapies and immunotherapy (Arvold *et al.*, 2016). However, treatment to brain metastasis is still mainly palliative. Therefore, it is crucial to find new therapeutic modalities in order to decrease the neurological defects, increase the quality of life of these patients and their overall survival.

3.1. Surgery

Surgery is used to obtain tissue for diagnosis in addition to reduce intracerebral pressure and to prolong survival by removing the bulk of the tumour (Achrol *et al.*, 2019). However, removing a brain metastatic lesion with surgery has been

described as palliative care more than a curative therapy due to moderate impact of overall survival of patients.

To be a good candidate to surgery, brain metastatic patients need to fulfil several parameters. The patient should have up to two metastases, should have well-controlled systemic disease, a good functional status (KPS ≥70), age <65 years old, and intact neurological function. The metastasis should be in an area of the brain that is surgically accessible with minimal risk of damage, and an absence of leptomeningeal infiltration (Arvold *et al.*, 2016). Surgery can be used alone or in combination with radiation therapy. Usually, whole brain radiotherapy is used as a prophylactic strategy to decrease the risk of local relapse of the tumour after debulking of the tumour mass (Arvold *et al.*, 2016).

3.2. Radiotherapy

Like surgery, radiation is largely used in brain metastatic patients as a palliative treatment, in order to decrease symptoms and improve the patient's quality of life. Historically, radiation has long been used to treat cancer. Radiation treatment can induce irreparable DNA damage, with many double-strand breaks, and thereby activate DNA damage-dependent apoptotic pathways.

There are two general types of radiotherapy protocols that are employed in patients: whole brain radiotherapy (WBRT), patients receive a fractionated dose of radiation administrated over the entire brain, and stereotactic radiosurgery (SRS), which treats only a defined region of the brain usually using a single dose of radiation. These protocols can be used alone or in combination with surgery or chemotherapy.

Whole brain radiation therapy (WBRT) is the treatment of choice for patients with multiple metastases, which corresponds to more than 60% of patients with brain metastasis. This treatment can be used also as a prophylactic adjuvant therapy after surgery, in order to prevent local relapse. WBRT has been described as an effective treatment for the control of symptoms in 80% of patients with brain metastases; however, the effect on overall survival is poor, with an average increase of survival between 3 to 7 months (Valiente *et al.*, 2018). Additionally,

treatment with WBRT increases patients' risk for developing neurologic deficits over time.

Recent clinical studies have opened the door for a discussion regarding an important question:

Does WBRT really offer meaningful benefits for patients with brain metastases?

There is significant controversy surrounding this issue; based on these studies, it seems that treating patients with WBRT does not increase overall survival or quality of life when compared with palliative care alone or stereotactic radiosurgery (Mulvenna *et al.*, 2016).

Stereotactic radiotherapy (SRS) is a modality of radiation therapy used to treat small tumours (less than 3cm diameter) in the brain of those patients with a low number of lesions on brain (1-3). The location is also an important parameter to consider in order to select a patient for this therapeutic modality. This type of radiotherapy can deliver precisely radiation only in areas of the brain affected by the metastasis. Unfortunately, SRS therapy has also some important issues, first of all SRS is a more complex and costly treatment and consequently could be not available in all the radiotherapy centres. Besides that SRS compared with WBRT are a higher risk of new BrM during follow-up (e.g., distant brain recurrences), and an increased risk of radio necrosis (focal damage of the nearby brain tissue caused by a high dose of radiation), depending on the volume of healthy brain tissue which is irradiated to a relatively high dose, tumour biology factors, and the location of the tumour. Important temporary or permanent neurologic symptoms could be discerned (Hartgerink *et al.*, 2018).

The difference between SRS and WBRT permits that a patient could receive in one session an amount of radiation (20-27Gy radiation dose) specifically delivered to the metastasis while WBRT would require 10 or more sessions and without the possibility of avoiding the irradiation of unaffected brain. Thus, less adverse effects to the patient are expected. However, studies comparing WBRT and SRS have found conflicting results. One study from 2016 showed that application of SRS after surgery resulted in better local disease control compared to just observation, but no difference in overall survival (Brown *et al.*, 2016). A

randomised clinical trial comparing adjuvant SRS with standard postsurgical monitoring replicated this finding (Kocher *et al.*, 2011) and observed a greater local control benefit for small resected areas (0-2,5cm) compared to large ones.

A second randomised trial compared postsurgical WBRT paired with SRS on nonresectable tumours to cavity-targeted SRS paired with SRS on nonresectable tumours (Marchan *et al.*, 2018). This group found that the use of WBRT led to greater neurocognitive deficit than SRS only, and no survival benefit. However, they also observed that SRS alone resulted in worse disease control, both locally and throughout the brain, compared to WBRT. The poor outcome of SRS only in this study could be due to microscopic metastases throughout the brain, which are not targeted by adjuvant SRS. In cases where micrometastasis are likely, combination of SRS with another treatment modality, such as targeted therapy or immunotherapy, might provide better disease control with fewer overlapping side effects. Overall, it is important to consider the relative importance of local control, whole-brain control, and the risk of neurocognitive deficits all together for each individual patient situation when choosing a therapy for brain metastasis.

In summary, WBRT remains the standard of care for patients with multiple brain metastases or a poor functional status. SRS is being implemented in many hospitals although is likely that its intrinsic limitation rather that substitute WBRT complement it for some patients.

More experimental studies are necessary in order to increase the efficacy of WBRT for the treatment of brain metastasis and to clarify the real profit of using this therapeutic option.

3.3. Chemotherapy

Chemotherapy is a classical type of systemic therapy used in cancer. In contrast to the primary tumour, where chemotherapy can easily reach the cancer cells, in the brain there are several factors which prevent the access of this therapy to the cancer cells and consequently limit the efficacy.

The blood brain barrier (BBB), the high interstitial fluid pressures and abnormal local perfusion affect the ability to drug delivery to brain metastasis and its efficacy to kill cancer cells in the brain. Besides, it has been described that brain

metastatic cells undergo significant genetic changes after leaving the primary tumour until they colonize the brain parenchyma due to diverse selection pressures leading to divergent evolution. These genetic alterations could result in a metastasis that is non-responsive to a drug despite the manifest sensitivity of the primary tumour.

Although chemotherapy has been used for decades, one of the main caveats is that it is not specific. Recent studies have demonstrated the importance of developing effective targeted therapies and immunotherapies that are tailored to each patient and each lesion, in order to exploit identifiable tumour vulnerabilities and boost response rates (Rosenberg, 2014; Melero *et al.*, 2015; Sharp *et al.*, 2016; Thallinger *et al.*, 2018).

3.4. Targeted therapy

Target therapies have been developed for the treatment of specific types of cancers with well-defined molecular alterations. Usually patients with brain metastasis have been excluded from these studies. However, new clinical trials have started to show a potential utility of these agents in patients with brain metastasis.

Some studies showed that EGFR and ALK tyrosine kinase inhibitors (TKIs) have good central nervous systems penetration, achieving response rates between 40% to 80% in EGFR-mutant or ALK-positive non-small-cell lung cancer and an increase of 15 to 22 months in overall survival, respectively (Ansari *et al.*, 2009; Grommes *et al.*, 2011; Welsh *et al.*, 2013). Additionally, for patients with brain metastasis from HER2-positive breast cancer, several clinical trials suggest that response rates are better when patients are treated with the combination of neratinib (a small molecule that is a dual inhibitor of HER2 and EGFR) and capecitabine (a chemotherapeutic agent that inhibits active form of thymidine, thymidine monophosphate, which is required for the *de novo* synthesis of DNA) compared to chemotherapy alone (Freedman *et al.*, 2016, 2017). For patients with ER-positive or PR-positive breast cancer brain metastasis, preliminary data also support the use of selective inhibitors of cell cycle proteins CDK4 and CDK6 (like Abemaciclib) (Tolaney *et al.*, 2017).

Targeted therapies have also been studied in patients with brain metastatic melanoma with relative success. Some studies have demonstrated an increase of response in 20% to 38% in melanoma brain metastasis BRAF-mutant treated with BRAF inhibitors like vemurafenib and dabrafenib (Long *et al.*, 2012; Dummer *et al.*, 2014; Davies *et al.*, 2017; McArthur *et al.*, 2017).

Taken together, these data suggest that targeted therapies, possibly in combination with chemotherapy or radiotherapy, are a promising treatment strategy for brain metastasis.

3.5. Immunotherapy

Immunotherapies are a novel therapeutic strategy that recently have begun to be explored for the treatment of brain metastatic patients. The use of immunotherapy in this setting is now being tested in clinical trials, and some promising results have been shown in the treatment of brain metastatic patients with melanoma and lung (NSCLC) cancer. Specifically, inhibitors of immune checkpoints targeting surface molecules CTL4 and PD-1 as well as anti-PDL1 have been applied in brain metastatic patients with promising results (Achrol *et al.*, 2019;Taggart *et al.*, 2018). Using these new drugs alone was associated with an intracranial response rate of 33% in NSCLC and 22% in melanoma with a sustained effect in some patients for more than 12 months (Goldberg *et al.*, 2016). Additionally, combination therapy with several immunotherapeutic agents or even the combination of immunotherapy with radiotherapy has been described as providing benefits for patients. For example, the combination of anti-CTL4 and anti-PD1 in patients with metastatic melanoma have shown even higher response with approaching 60%, than when treated separately (Goldberg *et al.*, 2016). It has been also described that the combination of anti-PDL1 with radiotherapy (SRS or WBRT) showed a synergism in response rates to dual therapies (Anderson *et al.*, 2017; Nardin *et al.*, 2018). However, it has to be noticed that all these data correspond to asymptomatic brain metastasis since the rate of intracranial responses is reduced (<5%) when patients are treated with symptomatic metastasis.

Besides all these promising preliminary results, the study of the underlying biology, molecular mechanisms, and potential side effects of these therapies specifically in the brain metastatic setting need to be very carefully evaluated.

4. Models of brain metastasis

4.1. Overview of experimental models of brain metastasis

As previously described in this introduction (see point 1 and 2), the formation of brain metastasis is the result of a complex process with several steps. This multi-step process that begins with tumour cell invasion, still at the primary tumour, and ends with the colonization and establishment of micro and macro metastases in brain tissue (Nguyen, Bos and Massague, 2009; Massague, Batlle and Gomis, 2017; Valiente *et al.*, 2018; Achrol *et al.*, 2019). Due to the complexity of the biology behind brain metastasis it is difficult to fully recapitulate all these processes *in vitro*. In the attempt to improve the ability to mimick the metastatic process that occur in brain metastatic patients, new models *in vitro*, *in vivo* and *ex vivo* are being used and accepted by the scientific community as a fundamental tool to study the different parts of the metastatic cascade and also to develop and use models that can give us a holistic view of the process (Bos *et al.*, 2009; Nguyen *et al.*, 2009; Li *et al.*, 2013; Sevenich *et al.*, 2014; Valiente *et al.*, 2014; Jilaveanu *et al.*, 2015; Martínez-Aranda *et al.*, 2015; Wrage *et al.*, 2015; Chen *et al.*, 2016; Priego *et al.*, 2018).

In order to study brain metastasis, investigators obtained cancer cells from patients, usually from pleural fluids or lymph node metastases. These cells were engineered with different reporters (e.g. GFP and Luciferase) with the purpose of its detection with non-invasive techniques (e.g. bioluminescence) and/or using histology or flow cytometry. These cells obtained from patients were used to generate new models of brain metastasis by using *in vivo* selection (Bos *et al.*, 2009) of the cancer cells that manage to reach the brain, going through the step of colonization and developing viable metastasis (Bos *et al.*, 2009; Nguyen *et al.*, 2009; Valiente *et al.*, 2014; Chen *et al.*, 2016; Priego *et al.*, 2018). These cellular models are essential tools for most studies on brain metastasis. Although *in vitro* studies have some limitations with regard to mimicking all processes of the

metastatic cascade, it is an important tool to study for example the passage of cancer cells through the BBB, drug screenings, discovery of new mediators of metastasis (Bos *et al.*, 2009).

Preclinical metastatic mouse models are a fundamental tool to develop new therapies and approaches to treat the disease. There are several different mouse models that can be divided in spontaneous metastatic models, which consists on mice genetically engineered, typically with oncogenes that have been either down or up-regulated, to induce the disease. The main difficulty of using these models is that it takes several weeks to months to generate brain metastasis. On the other hand, syngeneic models of brain metastasis are the best models to study the crosstalk between tumour cells and host microenvironment, including the immune system. In contrast, xenograft models require the use of human tumour cells into immunocompromised mice, either in orthotopic (tumour is implanted into its natural environment) or heterotopic (tumour is injected into a different tissue or organ) locations (Khanna and Hunter, 2005).

The use of *in vivo* models to examine brain metastasis is a powerful tool for understanding the interactions that occur between the infiltrating tumour cells and the resident brain cell population. Together with immunologic, molecular and microscopy techniques these models are a very good platform on which researchers can recapitulate the metastatic cascade.

In order to incorporate the highest degree of complexity, patient derived xenografts (PDX) models are becoming important to study brain metastasis. The use of PDX models could be relevant to evaluate personolized therapies. Unfortunately, these models present several caveats, they require immunosuppressed hosts and usually they are not easy models to incorporate genetic manipulations, thus compromising the monitoring of tumour evolution and the identification of the tumour cells on the host tissue by molecular or immunological techniques.

Summing up the develop and use of new models is very important in order to increase the identification novel and more effective therapeutics that block the metastatic process and find new mediators of therapy resistance.

4.2. Use of radiotherapy in experimental models of brain metastasis

Models to study brain metastasis include: *In vitro* models with brain metastatic cell lines, organotypic models from mouse and human brain tissue, xenografts, allografts, patient derived xenografts and spontaneous brain metastasis models. All these models are important for finding new mechanisms and mediators involved in brain metastasis and are also used to test new drugs and therapies.

Our main interest with this thesis work was to establish new experimental models to interrogate radiation resistance in brain metastasis. Previous studies using radiotherapy in experimental models of brain metastasis showed a limited response of cancer cells to radiation; however, all these studies had significant/important limitations and none of them suggested a potential mediator or mechanism that could explain the limited response to radiotherapy. Martinez-Aranda *et al.* (2013) in a preclinical protocol tested a multifractionated whole brain radiation therapy (WBRT) (with three 5,5Gy fractions delivered on consecutive days) in association with a chemotherapy agent, temozolomide (TMZ), a known chemotherapeutic agent used as a radiosensitizer in primary brain tumors (60mg/kg/day orally for five consecutive days) (Martinez-Aranda *et al.*, 2013). They observed doubling of survival in mice treated with this combination compared to controls. Additionally, Smart *et al.* (2015) developed a preclinical model for radiation therapy of brain metastasis in breast cancer. In this study, mice were randomized to groups receiving WBRT as delivered in the clinic (3Gy a day for 10 days) that was compared to another arm only receiving a single dose of radiation (Smart *et al.*, 2015). Fractionated radiation impaired the development of micrometastasis but failed to affect established brain metastases, which correspond to the clinically repevant scenario.

Finally, Leder et al. (2014) developed and tested a mathematical model of fractionated radiotherapy *in vivo*. They claim that treating at different hours during the day and with variable doses during the time of the treatment they will improve the effect of radiation in glioma (Leder *et al.*, 2014).

All published models were important tools as a starting point for our work. However, all protocols had limitations. In the Smart et al. protocol, they only saw a positive response in terms of radiation when brain metastases were very small.

As mentioned before this does not recapitulate the clinical situation since, at the time of diagnosis, brain metastases are big enough to be detected with MRI or, even worst, they generate neurological alterations. In the work of Leder et al., the mathematical model was designed for glioma rather than for brain metastases. Finally, considering the Martinez-Aranda et al. study, they did not clarify whether the phenotype was due to radiation or chemotherapy since they did not include single arms for the monotherapies.

5. S100A9

5.1. Molecular characterization

S100 calcium binding protein A9, also called calgranulin B and Myeloid related protein 14 (MRP-14), is a calcium and zinc-binding protein that plays a key role in the regulation of inflammatory processes and the immune response. S100A9 belongs to the S100 family of proteins, which are characterized/defined by containing 2 EF-hand calcium-binding motifs. S100A9 can be found as a monomer or as a heterodimer conjugated with S100A8; when conjugated with S100A8, it is called calprotectin (Nacken *et al.*, 2003).

S100A9 is expressed in a wide variety of cells (e.g. epithelial cells, different types of cancer cells), but it is in myeloid cells, (i.e. neutrophils, monocytes, keratinocytes and early differentiation states of macrophages), where S100A9 expression is more abundant. It can be found in different cellular compartments such as the cytoplasm, cytoskeleton, and plasma membrane, and is also known to be secreted (Gebhardt *et al.*, 2006).

S100A9 protein has been described to be involved in several important molecular functions. Intra- and extracellular mechanisms related to inflammation and immune response could be trigger for S100A9. S100A9 intracellular functions include: proinflammatory (recruitment of leukocytes, promotion of cytokine and chemokine production and regulation of leukocyte adhesion and migration), leukocyte arachidonic acid trafficking and metabolism, activation of neutrophilic NADH-oxidase, modulation of tubulin-dependent cytoskeleton during phagocytes and microbial activity, oxidant-scavenging and apoptosis-inducing activities. It

also stimulates innate immune cells through binding to TLR4 and RAGE receptor and consequently activating the MAP-kinase and NF-kappa-b signalling pathways resulting in an exacerbation of the proinflammatory cascade (Srikrishna, 2012; Markowitz and Carson, 2013; Leanderson, Liberg and Ivars, 2015; S. Wang *et al.*, 2018).

5.2. S100A9 in health and disease

S100A9 is an important mediator of inflammation and the immune response during an infection or another challenge, as described above. However, deregulated S100A9 expression has been implicated in different diseases, including autoimmune disease, cystic fibrosis (Lorenz *et al.*, 2008; Bargagli *et al.*, 2011), Crohn's disease (Pavlidis *et al.*, 2016; Jovanovic *et al.*, 2018), rheumatoid arthritis (van Lent *et al.*, 2008; Smith *et al.*, 2017; Nys *et al.*, 2019), chronic bronchitis and many types of cancers (Bergenfelz *et al.*, 2015; Lim *et al.*, 2016; Nedjadi *et al.*, 2018) and neurodegenerative disorders such as Alzheimer's (Chang, Kim and Suh, 2012; Wang *et al.*, 2014; Gruden *et al.*, 2016). Independent studies showed that the upregulation of the S100A9 gene plays an important role in the neuropathology and memory impairment in Alzheimer's disease, suggesting that the knockdown and knockout of this gene have a great therapeutic potential (Chang, Kim and Suh, 2012; Wang *et al.*, 2014; Gruden *et al.*, 2016).Horvath et al. (2016) suggests that S100A9 could be used as a robust biomarker to differentiate early stages of cognitive impairment in Alzheimer's disease (Horvath *et al.*, 2016).

The knowledge about the function of S100A9 in brain metastasis is scarce. Yan Liu et al., (2016) identified S100A9 as one of the inflammation mediators important in the preparation of the metastatic site and the attraction of cancer cells to that site (Liu and Cao, 2016). They describe the action of S100A9 as a consequence of the high expression of TNFα that causes a positive loop of expression of inflammatory mediators and an increase in the attraction of myeloid cells (Liu *et al.*, 2017).

Aim

Aim

The main objective of my PhD project was:

To establish new experimental models to interrogate the underlying biology of radiation resistance in brain metastasis and to find potential mediators of this process that can be used as biomarkers to predict radiation response in patients and/or use these resistance mediators to be targeted with radio-sensitizers.

In order to do this, we designed specific aims:

1. Establishment of a brain metastasis model treated with radiotherapy (Whole brain radiation therapy, WBRT).
2. Identification of potential mediators of radiation resistance.
3. Functional characterization of potential mediators of radiation resistance.
4. Validation of our findings in human samples.

Material and Methods

Material and Methods

1. Tissue Culture

1.1. Cell Culture

1.1.1. Adherent cells

Human (H2030-BrM3, MDA231-BrM2, PC9-BrM3) and mouse (ErbB2-BrM2, 393N1, 482N1) brain metastatic cell lines were previously described (Bos *et al.*, 2009; Nguyen *et al.*, 2009). MDA231-BrM2 (abbreviated as MDA231-BrM), ErbB2-BrM2 (abbreviated as ErbB2-BrM), 393N1, and 482N1 cells were cultured in DMEM media supplemented with 10% foetal bovine serum (FBS), 2 mM L-Glutamine, 100IU/ml penicillin/streptomycin and 1 mg/ml amphotericin B. H2030-BrM3 (abbreviated as H2030-BrM), PC9-BrM3 (abbreviated as PC9-BrM) and HCC1954-BrM1 (abbreviated as Hcc1954-BrM) were cultured in RPMI1640 media supplemented with 10% FBS, 2 mM L-Glutamine, 100IU/ml penicillin/streptomycin, and 1 mg/ml amphotericin B. 293T cells were cultured in DMEM media supplemented with 10% FBS, 2 mM L-Glutamine, 100 IU/ml penicillin/streptomycin, and 1 mg/ml amphotericin B.

1.1.2. Brain metastasis model E0771-BrM

To generate a new brain metastatic model, E0771-P (parental) cells were administered via intracardiac injection to obtain brain metastatic derivatives. Briefly, a cell suspension containing 10^5 E0771-P cells expressing a Luciferase construct (Addgene ref. 19166), in a volume of 100µl were injected in the left cardiac ventricle of anaesthetized 4–6-week-old C57BL/6 mice. Tumour development was monitored by bioluminescence imaging using the IVIS-200 imaging system every three days. Brain lesions were localized by *ex vivo* bioluminescence imaging (BLI) and resected under sterile conditions. Tissue was minced and placed in a culture medium containing a DMEM supplemented with 0.125% collagenase III and 0.1% hyaluronidase. Samples were incubated at 37° C for 1 h, with gentle rocking. After collagenase treatment, cells were briefly centrifuged, resuspended in 0.25% trypsin, and incubated at 37° C for 15 min.

Cells were resuspended in culture media and allowed to grow to confluence on a 10 cm dish. Two additional rounds of *in vivo* selection were performed.

Brain metastatic cells, E0771-BrM3 (abbreviated as E0771-BrM), transduced with a lentiviral vector encoding ZsGFP (Catalog No. 632179, Clontech) and sorted for further propagation in culture or inoculation in mice. E0771-BrM was cultured in RPMI1640 media supplemented with 10% FBS, 1% Hepes 1M, 2 mM L-Glutamine, 100IU/ml penicillin/streptomycin, and 1 mg/ml amphotericin B.

1.1.3. **Mouse glial cell culture**

Mouse glial cells were obtained from one to three-day old mice pups (Schildge *et al.*, 2013). In brief, brains were mechanically dissociated and filtered through 100 mm filters. The resulting cell suspension was cultured in a petri dish for 7 days in DMEM media supplemented with 10% FBS and 2nM L-Glutamine. Cells that survive the culture period are predominantly astrocytes, microglia and oligodendrocytes.

1.1.4. **Oncosphere assay**

Brain metastatic cell lines (H2030-BrM, E0771-BrM and 482N1), were plated in low-attachment plates with a density of $1x10^3$ cells per well in Humec (Gibco, ref: 12753018) medium supplemented with basic human fibroblast growth factor (bFGF, 10ng/mL, Gibco, ref: 13256-029), Epidermal growth factor (EGF, 20ng/mL, Sigma-Aldrich, ref:E9644), insulin solution from bovine pancreas (Sigma, 5ug/mL, ref:I0516), and B27 supplement (Gibco, 1x, ref: 17500-044). H2030-BrM and 482N1 cells were culture for 7 days on these conditions in order to form isolated oncospheres. E0771-BrM cells needed 4 days of culture to form equivalent (same size and number approximately) oncospheres to the others cell lines studied. When indicated, oncospheres were irradiated at 10Gy in a single dose (irradiator Mark I 30A, JLShepherd).

1.1.5. **Co-culture assays**

1.1.5.1. Co-cultures with insert

We performed co-cultures using a commercial cell culture insert (High density, translucent PET membrane 24 well 0,4µm pore size, Falcon, ref:353495). We plated 1,5X10^4 H2030-BrM cells in the lower chamber of the plate and 4,5x10^4 primary glial cells on top of the insert with RPMI1640 media supplemented with 0,25% FBS, 2 mM L-Glutamine, 100IU/ml penicillin/streptomycin, and 1 mg/ml amphotericin B. Co-cultures were irradiated 18h after plating and the results were measured 72h after irradiation.

1.1.5.2. Co-cultures without insert involving cell-cell contact

In a 24 well-plate, 1,5X10^4 H2030-BrM cells and 4,5x10^4 glial cells were plated within the same well. The cell mixture was cultured with RPMI1640 media supplemented with 0,25% FBS, 2 mM L-Glutamine, 100IU/ml penicillin/streptomycin, and 1 mg/ml amphotericin B. Cultures were irradiated 18h after culture and the results were measured 72h after irradiation.

1.1.6. **Organotypic cultures**

1.1.6.1. Initiation of metastasis

Organotypic slice cultures from adult mouse brains were prepared as previously described (Valiente *et al.*, 2014). In brief, brains were dissected in Hank's balanced salt solution (HBSS) supplemented with HEPES (pH 7.4, 2.5 mM), D-glucose (30 mM), CaCl2 (1 mM), MgSO4 (1 mM), and NaHCO3 (4 mM), and embedded in low-melting agarose (Lonza) preheated to 42°C. The embedded brains were cut into 250 µm slices using a vibratome (Leica). Slices were divided at the hemisphere into two pieces. Brain slices were placed with flat spatulas on top of 0.8 µm pore membranes (Millipore) floating on culture media (Dulbecco's modified Eagle's medium [DMEM], supplemented HBSS, 5% FBS, L-glutamine (1 mM), 100 IU/ml penicillin, 100 mg/ml streptomycin). 3x10^4 cancer cells resuspended in 2 µl of culture media were placed on the surface of the slices and incubated for 3 days.

1.1.6.2. Established metastasis

Brains with established metastasis were obtained at the experimental endpoint (5-7 weeks in human BrM cell lines, 2 weeks in mouse BrM cell lines). The methodology to generate the organotypic culture was the same as described above however without the need of plating the cancer cells since they are already within the tissue. Brain slices were imaged to confirm the presence of established metastases using BLI.

1.2. *In vivo* and *ex vivo* therapy

1.2.1. Radiation treatment assay

All cell types and organotypic cultures that were subjected to radiation received a single dose of 10Gy of gamma radiation (irradiator Mark I 30A, JLShepherd); source used was Cs-137 (662 KeV E.max).

BLI was acquired 18 hours after plating cancer cells (Day 0) and brain slices were irradiated immediately after that with 10Gy radiation dose. Subsequently, BLI was acquired again 3 days after radiation (Day 3). The growth rate was obtained by comparing bioluminescence fold increase between day 3 and day 0.

1.2.2. Drug treatment assay

FPS-ZM1 inhibitor (10uM, Selleck chemicals, cat. S8185) or Bay11-7082 inhibitor (50uM, Selleck Chemicals, cat. S2913) were administered once during the experiment at the same time that the cancer cells were plated on the surface of brain slices or when established metastases were placed on the culture membrane, by adding it directly into the media. A BrdU pulse (0.2 mg/ml, Sigma-Aldrich, ref. B9285) was given by adding it in the media four hours before fixing brain slices in paraformaldehyde (4%) overnight. Free-floating immunofluorescence was performed afterwards and mounted with Mowiol-Dabco anti-fade reagent.

2. *In Vivo* analysis:

2.1. Procedures on animals

All animal experiments were performed in accordance to a protocol approved by the CNIO, Instituto de Salud Carlos III and Comunidad de Madrid Institutional Animal Care and Use Committee. Athymic nu/nu (ENVIGO), and C57BL/6 mice 4–6 weeks of age were used. A brain metastatic derivative of the syngeneic E0771 model (E0771-BrM3) was established according to a previous protocol (Bos *et al.*, 2009; Nguyen *et al.*, 2009). For intracardiac models of brain colonization, 100 µl of PBS containing 100,000 cancer cells was injected into the left ventricle. Alternatively, 2 µl of PBS containing 25,000 cancer cells was intracranially injected (right frontal cortex, approximately 1.5 mm lateral and 1 mm caudal to the bregma, and to a depth of 2 mm) using a gas-tight Hamilton syringe and a stereotactic apparatus. Brain colonization was analysed *in vivo* and *ex vivo* by bioluminescence imaging. Briefly, mice were anesthetized using 3% isoflurane, injected retro-orbitally with D-Luciferin (150 mg/kg) and imaged with an IVIS Spectrum Xenogen machine (Caliper Life Sciences). Bioluminescence analysis was performed using Living Image software, version 3.

To study the radiation response of BrM cells injected subcutaneously in the head of the animal, $5x10^5$ cells were resuspended in 100uL PBS mixed with 50% reduced growth factor Matrigel (Corning Matrigel growth factor) and injected subcutaneously.

2.1.1. Radiation therapy protocols *In vivo*

The irradiator Mark I 30A (J.L. Shepherd & Associates, USA) system was used for irradiation of mice. Cranial irradiation was delivered using an opposed lateral-beam geometry, collimated to produce a 0.5 cm diameter field at the depth of interest. The body was protected by a 3 cm custom-made shield device that covers the mice except for the head.

The source used in this case was Cs-137 (662 KeV E.max). The source-to-axis distance was 20 cm, and the collimator-surface distance was 7 cm. Doses ranging between 2,0 and 5,5 Gy were delivered at a dose-rate of 1,54 Gy/min.

Activity at calibration date was 1100 Ci (10/10/2002). Calibration was performed by manufacturer (J.L. Shepherd & Associates, USA) following internal procedure using an MHS Industries Model 2025 x-ray monitor (S.N. 4212) with a 0.18cc probe (S.N. 8716-5), and converter (S.N. 8730). This meter is calibrated by J.L. Shepherd & Associates Cs-137 Model 89 calibration range (S.N. 8190), by use of N.I.S.T. Transfer dosimeters, National Institute of Standards and Technology Report #DB917/114, dated March 20, 1996.

The animal was placed in a methacrylate chamber and anesthetized using ketamine/xylazine as described below. None of the immobilization devices were in the beam path. The doses were not corrected for surface curvature or tissue heterogeneities. Dosimetry standardization was adequate for reliability and reproducibility of our findings.

Radiation protocol A: Based on Leder et al., who reported an optimized protocol for radiation therapy in glioblastoma patients (“Optimum-2”). Radiation schedule was as follows: Day1: Dose: 3Gy/ Time: 8am; Day2: Dose: 1Gy/ Time: 4pm; Day3: no radiation; Day4: Dose: three of 1Gy/ Time: 9am, 1pm, 5pm; Day5: Dose: three of 1Gy/ Time: 9am, 1pm, 5pm (Leder *et al.*, 2014).

Radiation protocol B: Based on a protocol established by Martinez-Aranda et al. who applied a chemoradiation protocol with Temozolomide (TMZ, Oral gavage, 60 mg/kg/day, for 5 consecutive days) on mouse models of brain metastasis. In our experiments, radiation was administered only to the head of the mouse. Radiation schedule was as follows: Day1: Radiation: Dose: 5,5Gy; Day2: Radiation: Dose: 5,5Gy; Day3: Radiation: Dose: 5,5Gy. Total radiation dose per mouse was 16,5Gy (Martinez-Aranda *et al.*, 2013).

Radiation protocol C: Based on the Smart et al. radiation protocol for brain metastasis. Radiation schedule was as follows: 3Gy for five days, two days without radiation and 3Gy for five additional days. Total dose per mouse was 30Gy (Smart *et al.*, 2015).

3. Tissue analysis:

3.1. Immunofluorescence

Slicing of whole brains was done using a vibratome, in case of fresh samples (Leica VT1000S), or sliding microtome (Thermofisher HM450), in case of fixed samples. Brain tissues sectioned by vibratome were later fixed in 4% PFA at 4º C. Brains to be sectioned with the microtome were initially fixed in 4% PFA at 4º C overnight and then dehydrated in sucrose 15% overnight and finally maintained in sucrose 30% until be sectioned.

Both types of brain slices (250 µm, vibratome, and 80 µm, microtome) were blocked in NGS 10%/BSA 2%/Triton 0.25% in PBS for 2 hr at room temperature (RT). Primary antibodies were incubated overnight at 4ºC in the blocking solution and the following day for 30 min at RT. After extensive washing in PBS-Triton 0.25%, the secondary antibody was added in the blocking solution and incubated for 2 hr at RT. After extensive washing in PBS-Triton 0.25%, nuclei were stained with bisbenzimide (1 mg/ml; Sigma) for 7 min at RT. The same protocol was applied to stain oncospheres.

Table 2. Antibodies list

Primary antibodies

- Anti-Green Fluorescent Protein (Aves Labs, ref. GFP-1020, dilution 1:1,000)
- Anti-BrdU (Abcam, ref. ab6326, dilution 1:500),
- Anti-S100A9 anti-human (Dako, ref. M747, dilution 1:200),
- Anti-s100a9 anti-mouse (Cell Signalling, ref: #73425, dilution 1:100),
- Anti-phospho-histone H2ax (Ser139) anti-human (Millipore, cat. #05-636, dilution 1:1000)

Secondary antibodies*

- Alexa-Fluor plus Goat anti-chicken488, (cat. #A11039)
- Alexa-Fluor plus Goat anti-rabbit555 (cat. #A21429)
- Alexa-Fluor plus Goat anti-mouse555 (cat. #A21422)
- Alexa-Fluor plus Rabbit anti-mouse633 (cat. #A21072)
- Alexa-Fluor plus Goat anti-mouse647 (cat. #A21236)

*All the secondary antibodies are from Invitrogen. We use a work dilution of 1:300 in all of them except for Alexa Fluor anti-chicken 488 with a dilution of 1:500.

3.2. Immunohistochemistry

A total of twenty-six human brain metastasis samples from lung cancer or breast cancer were obtained from the Soffietti lab (University Hospital Turin) (16 samples) and the Cohan-Jonathan Moyal lab (Institute du Cancer Toulouse) (10 samples). Immunohistochemistry (IHC) was performed at the CNIO Histopathology Core Facility using standardized automated protocols. Single immunohistochemistry (Autostainer Link, Dako or Ventana Discovery XT, Roche) was initiated by performing antigen retrieval with high or low pH buffer (depending on the primary antibody) and, after blocking of endogenous peroxidase (3% hydrogen peroxide), slides were incubated with the appropriate primary antibody, mouse monoclonal anti-S100A8/S100A9 (Myeloid/Histocyte Antigen, MAC 387, RTU, Dako, M0747). After the primary antibody, slides were incubated with the corresponding secondary antibodies and visualization systems when needed (EnVision FLEX+, Dako) conjugated with horseradish peroxidase. The immunohistochemical reaction was developed using 3,3-diaminobenzidine tetrahydrochloride (DAB). Nuclei were counterstained with Carazzi's haematoxylin. Finally, the slides were dehydrated, cleared and mounted with a permanent mounting medium for microscopic analysis. Expression of S100A9 in metastatic cells and in the microenvironment was independently evaluated and scored as 0, 1, 2 or 3 (no expression of S100A9, low-, intermediate-, and high-expression of S100a9, respectively) by clinical neuropathologists.

3.3. Image acquisition and analysis

Images were acquired with a TCS-SP5-X laser scanning confocal microscope (Leica-Microsystems) equipped with AOBS, a tuneable white light laser, a 10X/0.4NA and a 20X/0.7NA dry lenses, a 20X0.7NA multi-immersion lens, a 40X/1.25NA and 63X/1.4NA oil immersion lenses, and LAS AF software. Mosaic images of the oncospheres were imaged with a DM6000I workstation (Leica-Microsystems) equipped with a 5X/0.15NA (numerical aperture) dry lens, and

LAS AF and Leica HCS software. Acquired images were analysed with ImageJ software and Definiens developer XD 2.5.

3.4. Bioluminescent acquisition and analysis

3.4.1. *In vitro* and *ex vivo* assays

Bioluminescence images were taken using an IVIS Spectrum (Perkin Elmer, Waltham MA). Five minutes before imaging BrM cells *in vitro* and brain slices *ex vivo*, 20uL/mL of D-Luciferin (15mg/mL, Caliper Life Sciences, part number #119222) was added to the media

3.4.2. *In vivo*

For *in vivo* imaging, mice were anesthetized with 3% isoflurane gas anaesthesia and then injected retro-orbitally with 100 µL of 15 mg/mL D-luciferin stock solution. After the D-luciferin injection, the animals were placed on the stage of the IVIS Spectrum in a prone position with the animal's dorsal side facing the CCD camera. Default bioluminescent settings of Living Image 4.0 were used. Regions of interest (ROI) were drawn on the 2D bioluminescent image over the brain metastasis lesions and total photons emitted were calculated. The image analysis and quantification were done using Living Image 4.0 software and the luminescence was reported in photon flux.

4. Flow-cytometry

4.1. Sorting

Brain metastatic cells were detached using trypsin (Gibco, ref: 25300-054). The cell pellet was resuspended in RPMI media supplemented with 0,25% FBS, 2 mM L-Glutamine, 100IU/ml penicillin/streptomycin and 1 mg/ml amphotericin B, at a final concentration of 5-10x10^6 cells/mL. Before sorting, cells were filtered in a 50um sterile filter (Sysmex, ref:04-004-2327) and 2uL/mL of DAPI solution (stock solution 200ug/mL; Sigma, ref: D9542) was added. Sorted cells were collected in RPMI media supplemented with 10% FBS, 2 mM L-Glutamine,

100IU/ml penicillin/streptomycin and 1 mg/ml amphotericin B, centrifuged, and plated in a 10 cm dish with fresh culture media.

All sorting steps were conducted using an Influx cell sorter (BD, San Jose CA) with a nozzle of 100um. E0771-BrM cells were selected based on expression of green fluorescent protein (GFP). H2030-BrM were isolated from the co-culture with glial cells based on GFP+ expression as well.

To clarify whether NFκβ is activated by S100A9 and if this pathway is the responsible for the radiation resistance phenotype, we infected BrM cells with a lentivirus containing a NFκβ reporter (cdc-5NF-mCherry) and a colour marker (mCherry) (Badr *et al.*, 2009).

In order to select the cells infected by the lentivirus with the NFκβ reporter vector, H2030-BrM mCherry positive BrM cells were treated with recombinant human TNFα (cat: 300-01A, Peprotech), an activator of NFκβ pathway, for 28h to then sort out the mCherry+.

5. Molecular analysis:

5.1. Transcriptomic analysis

5.1.1. Real-time quantitative PCR (qRT-PCR)

Whole RNA was isolated using an RNAeasy Mini Kit (QIAGEN). 1000 ng RNA was used to synthesize cDNA using an iScript cDNA Synthesis Kit (Bio-Rad, ref. 1708890). RNA obtained from mouse brains included micro-dissected established metastases from human BrM cells. In these cases, the microenvironment was analysed using mouse primers, while human primers were utilized to analyse the cancer cells. RNA from BrM cell lines was obtained from a confluent well of a 6-well plate. RNA from oncospheres was obtained from cells cultured in low attachment 24-well plates or 10 cm plates. Quantitative PCR (qPCR) reactions were conducted using SYBR green gene expression assays (GoTaq® qPCR Master Mix Promega, ref. A6002). qPCR reaction was performed on QuantStudio 6 Flex Real-Time PCR System (Applied Biosystems) and analysed using QuantStudio 6 and 7 Flex Software.

Table 3. Primers used for human genes (5´->3´):

Gene	Forward	Reverse
S100A9	TGGAACGCAACATAGAGACCA	CGCCATCAGCATGATGAACT
TNFα	CGAGTGACAAGCCTGTAGC	GGTGTGGGTGAGGAGCACAT
TNFR1	CGCTACCAACGGTGGAAGTC	CAAGCTCCCCCTCTTTTTCAG
TNFR2	CAAGCCAGCTCCACAATGG	TGACCGAAAGGCACATTCCT
RAGE	GCAGTCGGAGCTAATGGTGA	TCCACCACCAATTGGACCTC
TLR2	GCCAAAGTCTTGATTGATTGG	TTGAAGTTCTCCAGCTCCTG
TLR4	GGTCAGACGGTGATAGCGAG	GGGAGGTTGTCGGGGATTTT

Table 4. Primers used for mouse genes (5´->3'):

Gene	Forward	Reverse
s100a9	CACAGTTGGCAACCTTTATG	CAGCTGATTGTCCTGGTTTG
Tnfα	AGGGATGAGAAGTTCCCAAATG	GCTTGTCACTCGAATTTTGAGAAG

Relative gene expression was normalized to *Beta 2 Microglobulin (B2M* - human) or beta 2 microglobulin (*b2m* - mouse) using the primers below:

Table 5. Human genes (5´->3´, forward; reverse):

Gene	Forward	Reverse
B2M	AGATGAGTATGCCTGCCGTG	TCATCCAATCCAAATGCGGC

Table 6. Mouse genes (5´->3´):

Gene	Forward	Reverse
b2m	GACCGGCCTGTATGCTATCC	CAGTAGACGGTCTTGGGCTC

5.1.2. **RNAseq**

Total RNA was extracted using a RNeasy kit (QIAGEN). Cells were lysed with RLT + 1% β-mercapto-ethanol (RNAeasy kit, Quiagen). RNA integrity numbers ranged from 7.6 to 9.4 (average 8.7) when assayed on an Agilent 2100 Bioanalyzer. The PolyA+ fraction was purified and randomly fragmented, converted to double stranded cDNA, and processed through subsequent enzymatic treatments of end-repair, dA-tailing, and ligation to adapters as in Illumina's "TruSeq Stranded mRNA Sample Preparation Part # 15031047 Rev. D" kit (this kit incorporates dUTP during 2nd strand cDNA synthesis, which implies that only the cDNA strand generated during 1st strand synthesis is eventually sequenced). An adapter-ligated library was completed by PCR with Illumina PE primers (9 cycles). The resulting purified cDNA library was applied to an Illumina flow cell for cluster generation and sequenced on HiSeq2500 (Illumina) following the manufacturer's protocols. Image analysis, per-cycle base calling and quality score assignment were performed with Illumina Real Time Analysis software. Conversion of Illumina BCL files to bam format was performed using Illumina2bam. Single read sequences were analysed by Nextpresso pipeline (Grana et al. 2016). Sequencing quality was analysed with FastQC (http://www.bioinformatics.babraham.ac.uk/projects/fastqc/); reads were aligned to the human genome (GRCh37/hg19) using TopHat-2.0.10 (Kim et al., 2013), Bowtie 1.0.0 (Langmead and Salzberg, 2012) and Samtools 0.1.19.0 (Li et al., 2009); and transcripts assembly, abundances estimation and differential expression were calculated with Cufflinks 2.2.1 (Trapnell et al., 2010). The estimated significance level (P value) was corrected to account for multiple hypotheses testing using a Benjamin and Hochberg False Discovery Rate (FDR) adjustment. Genes with FDR less than or equal to 0.05 were selected as differentially expressed. PCA plots, hierarchical clustering (Pearson’s Dissimilarity), and heatmaps were generated in R and Partek.

5.1.3. **Gene set enrichment analysis**

Gene set enrichment analysis (GSEA) of differentially expressed genes was performed using the GSEA software, Version 2.0.6, obtained from the Broad Institute (Subramanian *et al.*, 2005). GSEA was performed to analyse the enrichment of gene sets following the developer's protocol and using pathway annotations from the Gene Ontology, Reactome, Biocarta and Kyoto Encyclopaedia of Genes and Genomes (KEGG) databases.

All previously obtained differentially expressed genes were ranked according to their t-statistic. This ranked file was used as input for the enrichment analysis. All basic and advanced fields were set to default and only gene sets significantly enriched at a False Discovery Rate (FDR) q-value < 0,25 were considered.

5.1.4. **Gene Ontology Molecular function**

Gene Ontology analysis was performed using the EnrichR software.

5.1.5. **Loss of function approaches**

5.1.5.1. Lentivirus production and cancer cell infection

In order to generate stable knockdown cell lines lacking expression of *S100A9*, two different short hairpin RNAs were employed. For human cells, TRC lentiviral Human S100a9 shRNA (ref: RHS4533-EG6280, Dharmacon), was utilized, and for mouse cell lines, TRC lentiviral Mouse S100a9 shRNA (ref: RMM4534-EG20202, Dharmacon) was used. Both lentiviral plasmids carry a puromycin resistance gene.

Lentivirus was produced in HEK293T cells grown to 50-70% confluence on the day of transfection. The transfection was conducted using 8,75ug of TRC lentiviral shRNA (mouse or human) mixed with VSVG, RRE and REV packaging vectors in a 1:1 ratio as per manufacturer's protocol. The lentiviral and packaging vectors were mixed in 105uL of lipofectamine transfection reagent (Lipofectamine 2000 ref: 11668-030, Invitrogen) and 5mL Opti-Mem (ref: 31985-070, Gibco), then added to a final volume of 15mL transfection media (Tfm; DMEM, FBS 11,4%, Glutamine 1%, Sodium Pyruvate 1%) and incubated overnight. To

enhance the efficiency of infection, cells were treated with polybrene (1ug/mL; Sigma Aldrich). On the day after transfection, the media was changed to fresh transfection media and cells were incubated for 36h under standard growth conditions.

Following infection, cells were selected using 2mg/mL puromycin (Sigma Aldrich). After three days treated with puromycin all the control cells were dead. Selected cells were maintained in culture with a supplement of puromycin in the media for two weeks after selection.

6. **Statistical analysis**

Data are represented as the mean values ± S.E.M. When comparisons were done between two experimental groups, an unpaired Student's t test was used. Overall survival was calculated using Kaplan–Meier survival curves. For survival curves, P values were obtained with log rank (Mantel-Cox) test. Heatmaps were generated using Morpheus software (https://software.broadinstitute.org/morpheus/).

Results

Results

1. Establishment of a new breast cancer model to study brain metastasis

There are a limited number of experimental models that allow studying brain metastasis in an immunocompetent background (Valiente *et al.*, 2018), and recent work has suggested that the immune system is important for the radiation response (Twyman-Saint Victor *et al.*, 2015). Thus, immunocompetent models are necessary to investigate the potential mechanisms involved in the response to radiation. Taking advantage of the ability of E0771, a well-characterized syngeneic breast cancer cell line, to be used in an immunocompetent setting, we established a model of breast cancer brain metastasis.

We performed intracardiac (IC) injection of E0771 parental cell line (E0771-P), a basal triple negative breast cancer cell line (Johnstone *et al.*, 2015), that we initially engineered to express a plasmid encoding the enzyme luciferase in a group of 10 C57BL/6 mice. Expression of luciferase allows non-invasive tracking of metastasis progression with bioluminescence imaging (BLI). Seven days after IC injection, we started to detect bioluminescence in different regions of the body, including lumbar region, abdomen, and head. At day 15 after IC injection, mice were sacrificed based on evident worsening of the general health status or weight loss equal to or greater than 20%. *Ex vivo* BLI confirmed extensive metastatic load in multiple organs, such as the lung, lymph nodes, and liver. Brain metastases were only detected in 2/10 mice, in contrast to lung metastases, which were detected in 10/10 mice. Consequently, the E0771-P cell line is highly metastatic to multiple organs but has limited ability to colonize the brain, as previously reported (Contreras-Zarate *et al.*, 2019).

To increase tropism to the brain, we dissected the brain metastasis with the highest *ex vivo* bioluminescence value ($9x10^3$ average radiance (p/s/cm2/sr). The dissected lesion was then enzymatically dissociated in the appropriate media (see Methods) and the cancer cells were isolated and cultured *in vitro*. After two passages *in vitro*, adherent cells were tested with BLI. When bioluminescence was confirmed, the resulting cell line was named E0771-BrM1 (BrM, brain

metastatic). Two additional rounds of *in vivo* selection (Bos *et al.*, 2009; Nguyen *et al.*, 2009) generated the E0771-BrM3 cell line. The new cell line was then transfected with a plasmid encoding for ZsGFP (Catalog No. 632179, Clontech), which helps to identify cancer cells by means of histology. In order to confirm the increased brain tropism of E0771-BrM3 cells compared to the parental counterpart (E0771-P), we performed a final experiment *in vivo* injecting 10 mice with each cell line. Fifteen days after IC injection, *in vivo* bioluminescence signal in the head was detectable at higher levels in those injected with E0771-BrM3 cells ($2x10^5$ average radiance (p/s/cm2/sr) compared to those inoculated with E0771-P ($5x10^4$ average radiance (p/s/cm2/sr) (Figure 1A). Analysis of *ex vivo* brain bioluminescence confirmed a significant increase in brain metastatic burden in those animals injected with E0771-BrM3 cells compared with the group of mice injected with E0771-P (Figure 1B). In contrast, we did not observe any significant difference in extracranial metastasis (Figure 1C), which could explain the lack of any difference in survival (Figure 1D) (P= 0,1149). The new model E0771-BrM3 is identified as E0771-BrM in the rest of the text for simplicity. This model has been incorporated to the broad repository of experimental brain metastatic cell lines available in the laboratory.

Figure 1. A new syngeneic breast cancer model to study brain metastasis.

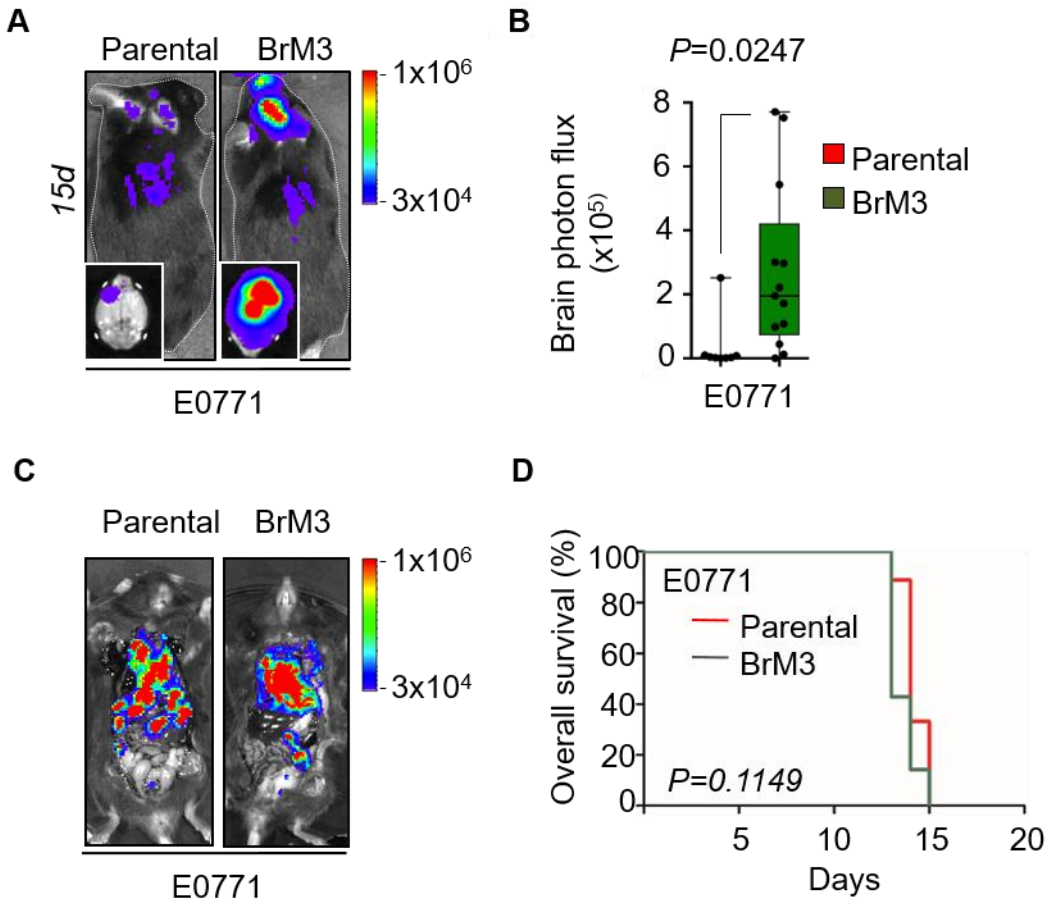

Figure 1. A. Bioluminescence images *in vivo* and *ex vivo* at day 15 after intracardiac injection. B. Quantification of *ex vivo* bioluminescence of brains comparing E0771-P with E0771-BrM3 (E0771-P n=7, E0771-BrM3 n=13; P= 0.024). C. *Ex vivo* bioluminescence from thoracic and abdominal cavities at day 15 show no differences between E0771-P and E0771-BrM3 cells. D. Overall survival graph comparing mice injected with E0771-P and E0771-BrM3 cells (Parental n =4, BrM3 n=5, P=0.1149).

2. **Sensitivity of brain metastatic cells to radiation *in vitro***

We analysed the efficacy of radiotherapy to impair the viability of brain metastatic (BrM) cell lines. Specifically, we tested lung cancer BrM (H2030-BrM; PC9-BrM; 393N1; 482N1) and breast cancer BrM (MDA231-BrM; CN34-BrM; ErbB2-BrM; Hcc1954-BrM1a; Hcc1954-BrM1b; E0771-BrM) models. These models include both mouse (393N1; 482N1, E0771-BrM) and human (H2030-BrM; PC9-BrM,

MDA231-BrM; CN34-BrM, ErbB2-BrM, Hcc1954-BrM1a; Hcc1954-BrM1b) cell lines (Figure 2C) and represent clinically relevant oncogenomic profiles for each tumour type (data not shown).

We cultured each BrM cell line *in vitro* under normal culture conditions and divided them in two experimental groups, a non-irradiated control group and another group that received a single dose of radiation (10Gy of gamma radiation (γ-IR) (Figure 2A). Seventy-two hours later, cells were fixed and stained with DAPI. Five different fields from three coverslips per cell line and condition were imaged using a fluorescence microscope and quantified for the percentage of viable cells (Figure 2B). All models tested presented high sensitivity to radiation, which decreased the percentage of viable cells by 45- 83%, depending on the model (Figure 2C).

These results prove that BrM cells lines present a high sensitivity to radiation *in vitro* independently of their species, tissue of origin, or oncogenomic profile.

Figure 2. Experimental brain metastases are highly sensitive to radiation *in vitro*.

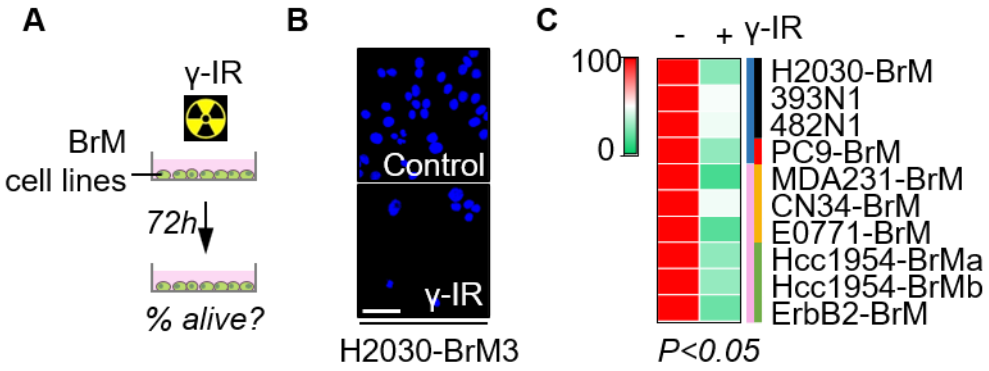

Figure 2. A. Schema of experimental design. B. Representative images of control and irradiated cells (single dose of 10Gy) of H2030-BrM in adherent culture conditions. Staining with DAPI. C. Heatmap depicting the percentage of DAPI+ cells in the coverslip (H2030-BrM = 75%, P= 0.002; PC9-BrM= 58%, P= 0.026; 393N1= 72%, P= 0.02; 482N1= 72%, P= 0.015; MDA231-BrM= 70%, P= 0.011; CN34-BrM= 52%, P= 0.007; ErbB2-BrM= 76%, P= 0.012; Hcc1954-BrM1a= 45%, P= 0.029; Hcc1954-BrM1b= 72%, P= 0.02; E0771-BrM= 83%, P= 0.0001)

3. Sensitivity of Brain metastasis cells to radiation *in vivo*

3.1. Human lung adenocarcinoma in an immunodeficient mice model (Athymic Nude-Foxn1^{nu})

To determine whether the sensitivity to radiation we observed *in vitro* is recapitulated *in vivo*, we tested several radiotherapy protocols on mice with brain metastatic tumours. We chose H2030-BrM, a human lung adenocarcinoma cell line, since it was among the most radiosensitive *in vitro*.

In order to generate established metastases in the brain, we performed IC injection of 1x10^5 cancer cells per mouse (Nguyen *et al.*, 2009). Given the human origin of the H2030-BrM lung adenocarcinoma model, we used immunodeficient mice (Athymic Nude-Foxn1^{nu}).

Fourteen days after IC injection we confirmed the presence of established brain metastases by BLI (Figure 3A), defined as heads with photon flux values >10^4 (measured as p/s/cm2/sr). In fact, average value was 1,84x10^5 at the time the radiation protocols were initiated (Figure 3B), thus, mimicking very closely the clinical situation where fully established metastases are treated. We applied three different radiation protocols previously reported in experimental brain tumours (Martinez-Aranda *et al.*, 2013; Leder *et al.*, 2014; Smart *et al.*, 2015). To avoid extracranial radiotoxicity, we designed and validated a lead metal shield that allowed us to irradiate only the heads of mice (Figure 3A and C). To perform the experiment, we divided the animals into four different treatment groups: Group 1. Non-irradiated control group, n= 14 mice; Group 2. Irradiated group with protocol A (Leder *et al.*, 2014), n= 20 mice; Group 3. Mice subjected to protocol B (Martinez-Aranda *et al.*, 2013), n= 7 mice; Group 4. Mice subjected to protocol C (Smart *et al.*, 2015), n= 5 mice. Although the details of each protocol can be found in the Methods section, they are briefly summarized here.

Protocol A: mice were treated with a fractionated dose of 1Gy and 3Gy over five days. Total dose of 10 Gy per mouse (Leder *et al.*, 2014) .

Protocol B: mice received a fractionated dose of 5,5Gy/day for 3 days. Total dose of 16,5Gy of radiation per mouse (Martinez-Aranda *et al.*, 2013).

Protocol C: mice received a fractionated dose of 3Gy/day of radiation dose for 10 days, reaching a total amount of 30Gy per mouse. Protocol C is the closest to the clinical standard of care (Smart *et al.*, 2015).

Surprisingly, no impact of radiation on brain metastasis progression scored by non-invasive BLI could be detected with any of the protocols used (Figure 3D). Consequently, mice succumb to the disease at the same time than the non-irradiated group (Figure 3E). BLI analysis showed that there was no difference in terms of the BLI signal in the different groups of irradiated mice compared with the non-irradiated group (Figure 3D). In terms of overall survival, we observed no difference between any of the treatment groups. All of the animals died between day 21 and day 55 after IC (Figure 3E).

These results suggest that, in contrast to what we observed *in vitro*, radiation does not impair the viability of brain metastasis *in vivo.*

Figure 3. *In vivo* response to radiation in immunodeficient mice.

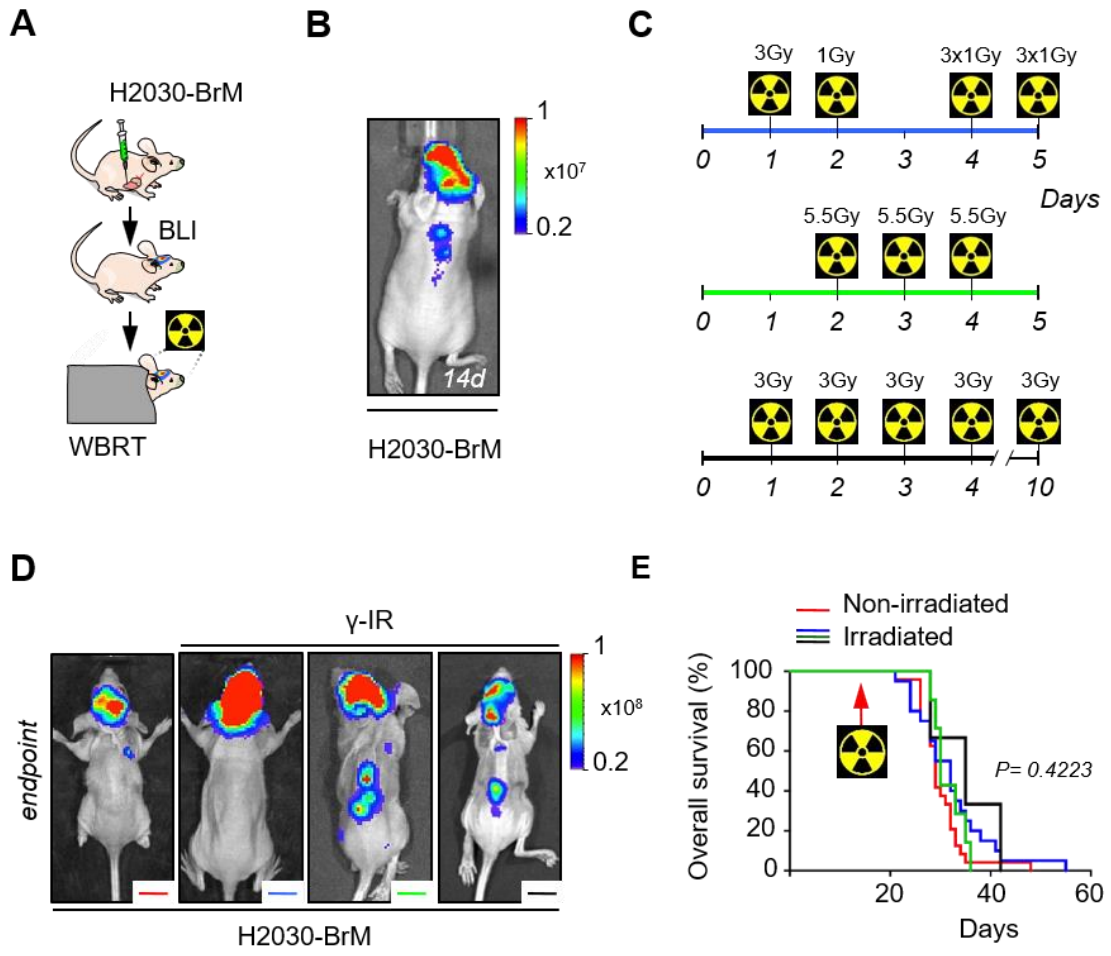

Figure 3. A. Schema of experimental design. B. Bioluminescence representative image at day 14 after intracardiac injection. C. Schematic representation of radiation protocols tested *in vivo.* Blue line represents protocol A; Light green line represents protocol B; and black line represents protocol C. D. Bioluminescence representative images of control and animals for the three different groups treated with radiation (Red: non-irradiated group; blue: protocol A; light green: protocol B; black: protocol C) at the humane endpoint. E. Survival curves comparing all groups analysed using Log-rank Mantel-Cox test (P= 0.4223). (Red, non-irradiated: n= 24; blue, protocol A: n=20, P=0.1649; light green, protocol B: n=7, P=0.3057; black, protocol C n=5, P=0.2019)

3.2. Mouse breast adenocarcinoma in an immunocompetent model (C57BL/6)

To ensure that this phenotype is also replicated in an immunocompetent background and in an additional cancer type, we performed *in vivo* irradiation of E0771-BrM established brain metastases using protocol C (Smart *et al.*, 2015). Given that our objective was to irradiate established metastases and that survival of mice inoculated with the syngeneic cell line is very close to the duration of the therapeutic intervention (Figure 1D and 3C), we incorporated a modification in the experimental design. We performed intracranial injection ($2,5X10^4$ cells), waited for 3 days, and started the protocol when the BLI signal in the brain reached 10^4 photon flux values (Figure 4A). This way we were able to mimic the clinical situation using an immunocompetent background. Similarly, to the immunosuppressed hosts, we found no differences in BLI signal between non-irradiated and irradiated mice (Non-Irradiated: n=4; Irradiated: n=4; P=0.456) (Figure 4B and C). We additionally measured the mean area of the metastases using histology and confirmed that there was no difference between treatment groups (Non-Irradiated: n=4; Irradiated: n=4; P=0,350) (Figure 4D). Although the E0771-BrM model was engineered to express GFP, we have consistently observed that it tends to lose the expression of this reporter *in vivo*. These findings have been reported in other syngeneic and hypothesize to reflect the action of the immune system. However, this unexpected limitation did not involve a major impact in our main aims.

In conclusion, *in vivo* irradiation following clinically relevant protocols applied to established brain metastases from lung or breast cancer in an immunocompetent or immunosuppressed host has no significant effect on local progression and, thus, it does not impact survival.

Figure 4. *In vivo* response to radiation in a syngeneic mouse model of brain metastasis.

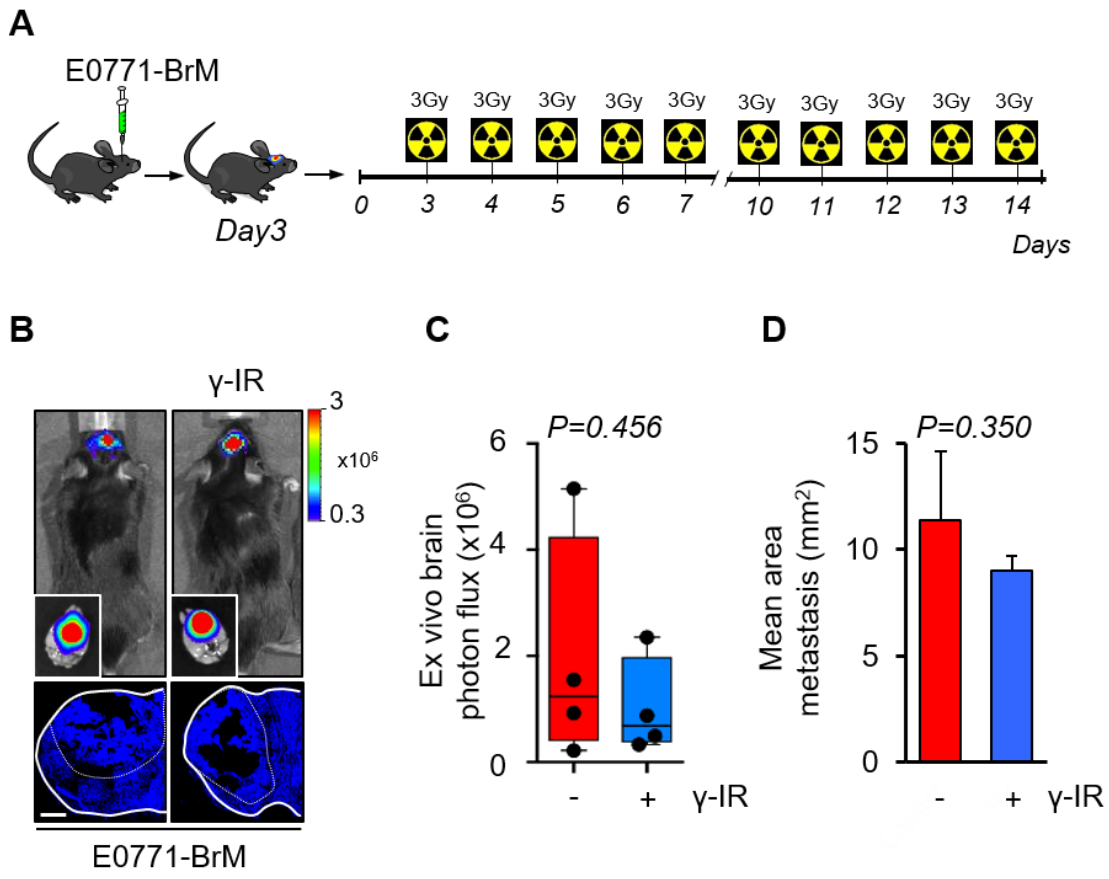

Figure 4. A. Schema of experimental design. B. Representative bioluminescence images *in vivo* and *ex vivo* at day 14 after intracranial injection. Representative images of brains from non-irradiated and irradiated mice, respectively, stained with DAPI. White lines surround the brain metastatic lesion. C. Quantification of *ex vivo* bioluminescence of non-irradiated and irradiated brains (Non-irradiated n=4; irradiated n=4; P= 0.456). D. Quantification of the mean area of brain metastasis lesions from non-irradiated and irradiated brains (Non-irradiated n=4, mean 11.35 ± 3.25; irradiated n=4, mean area= 8.97 ± 0.695; P= 0.350).

3.3. Brain metastasis cells are radio-sensitive *in vivo* when growing extracranially

In order to analyse whether resistance to radiation *in vivo* is dependent on the presence of BrM cells in the brain parenchyma and not acquired through a more general *in vivo*-dependent mechanism, we generated H2030-BrM tumours in the

subcutaneous space of the head and treated them with radiation (Figure 5A). $1x10^5$ cells H2030-BrM cells resuspended in Matrigel (1:2) were allowed to grow for 15 days to mimic the protocol applied to brain metastasis. At this moment, a mass could be detected in the head. The established tumour was irradiated with a single dose of 10Gy (Figure 5A). Given that the BLI was saturated in the control animals and thus not compatible to be used in the analysis, we performed histology. 72 hours after irradiation, a BrdU pulse was administered (0,8mg/kg – 100uL of a stock solution 0,2mg/mL) and 4 hours later mice were sacrificed. The proliferation index of the control and irradiated groups was determined (Figure 5B). A significant decrease in BrdU was detected in irradiated tumours (p-value=0,0071) (Figure 5C).

Our experiment suggests that resistance of BrM cells to radiation therapy might be specifically induced in the brain parenchyma. This finding might involve that this form of resistance can be modulated and thus its molecular regulation could be used to generate better ways to apply this therapy.

Figure 5. Subcutaneous H2030-BrM tumours are sensitive to radiotherapy.

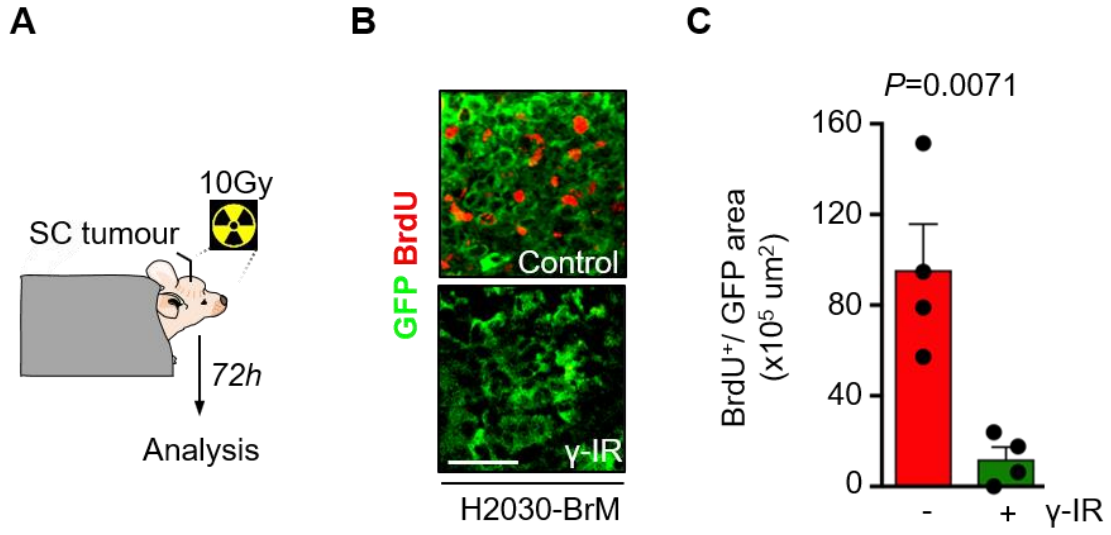

Figure 5. A. Schema of experimental design. Tumours were irradiated 15 days after a subcutaneous inoculation (SC: subcutaneous). B. Representative images of subcutaneous tumours stained against green fluorescence protein (GFP) and

BrdU to identify proliferating cells after irradiation. C. Quantification of BrdU+ cells per GFP area (Non-irradiated: n=4; irradiated: n=4; P= 0.0071).

4. **Resistance to radiotherapy can be modulated.**

The previous data suggest that BrM cells have different sensitivity to radiation when evaluated *in vitro* versus *in vivo*. To test this hypothesis, we reasoned that there should be conditions present in the *in vivo* environment that might induce the resistance. Metastatic cells must have the ability to re-initiate the tumour in secondary organs. This ability has been linked to stem cell-like properties (Celià-Terrassa and Kang, 2016; Lambert, Pattabiraman and Weinberg, 2017). Cancer stem cells have been previously shown to correlate with increased resistance to therapy, including radiotherapy (Rycaj and Tang, 2014; Krause *et al.*, 2017). In addition, another attribute of metastatic cells includes their ability to interact with the microenvironment, which has been also proved to mediate therapeutic resistance in a variety of different pre-clinical models (Sun *et al.*, 2012; Qu *et al.*, 2019). Consequently, we designed *in vitro* experiments to mimic stem cell-like properties and the crosstalk with the microenvironment in order to evaluate their potential impact on increasing radiation resistance.

4.1. *In vitro* conditions that increase radiation resistance.

4.1.1. **Tumour spheres are resistant to radiotherapy.**

First, to test the impact of stem cell-like properties on radioresistance, H2030-BrM cells were grown under low attachment conditions to induce the generation of oncospheres. Oncospheres have been shown to enrich cancer cells with superior tumour initiating abilities that are more effective in generating metastases.

BrM were cells were cultured for seven days under low attachment conditions. On day 7, oncospheres were irradiated (single dose of 10Gy) and then incubated for 72 hours, mimicking our previous *in vitro* assays. Subsequently, we analysed the effect of radiation by measuring the number and size of the spheres (Figure 6). We observed no difference in terms of size or number in any of the BrM cells

tested, which represent different tumour types and mouse/ human origins (H2030-BrM, P=0,504; E0771-BrM, P=0,7376; 482N1 P=0,668).

These results suggest that oncospheres can be considered an *in vitro* surrogate with a superior resistance to radiation.

Figure 6. Oncospheres are resistant to radiotherapy.

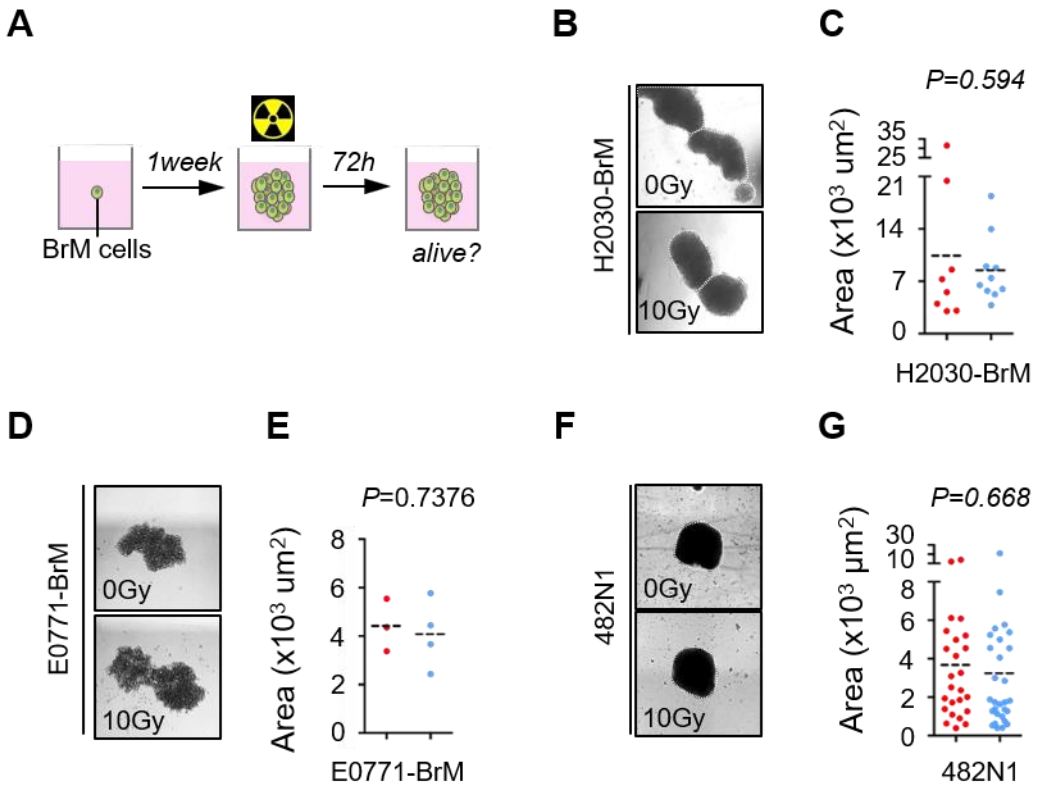

Figure 6. A. Schema of experimental design. B, D and F. Representative images of H2030-BrM (B), E0771-BrM (D) and 482N1 oncospheres (F). In each image set, the upper image represents the control group and the lower image represents oncospheres irradiated with a single dose of 10Gy. C, E and G. Quantification of the area of spheres ($x10^3$ μm^2) in the non-irradiated and irradiated groups of H2030-BrM (p=0.504), E0771-BrM (p=0.7376) and 482N1 (p=0.668), respectively.

4.1.2. **Co-culture of glial cells increases resistance of brain metastasis cells to radiation**

One of the most abundant components of the brain metastasis microenvironment are glial cells, including astrocytes as well as microglia (Quail and Joyce, 2017). Given the known influence of these cellular components on therapeutic resistance (Chen *et al.*, 2016), we tested whether they could also influence the sensitivity of BrM cells to radiation.

Glial cells were obtained from P0-P3 embryos, which is a commonly used protocol to isolate these cells for primary cultures (Schildge *et al.*, 2013). BrM and glial cells were co-cultured under two conditions: without direct cell-cell contact, using an insert chamber; or with direct cell-cell contact, by plating cancer cells and glial cells together. The proportion of cancer cells (H2030-BrM and MDA231-BrM) ($1,5x10^4$) to glial cells ($4,5x10^4$) was prepared at 1:4. By performing these two approaches we were able to analyse the influence of the glial cell secretome (paracrine interactions) versus direct cell-to-cell interactions in radiation resistance.

Interestingly, although exposure to the secretome of glial cells alone was not sufficient to change the sensitivity of BrM cells to radiation, as measured by the proportion of GFP+ cells remaining after treatment (Figure 7B), resistance to radiation was partially reduced when cancer cells were co-cultured with glial cells in the same well (Figure 7D). These results were reproduced in two different BrM cell lines from different primary tumours (H2030-BrM and MDA231-BrM). Consequently, cell-cell interactions with glial cells seems to correlate with an increased resistance of BrM cells to radiation.

Figure 7. Co-culture of brain metastatic cells with glial cells increases resistance to radiation.

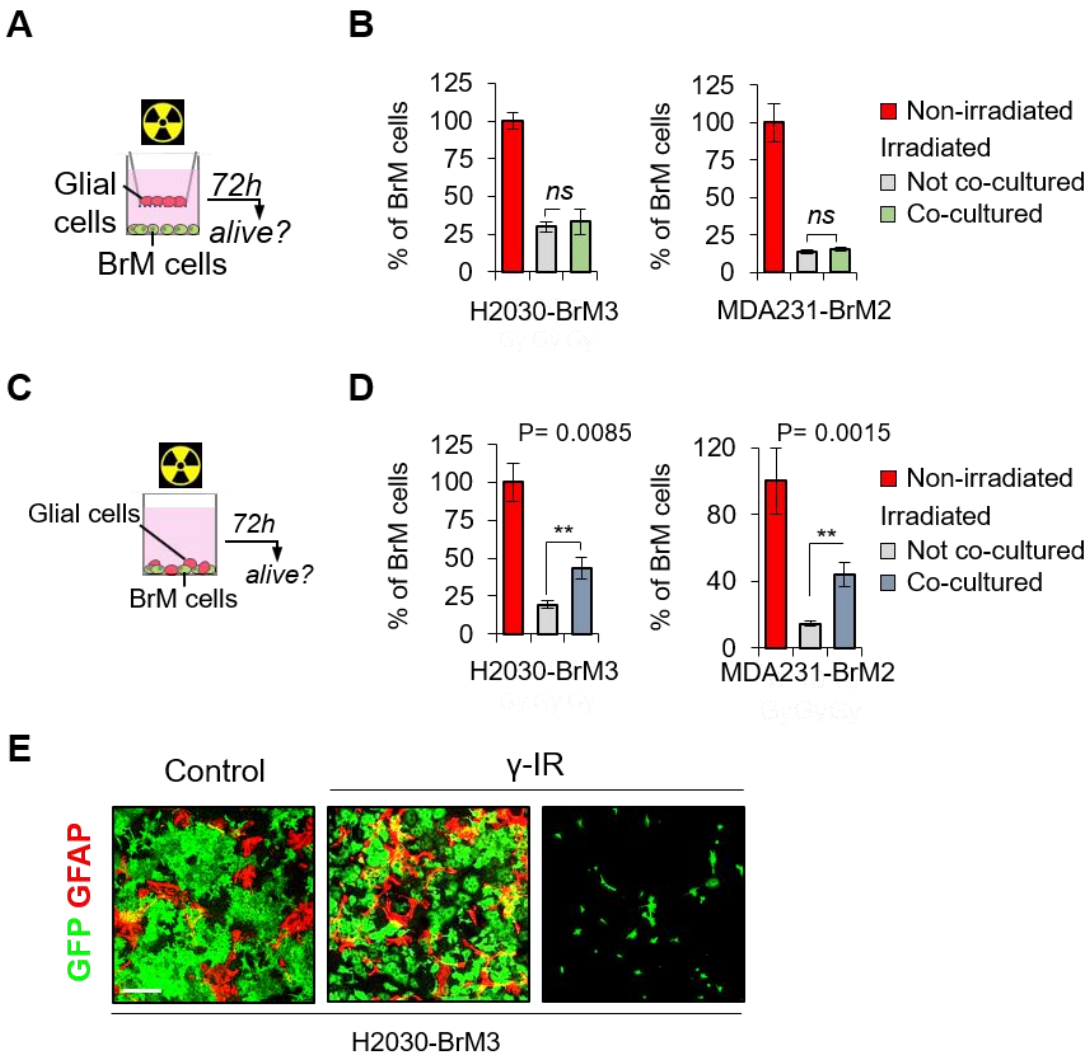

Figure 7. A, C. Schema of experimental design including co-cultures with insert chamber (A) and with cell-to-cell interactions (C). B. Quantification of the percentage of brain metastatic cells (H2030-BrM and MDA231-BrM) alive 72h after irradiation, in non-irradiated (red), irradiated cells in adherent conditions (gray) and irradiated cells cultured with the insert containing the glia (green) (H2030-BrM irradiated not co-cocultured: 29.85% ±3.47 , irradiated co-cultured: 33.4% ±8.50, P=0.611; MDA231-BrM irradiated not co-cocultured: 13.39% ±1.43, irradiated co-cultured: 15.55% ±2.15, P=0.475). D. Quantification of the percentage of brain metastatic cells (H2030-BrM and MDA231-BrM) alive 72h after irradiation, in non-irradiated (red), irradiated cells in adherent conditions (gray) and irradiated co-culture with cell-to-cell interaction (blue) (H2030-BrM

irradiated not co-cocultured: 19%± 2.57, irradiated co-cultured:43,5% ± 7.76, P=0.0085; MDA231-BrM irradiated not co-cocultured: 15%± 1.77, irradiated co-cultured:40,5% ± 5.12, P=0.0015).

4.2. Ex vivo

4.2.1. **Rationale to use organotypic brain cultures**

We next looked for more sophisticated models that recapitulate both tumour initiation and interactions with the microenvironment. Brain organotypic cultures satisfy both demands when combined with BrM cells. This preparation has been extensively used to study the molecular mechanisms underlying metastatic colonization including the initiation of metastasis as well as the crosstalk between cancer cells and the microenvironment. Consequently, brain organotypic cultures are considered as an excellent surrogate to functionally validate brain metastasis mediators before testing them *in vivo*. Importantly, the flexibility of this assay allows mimicking both early and late stages of colonization.

4.2.2. **Brain organotypic cultures recapitulate *in vivo* resistance to radiation**

In order to generate brain organotypic cultures brains from healthy mice were sectioned to generate thick brain slices (250 µm) using a vibratome. Brain slices were then placed on top of a membrane floating on the culture media (see Methods). Each brain slice received $3x10^4$ BrM cells, that were plated on the surface of the brain cultures, which is known to mimic the early stages of colonization. After overnight incubation, BLI emitted by BrM cells was acquired (day 0) and then brain slices were divided into 2 groups, non-irradiated and irradiated. The irradiated group received 10Gy in a single dose. 3 days after radiation, BLI was obtained again. The ratio between the BLI obtained at day 3 versus day 0 for each individual slice indicates the growth rate of BrM cells after being irradiated.

Our data show that, using this *ex vivo* model, a single dose of radiation of 10Gy is not able to compromise the growth rate of either H2030-BrM human lung cancer cells (Non-Irradiated: n= 20 ; Irradiated: n= 20 brain slices per condition,

P= 0.2385) or the E0771-BrM mouse breast cancer cells (Non-Irradiated: n= 8; Irradiated: n= 8 brain slices per condition, P= 0.2303). This is in sharp contrast to the radiation sensitivity observed for these cell lines *in vitro* (Figure 2C) and suggest that the induction of radiation resistance is highly dependent on the brain microenvironment.

Plating cancer cells on top of brain slices is a useful surrogate for the initial phases of brain metastasis but does not allow to interrogate very closely the clinical situation in which radiation is typically applied on well-established brain metastasis. Therefore, we decided to repeat this experiment but considering established brain metastases. Organotypic cultures were generated from brains containing established brain metastases generated after 5 weeks from intracardiac injection of H2030-BrM cells. Established brain metastases were confirmed as previously described (see material and methods) using BLI values *in vivo* and *ex vivo*. Brains with confirmed established metastases were sectioned and those slices with BLI values between $5x10^4$ to $1x10^6$ photon flux were selected at day 0 for the experiment. Brain slices were then divided into irradiated (10Gy, single dose) and non-irradiated (control) groups and cultured for 3 days. At day 3 after irradiation, BLI images were taken and the growth rate of metastases was estimated by calculating the fold-increase compared to baseline values at day 0.

As in the experiments scoring the early stages, radiation did not impair the growth of established metastases from H2030-BrM (Non-Irradiated: n= 10; Irradiated: n= 10 brain slices per condition, P= 0.7111).

In summary, organotypic cultures containing brain metastases reproduce the resistance to radiation observed *in vivo*, suggesting that this model could help to dissect the underlying resistance mechanisms.

Figure 8. Organotypic cultures recapitulate resistance to radiation.

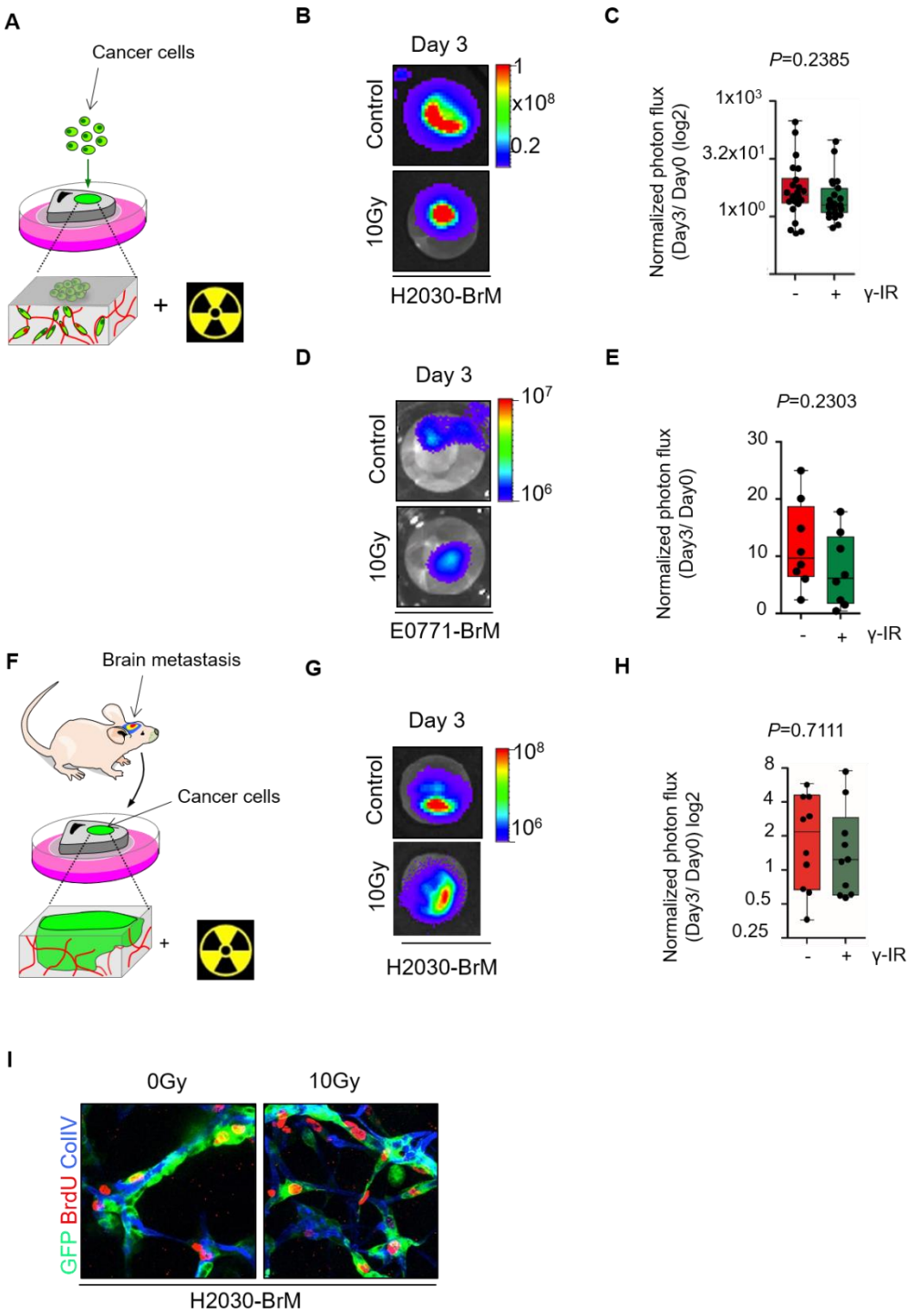

Figure 8. A. and F. Schema of the experimental design including plating BrM cells on the brain slices (A), which mimics initial stages, as well as cultures obtained from mice with established brain metastasis (F). B, D and G. Representative images of cultured brain slices for 3 days. BLI is shown in non-irradiated brain slices (top image) and irradiated slices (bottom image). B and D correspond to

results after plating BrM cells while G correspond to established metastases. C, E and H. Quantification of normalized photon flux in organotypic cultures of initial stages organotypic cultures of H2030-BrM (C) (Non-irradiated n= 23, 27.38± 15.06; Irradiated n= 24, 8.95± 4.45; P= 0.2385) and E0771BrM (E) (Non-irradiated n= 8, 11.88± 2.69; Irradiated n= 8, 7.49± 2.24; P=0.2303). Quantification of establish brain slices of H2030-BrM model (H) (Non-irradiated n=10, 2.52± 0.62; Irradiated n=10, 2.16± 0.74; P=0.7111) I. Representative images of immunofluorescence of non-irradiated and irradiated organotypic cultures with H2030-BrM cells. GFP: green fluorescence protein (green). BrdU: bromodeoxyuridine (red). ColIV: collagen IV (blue).

5. **Induced resistance to radiation is transient.**

In order to determine if the radiation resistance observed in oncospheres and glial co-cultures is permanently fixed in BrM cells or, on the contrary requires from constant induction, we performed re-irradiation experiments. BrM cells that were induced to be resistant to radiation after being cultured in oncospheres or with glial cells were re-plated in regular adherent culture conditions and interrogated for their ability to still resist radiation (see Figure 9A and 9C). Oncospheres were disaggregated and plated under adherent conditions and BrM cells were sorted from the glial cell culture and cultured under adherent conditions. A new dose of radiation (10Gy in a single dose) was given to these cells and 72 hours later we analysed the percentage of DAPI positive cells in both groups (Figure 9B and 9C). Given that the sensitivity to a single dose of radiation (10Gy) reduced cell viability (Figure 9B, D) to the levels detected in those BrM cells irradiated *de novo* (Figure 2C), we conclude that resistance is not permanently induced in BrM cells after special culture conditions. In order to be maintained, the resistance requires constant induction.

We also proposed that these *in vitro* surrogates inducing resistance could be dissected at the molecular level to interrogate potential sources responsible to decrease the sensitivity to this therapy.

Figure 9. Radiation resistance is a transient phenotype.

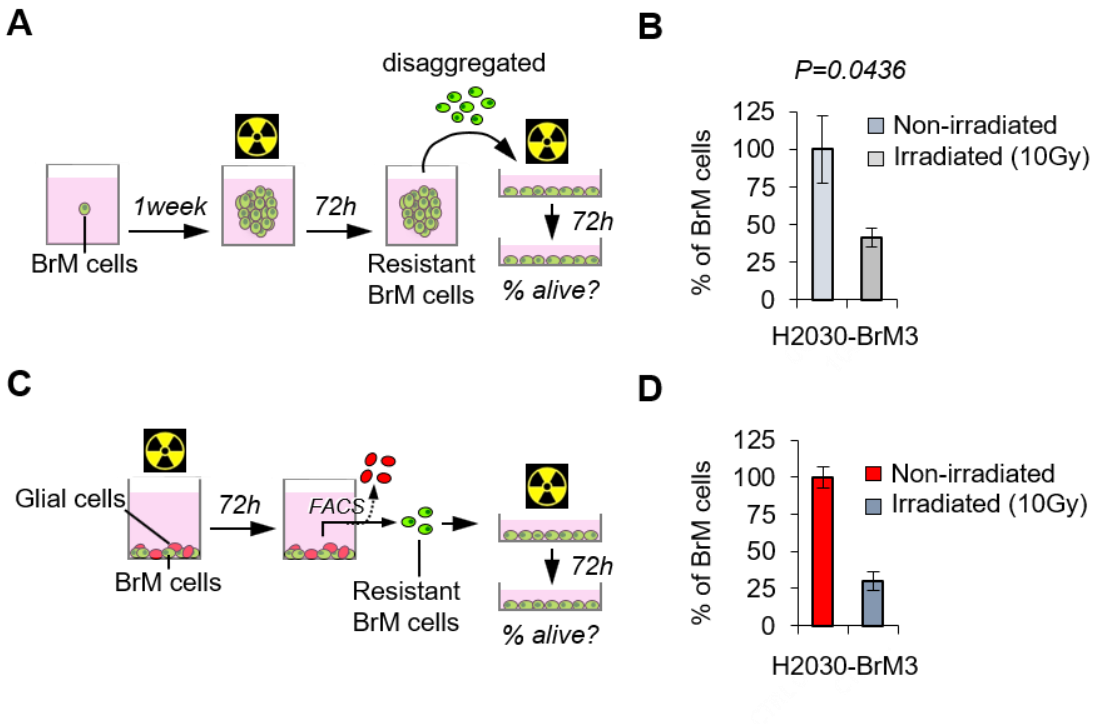

Figure 9. A and C. Schema of experimental design. B and D. Quantification of H2030-BrM 72 hours after being re-irradiated when compared with the control group (non-irradiated). Nor H2030-BrM obtained from oncospheres (B) neither from co-cultures were able to show any resistance (B and D, 5 fields of view were quantified from 5 images per coverslip from 3 different coverslips per condition (B, n= 15, 41.28± 6.07, P=0.0436; D, n= 5, 26.32± 3.54, P= $9.89x10^{-7}$).

6. Resistance to radiation correlates with more efficient DNA damage repair

To obtain molecular evidences of the radiation resistance phenotype, we analysed the level of γ-H2AX, a classical marker of DNA damage (Sak and Stuschke, 2010), in BrM cells after irradiation. Radiation causes DNA damage that activate DNA repair mechanisms. γ-H2AX is one of the pioneer sensors of DNA damage and accumulate in these lesions forming foci that could be visualized by immunofluorescence. Sustained levels of γ-H2AX is indicative of persistent damage that is not repaired, which could lead to apoptosis (Rogakou *et al.*, 1998).

BrM cells cultured under regular adherent conditions that received radiation (single dose of 10Gy), showed an increase of expression of γ-H2AX 1 hour after irradiation (Figure 10A). 24 hours after irradiation, we observed that BrM cells maintained high expression of γ-H2AX in their nuclei (Figure 10A). This finding, which might suggest the inability of BrM cells to resolve the radiation-induced DNA damage, could be the underlying cause leading to cell death detected after 72h (Figure 2C).

In contrast to this observation, when the same protocol of radiation was applied to the H2030-BrM cells grown under conditions correlating with radio-resistance (oncospheres, co-cultures, organotypic cultures and brain metastasis *in vivo*), the levels of γ-H2AX 24 hours after irradiation were drastically reduced (Figure 10B,C,D). In all the conditions we analysed 5 fields of view from 3 slices of 3 different wells of cells (A) or oncosphere cultures (B), six different brains were used to obtain *ex vivo* (C) and *in vivo* samples (D), three for each experiment.

In conclusion, we propose that one of the underlying mechanisms of resistance that could explain the lack of sensitivity to radiotherapy might involve a superior ability to repair DNA lesions.

Figure 10. Resistance to radiation correlates with less persistent DNA damage.

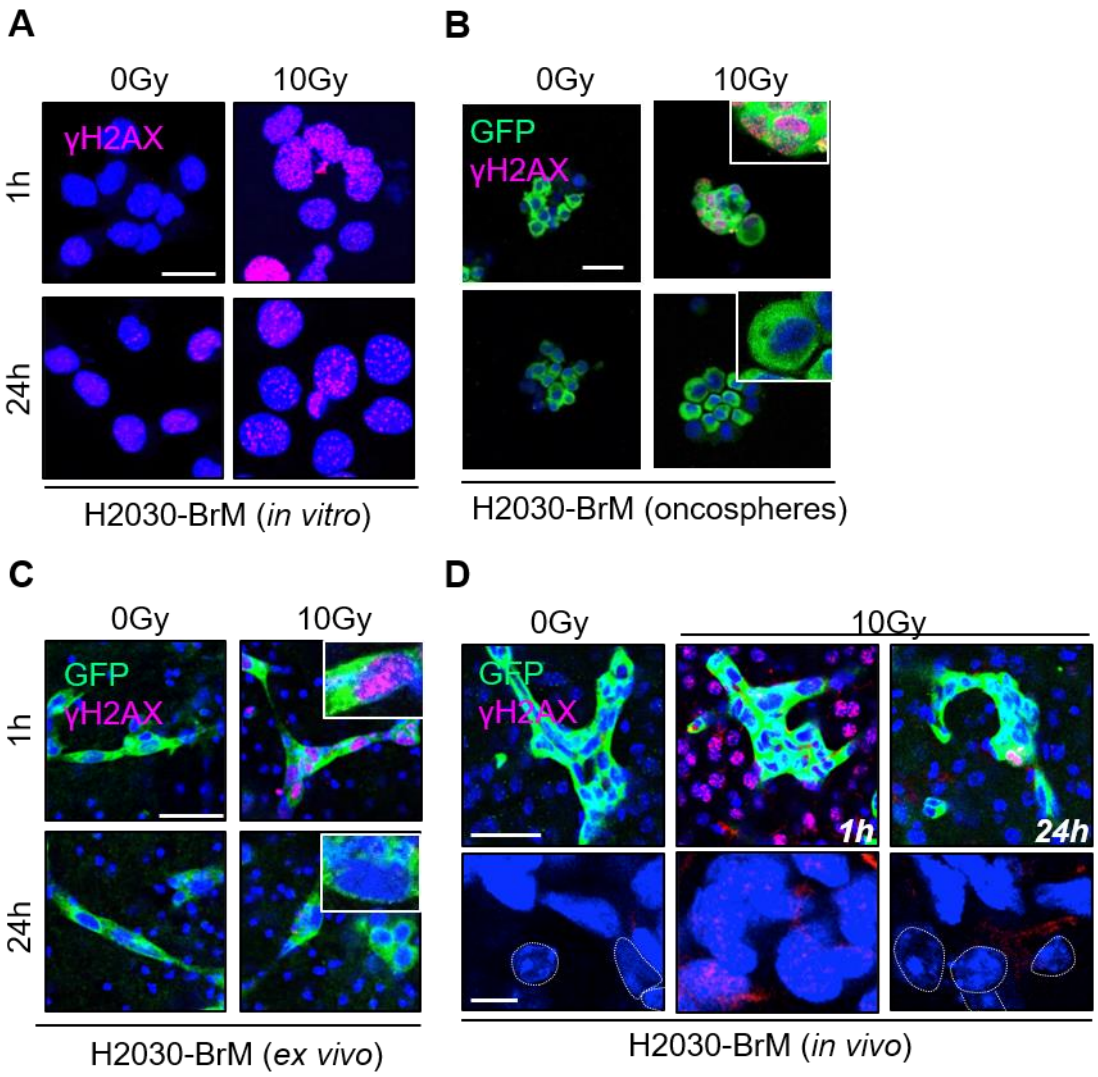

Figure10. Representative images of H2030-BrM cells stained with γ-H2AX antibody to score persistence of DNA damage over time. A. Adherent H2030-BrM cells maintain a high expression of γ-H2AX 24h after irradiation. B, C and D. H2030-BrM grown as oncospheres (B), on organotypic cultures *ex vivo* (C) or in vivo as brain metastases (D) efficiently reduced γ-H2AX levels 24 hours after irradiation.

7. **Molecular dissection of radiation resistance**

Given that our main goal was to improve the efficacy of radiotherapy, we reasoned that the transcriptome of resistant surrogates might identify de-

regulated genes that could be responsible for the phenotypes observed. In this sense we argue that different culture conditions correlating with radiation resistance might share commonly deregulated genes that might be responsible for the resistance phenotype. We hypothesize that it is the culture condition itself rather than the radiotherapy per se the inducer of potential transcriptomic changes. Thus, we focused on deregulated genes independently of the application of radiation, although their expression should not be influenced in an opposite way by this treatment.

In order to avoid any influence of radiation in cell death, we collected our samples 24 hours after applying radiation, since at this stage no changes in this sense were detected (data not shown). We focus our transcriptomic analysis on the H2030-BrM cell line, but we expanded the validation to other models. Three independent replicas were generated in each *in vitro* culture condition, including oncospheres and co-cultures with cell-cell-interactions. In the case of co-cultures, we isolated cancer cells by sorting based on GFP expression 24h after radiation and extracted RNA from those cells. All samples were tested for integrity using the bioanalyzer and submitted for RNA sequencing. The library generated by RNA sequencing was analysed to compare radiosensitive and radioresistant conditions.

7.1. Transcriptomic profile of radiation resistance in BrM cells

We focused our analyses on deregulated genes that were equally present in the two resistant surrogates, oncospheres and co-cultures with glial cells. Although the two resistant conditions are very different, we reasoned that if there was a key mechanism to resist radiation, it would be enriched in both conditions independently of the upstream stimuli that activated it, which is expected to be specific to each surrogate. Under these criteria, only ten genes were identified as deregulated across groups. Of these, two genes were up-regulated (*S100A9, CITED4*) and 8 genes were down-regulated (*ADM2, SLC1A4, B7H6, ASNS, PPP1R15A, FAT4, SESN2, MAP1B*). The 10 gene signature was also present in the non-irradiated resistant surrogates, which suggest that its acquisition is not depending on receiving radiation but on the culture conditions.

Figure 11.Transcriptomic profile of *in vitro* resistant surrogates.

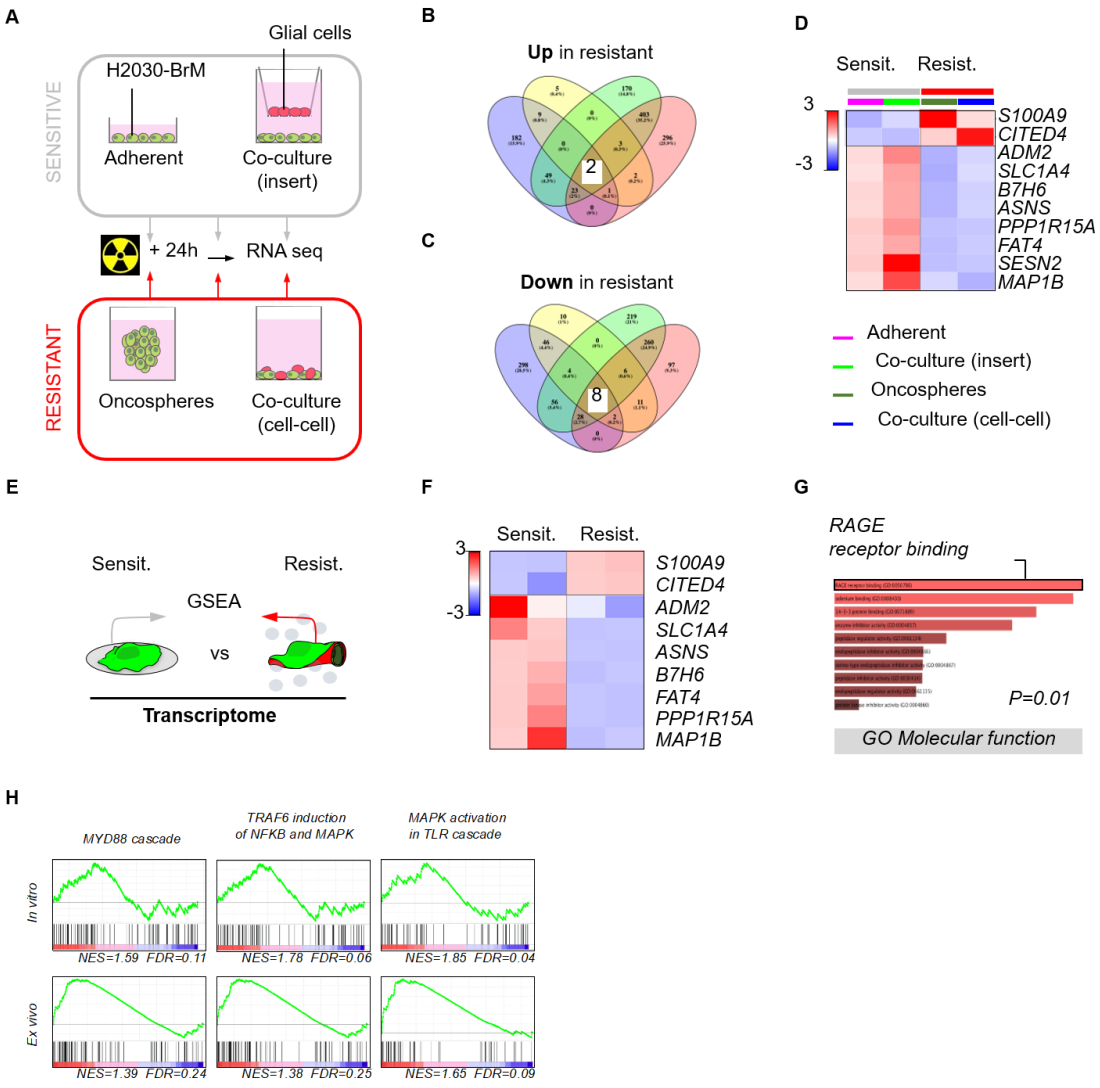

Figure 11. A and E. Schema of experimental design represents the conditions tested by GSEA analysis, including *in vitro* surrogates' analysis (A) and the analysis comparing adherent cells vs co-opting cells transcriptome (E). B. and C. Representation in a Venn diagram of the up regulated genes (B) and the down regulated genes (C) across the resistant groups. D. Heatmap representing gene expression of the 10 genes identified as deregulated across resistant groups. (up regulated – *S100A9, CITED4*; down regulated - *ADM2, SLC1A4, B7H6, ASNS, PPP1R15A, FAT4, SESN2, MAP1B)* at the comparation of sensitive (adherent cells and insert co-cultures) vs resistant surrogates (oncospheres and cell-cell contact co-culture). F. Heatmap representation of gene expression of the 10

genes of interest when we compared cells in adherent condition vs co-option cells. G. Gene ontology analysis graph of RAGE receptor H. Gene set enrichment representative graphs of the pathways found to be enriched.

Given that cancer cells growing in organotypic brain cultures also become highly resistant to radiation, we made use of the data generated in our previous publication (Valiente *et al.*, 2014) profiling H2030-BrM growing in brain slices in comparison to the same cell line under regular adherent culture conditions. Interestingly, in this very different experimental condition, the same 10 gene signature was also present (Figure 11).

Out of the 10 gene signature of radiation resistance, we decided to further assess *S100A9* because it was the highest up-regulated gene in each of the three resistance surrogates (oncospheres, co-cultures and organotypic cultures).

S100A9 is a calcium binding protein that has been reported to be involved in inflammatory processes and cancer progression (Gebhardt *et al.*, 2006). This protein can be found in the cytoplasm of myeloid cells and cancers cells but it can also be secreted, usually under circumstances involving stress (Tardif *et al.*, 2015; Jonasson *et al.*, 2017). Secreted S100A9 binds RAGE and TLR receptors that activate various downstream signalling pathways, including the NFκβ pathway (Riva *et al.*, 2012), a pathway that has been linked to radiation resistance in brain tumours (Bhat *et al.*, 2013).

Gene Set Enrichment Analysis (GSEA) showed significant enrichment of pathways related to NFκβ activation including MYD88 cascade; TRAF6 induction of NFκβ and MAPK; and MAPK activation in TLR cascade (Figure 11H). This finding applied to all *in vitro* and *ex vivo* conditions, which reinforces the potential involvement of this pathway in the resistance to radiation of brain metastasis surrogates. In addition to the identification of potential pathways activated by S100A9, we also found the enrichment of one of its receptors, RAGE, using the gene ontology (Figure 11G).

8. Identification of S100A9-RAGE-NFKB axis as a potential inducer of radiation resistance

8.1. Validation of S100A9 enrichment in brain metastasis and development of a loss of function strategy.

Given the increased expression of *S100A9* at the transcriptional level in all resistant surrogates, we hypothesized that it could be an important mediator of radiation resistance *in vivo*. First, we validated by qRT-PCR the increased expression of *S100A9* in oncospheres compared to adherent cells independently of irradiation (0Gy, P=0,0148; 10Gy, P=0,00157) (Figure 12A). In addition, we analysed S100A9 expression levels *in situ* by using S100A9 specific primers to human gene in brains containing human metastatic cells from H2030-BrM and brains with metastatic lesion of MDA231-BrM cells (figure 12 B). In these two models increased expression levels were evident when comparing cells growing under adherent conditions *in vitro* and cells growing inside the mouse brain (P=0,0108; P=0,0003, respectively). Besides that, we expanded the analysis to the protein levels of S100A9 and we included an additional model, including the E0771-BrM (Fig12C).

Figure 12. Validation of S100A9 enrichment in brain metastasis

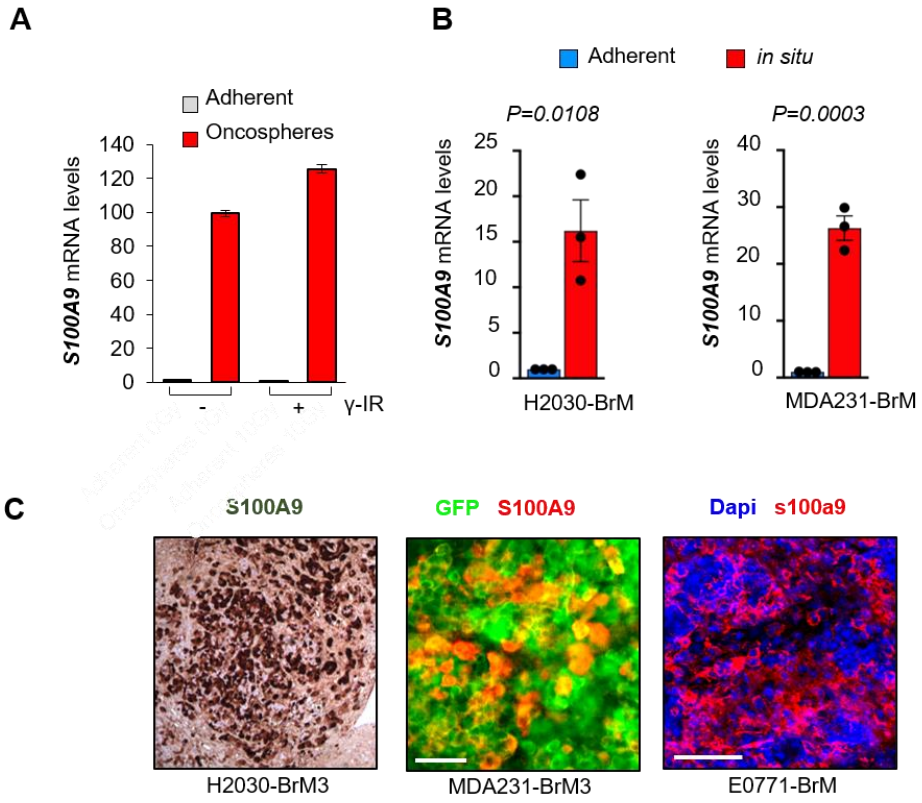

Figure 12. A. Quantification of *S100A9* mRNA levels in oncospheres compared to adherent cells in irradiated and non-irradiated conditions. B. Quantification of *S100A9* mRNA levels in adherent cells compared to BrM cells growing on a mouse brain (*in-situ*) in non-irradiated samples of H2030-BrM (left) and MDA231-BrM (right). C. Representative images of S100A9 protein expression levels (brown and red colour) on BrM cells (green). samples brains from mice with brain metastatic lesions from three different BrM cell lines (H2030-BrM on the left, MDA231-BrM on the middle and E0771-BrM on the right picture).

In order to functionally address whether the increased levels of S100A9 are responsible for mediating radiation resistance, we performed a knockdown in two different BrM models. 5 different shRNAs lentiviral vectors (pLKO.1 vectors) against the human *S100A9* gene and 5 different shRNAs lentiviral vectors against the mouse *s100a9* gene were used in the H2030-BrM and the E0771-BrM cell lines, respectively. Two shRNA that yielded more than 80% reduction in gene expression in each BrM model (Figure 13) were selected for the functional

validation *ex vivo* and *in vivo*. None of the cell lines showed any defect *in vitro* under normal adherent culture conditions (data not shown).

Figure 13. S100A9 knockdown selection for human and mouse BrM cell.

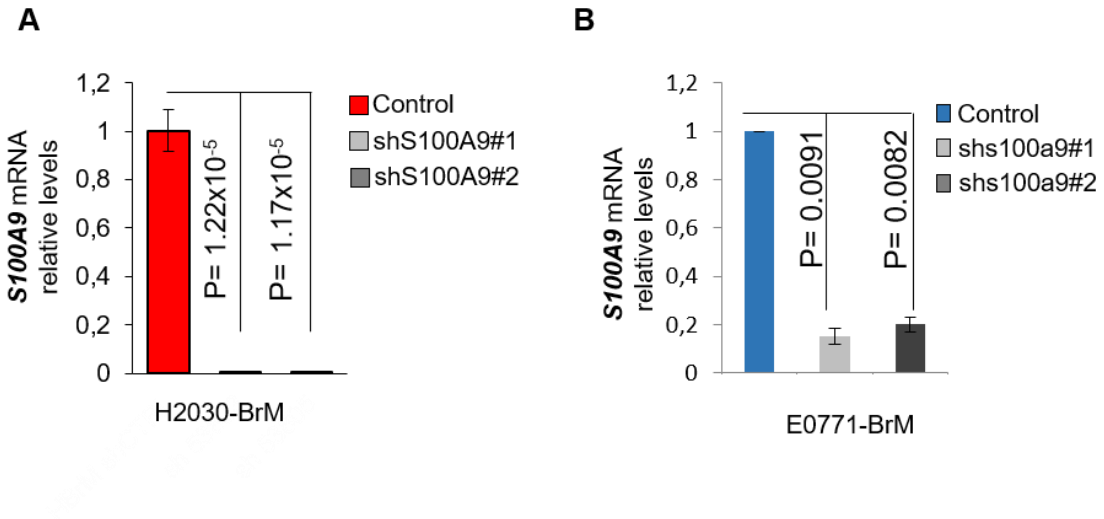

Figure 13. A. Quantification of S100A9 mRNA levels in H2030-BrM control cells compared to H2030-BrM cells engineered with two different knockdowns (ShS100A9#1 and ShS100A9#2). B. Quantification of S100A9 mRNA levels in H2030-BrM control cells compared to E0711-BrM cells engineered with two different knockdowns (Shs100a9#1 and Shs100a9#2)

8.2. *Ex vivo* evidence of the role of S100A9 as a mediator of radiation therapy.

In order to evaluate the potential role of S100A9 in mediating radiation resistance of brain metastatic (BrM) cell lines we use organotypic cultures. BrM cells ($3x10^4$ of cancer cells) engineered with control shRNA or shRNA targeting *S1009* were plated on top of alive brain slices. Plated BrM cells and brain slices were incubated overnight and the bioluminescence derived from the cancer cells, engineered to express luciferase, was acquired 18 hours after plating (Day 0). Subsequently, organotypic cultures were divided into two groups, one that received a single dose of 10Gy of radiation and another that was not treated. Brain slices were incubated for 3 days, after which bioluminescence imaging (BLI) was performed again before fixing the tissue. In order to estimate the growth rate

of BrM cells from each slice, we calculated the ratio of bioluminescence between day 3 and day 0 and termed this value as “fold increase”.

Control H2030-BrM cells demonstrated resistance to radiation, as expected (see figure 2C). Strikingly, *S100A9*-knockdown cells, which do not show any growth rate disadvantage with respect to control cells in the non-irradiated group, showed decreased bioluminescence levels in the irradiated group (Non-irradiated: shControl, n =9; sh*S100A9*#1, n= 6; sh*S100A9*#2, n= 13 brain slices per group, P= 0.5231; Irradiated: shControl, n= 10; sh*S100A9*#1, n= 4; sh*S100A9*#2, n=10 brain slices per group, P= 0.005).

Figure 14. *Ex vivo* evidence of the role of S100A9 as a mediator of radiation therapy

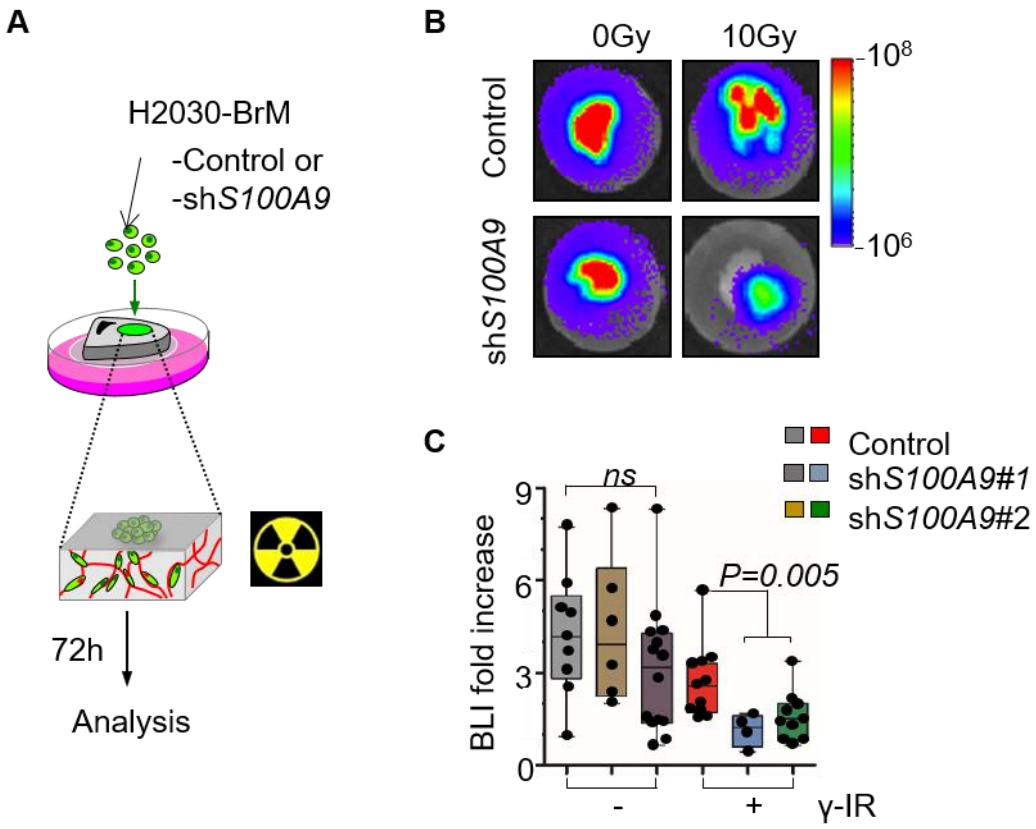

Figure 14. A. Schema of experimental design. B. Representative images of cultured brain slices for 3 days. BLI is shown in H2030-BrM control cells (top images) and in stable knockdown H2030-BrM cells lacking expression of *S100A9* (bottom images), in non-irradiated brain slices (left images) and irradiated slices (right images) conditions. C. Quantification of normalized BLI fold increase in

organotypic cultures of H2030-BrM cells (Control) and two different H2030-BrM knockdown cell lines (*shS100A9*#1 and #2). We compared the different groups (control vs knockdown) stratified by irradiation treatment.

8.3. Targeting *S100A9* in clinically relevant experimental models confirms its involvement in therapy resistance

In the clinical setting, brain metastases are usually treated when they have already formed macrometastases, which does not correspond with our previous data generated by plating BrM cells in brain slices. Therefore, in order to validate our findings in clinically relevant models, we generated established brain metastases in mice, generated organotypic cultures and irradiated them *ex vivo*.

First, we evaluated the ability of H2030-BrM sh*S100A9* cells to generate brain metastases. Intracardiac injection of shControl (n=10, nude Foxn1-/- mice) and sh*S100A9* (sh#1: n=5, nude Foxn1-/- mice; sh#2, n=5 nude Foxn1-/- mice, sh#2) H2030-BrM cells developed brain metastases with similar growth rates as measured by non-invasive BLI (add BLI values and P value) and showed similar metastatic load in the brain at the endpoint, as confirmed by *ex vivo* BLI.

Brains with established metastases were processed at 5 weeks after intracardiac injection. Organotypic cultures with metastases were exposed to a single (10Gy) dose of radiation. Three days later, we pulsed the slices with BrdU for four hours and fixed them using paraformaldehyde. Immunofluorescence imaging of BrdU incorporation demonstrated that *S100A9*-knockdown H2030-BrM cells significantly decreased proliferation rates 72h after radiation (n=15 , P<0,001).

Figure 15. S100A9 is responsible for resistance to radiation in established metastasis *ex vivo*

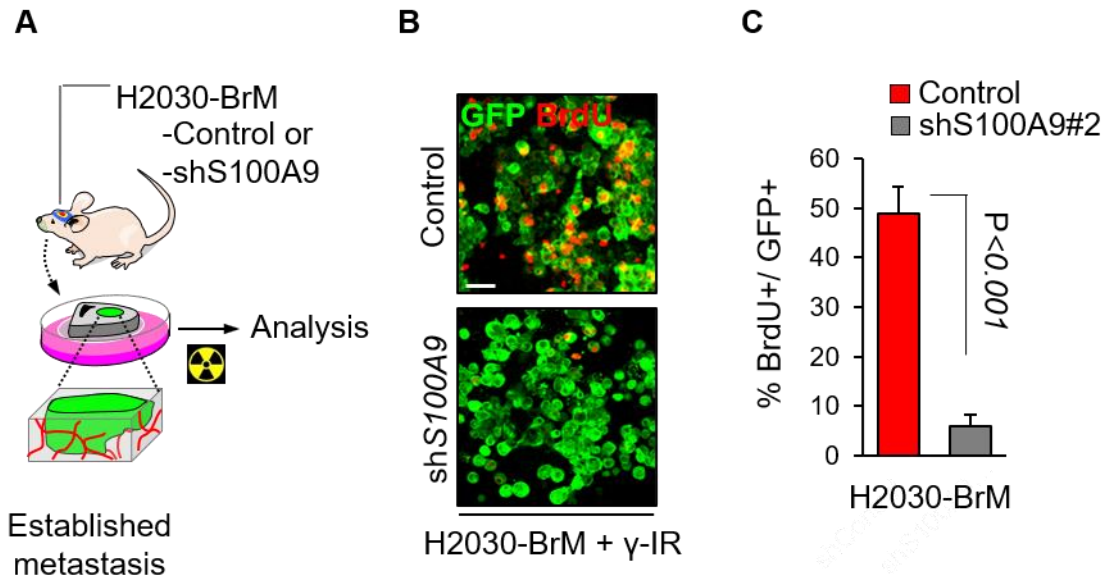

Figure 15. A. Schema of the experimental design including cultures obtained from mice with established brain metastasis. B. Representative images of immunofluorescence of irradiated brain slices, three days after irradiation. Immunofluorescence images shown levels of expression of BrdU on H2030-BrM control cells (top image) and in stable knockdown H2030-BrM cells lacking expression of *S100A9* (bottom image) both in establish brain slices. GFP: green fluorescence protein (green). BrdU: bromodeoxyuridine (red). C. Quantification of percentage of $BrdU^+$ cells per GFP^+ cells. (Control n=15 FOV; shS100A9#2 n=15 FOV; P<0.001)

We next performed an *in vivo* experiment to further test the potential role of S100A9 as a mediator of radiation resistance in brain metastasis. Three groups of mice were intracardiacally injected with three stably transfected cell lines derived from H2030-BrM: shControl, sh*S100A9*#1 or sh*S100A9*#2.

Brain metastases were established during the second week after the injection (Mean bioluminescence value ± SEM: shControl n= 10, $1.39x10^4 \pm 1.41x10^3$, sh*S100A9*#1 n=10, $1.02x10^4 \pm 1.76x10^3$ or sh*S100A9*#2 n=10, $1.14x10^4 \pm 1.50x10^3$). We applied protocol C (Figure16 E) of whole brain radiotherapy (WBRT) that includes a fractionated dose of 3Gy per day for 10 days, achieving

a total dose of 30Gy per mouse. This is the most clinically relevant of the commonly used radiation protocols (see Methods). Mice were followed weekly with non-invasive BLI until week 5 after intracardiac injection. At this time-point the humane endpoint is reached, and mice were sacrificed.

BLI *in vivo* showed a reduction in brain metastases burden in the groups injected with *S100A9* knockdown cells. In fact, this finding was already evident when only half of the total radiation dose had been delivered (shControl: n=8, 5.39E+05±1.06E+05; sh*S100A9*#1: n=8, 4.45E+04±2.33E+04; P=0,001; sh*S100A9*#2: n=8, 1.23E+05±3.83E+04; P=0,005) (Figure 15 F and G). Although brain metastases with *S100A9* knockdown continue growing, the growth rate was highly reduced compared to non-irradiated mice (Figure 15). *Ex vivo* bioluminescence taken at the endpoint confirmed reduced brain metastatic burden in irradiated mice harbouring *S100A9*-knockdown as compared to irradiated mice harbouring control tumours (shS100A9#1: n=8; P=0,016; shS100A9#2: n=8 P=0,044). Similarly, analysis of the histology confirmed that reduced levels of *S100A9* correlated with less GFP^+ metastases (shS100A9#2; P<0,001). Of note, extracranial metastases (non-irradiated) grew similarly in both groups.

These results unequivocally demonstrate that S100A9 mediates radiation resistance in lung adenocarcinoma brain metastasis.

Figure 16. S100A9 is responsible for resistance to radiation in established metastasis *in vivo.*

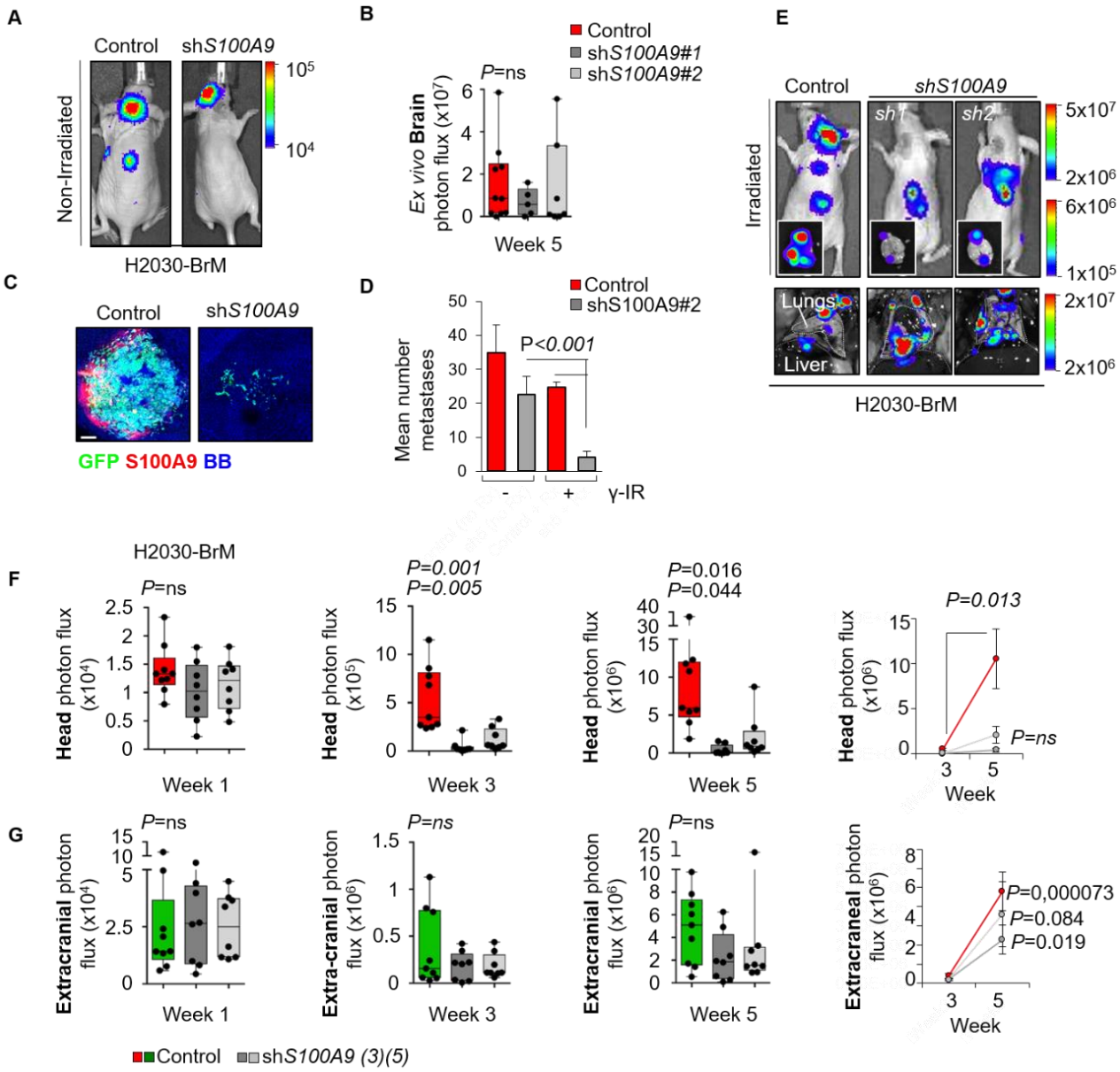

Figure 16. A. Representative bioluminescence images *in vivo* and *ex vivo*, 5 weeks after intracardiac injection. BLI is shown brain metastatic lesions in mice injected with H2030-BrM control cells (left image) and mice injected with a stable knockdown H2030-BrM cells lacking expression of *S100A9* (right image), in non-irradiated conditions. B. Quantification of *ex vivo* bioluminescence of control, shS100A9#1 and shS100A9#2 brains in non-irradiated conditions (Control n=10; shS100A9#1 n=5; shS100A9#2 n=5; P= ns.). C. Representative images of brains from irradiated mice, stained the nuclei with DAPI (blue), cancer cells identify by

GFP reporter (green) and S100A9 protein (red). D. Quantification of the mean number of brain metastasis lesions from H2030-BrM control cells and stable knockdown H2030-BrM cells lacking expression of *S100A9* in non-irradiated and irradiated brains (Non-irradiated: control n=2, mean 35± 8; shS100A9#2 n=2, mean 22.5 ± 5.5; irradiated: control n=5, mean 24.6± 1.66; shS100A9#2 n=5, mean 4.2 ± 1.77 ; P< 0.001). E. Representative bioluminescence images *in vivo* and *ex vivo* at 5 weeks after intracranial injection. BLI images shown *in vivo* control (left image), shS100A9#1 (central image) and shS100A9#2 mice (left image) from mice treated with 30Gy of radiation (protocol C, described before), respectively. As well as shown *ex vivo* bioluminescent images of brains and extracranial metastasis from control, shS100A9 #1 and #2 mice. F. and G. Quantification of *in vivo* bioluminescence of irradiated brains from control (left image), shS100A9#1 (central image) and shS100A9#2 mice (left image), respectively. (Week1: control n=9, mean 1.39E+04 ± 1.41E+03;shS100A9#1 n=8, mean 1.02E+04 ± 1.76E+03; shS100A9#2 n=8, mean 1.14E+04 ± 1.50E+03; P=ns; Week3: control mean 5.39E+05± 1.06E+05; shS100A9#1, 4.45E+04± 2.33E+04, P=0,001; shS100A9#2, mean 1.23E+05±3.83E+04; P=0,005; Week5: control, mean 1.05E+07± 3.28E+06; shS100A9#1, mean 4.47E+05± 2.14E+05, P=0,016; shS100A9#2, mean 2.10E+06± 9.48E+05, P=0,044)

Given that limited response to WBRT has been observed not only in patients with lung cancer but also in breast cancer brain metastases we wanted to know whether S100A9 could be also important in other model established from a different cancer type. Our hypothesis however proposed that S100A9 might be induced by aspects inherent to the process of colonization of cancer cells within the brain tissue environment.

Consequently, we performed an additional *in vivo* approach targeting *s100a9* in a mouse BrM model of triple negative breast cancer that we established (Figure 1). In addition to validate S100A9 in a different cancer type, this model also allows us to confirm our hypothesis in an immunocompetent host.

As previously described (Figure 4), we performed these experiments by intracranial injection. We confirmed that knockdown of *s100a9* does not impact

the ability of E0771-BrM cells to colonize the brain (data not shown). We sacrificed the animals at day 15 after intracranial injection and analyze the BLI. There were no differences in brain metastasis formation when we compared the irradiated control group with the knockdown (E0771-BrM control: n=10; E0771-BrM sh*s100a9*#43: n=10; E0771-BrM sh*s100a9*#43: n=10; P= 0,4981).

Subsequently, to test the role of S100A9 in radiation resistance on a syngeneic model, we inoculated a group of 10 mice per condition including shControl, sh*s100a9*#43 and sh*s100A9*#44 E0771-BrM cells. Three days after injection, once brain metastasis had been established (Mean bioluminescence value ± SEM: shControl= $2.68x10^4 \pm 9.23x10^3$, sh*s100a9*#43= $2.83x10^4 \pm 1.08x10^4$ or sh*s100a9*#44= $3.03x10^4 \pm 1.28x10^4$), we started the radiation protocol. Mice received a fractionated dose of 3Gy per day for 10 days to reach a total radiation dose of 30Gy at the end of treatment. Metastasis growth in the brain was evaluated by BLI images every 3 days. Fourteen days after intracranial injection, the animals were sacrificed, and the brains were analysed by BLI *ex vivo*.

We observed a clear trend of lower bioluminescence in the brains *s100a9* knockdowns when compared with the control group (E0771-BrM shControl: n=10; E0771-BrM sh*s100a9*#43: n=8; P= 0.0606; E0771-BrM sh*s100a9*#44: n=7; P= 0,1225).

Although we require to increase the number of mice, these results suggest that S100A9 is relevant for radiation resistance in an immunocompetent model.

Figure 17. Validation of S100A9 as a mediator of radiation resistance in a syngeneic model of brain metastasis.

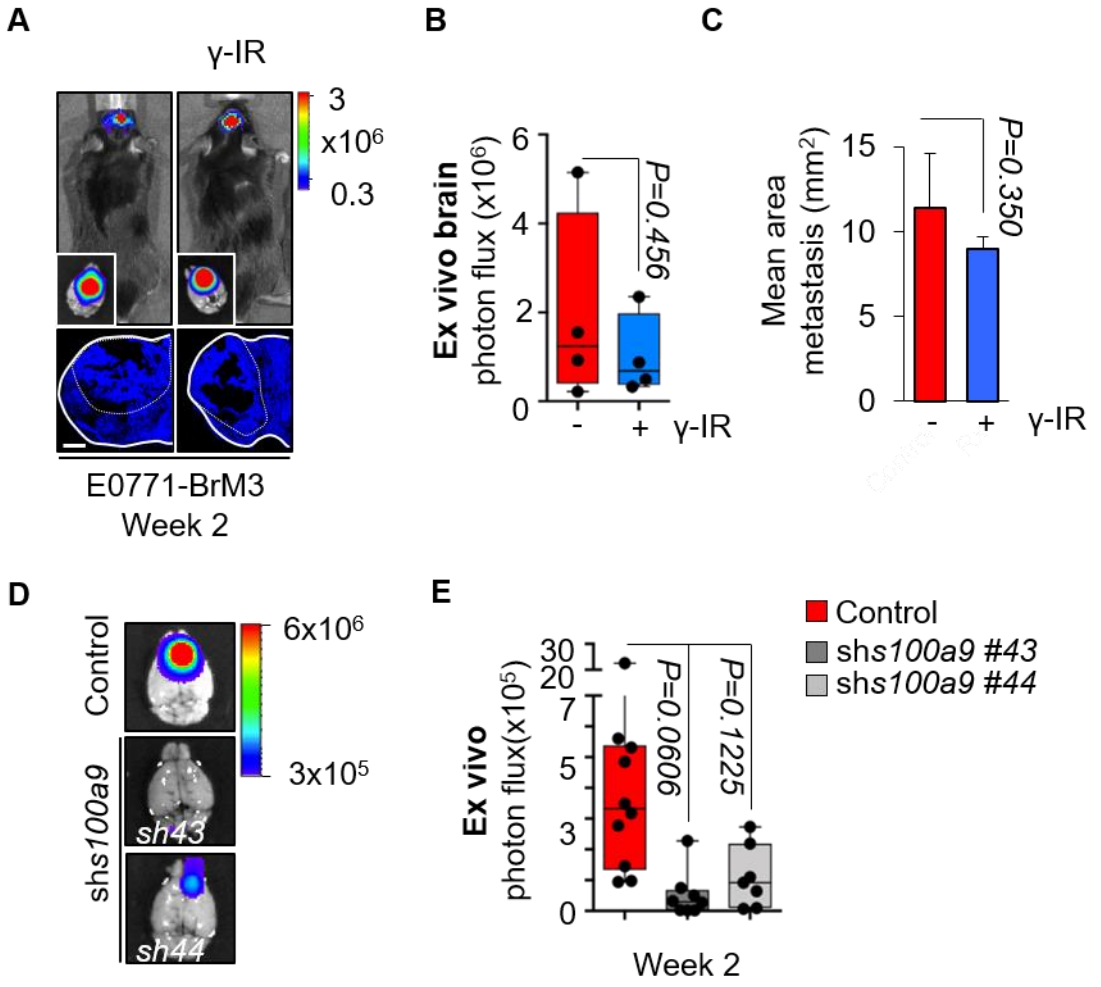

Figure 17. A. Representative bioluminescence images *in vivo* and *ex vivo* at day 14 after intracranial injection. Representative images of brains from non-irradiated and irradiated mice, respectively, stained with DAPI. White lines surround the brain metastatic lesion. B. Quantification of *ex vivo* bioluminescence of non-irradiated and irradiated brains (Non-irradiated n=4; irradiated n=4; P= 0.456). C. Quantification of the mean area of brain metastasis lesions from non-irradiated and irradiated brains (Non-irradiated n=4, mean 11.35 ± 3.25; irradiated n=4, mean area= 8.97 ± 0.695; P= 0.350). D. Representative BLI images of brains from shControl (top image) and shs100a9 #43 and #44 mice (bottom) at day 15 after intracranial injection. E. (E0771-BrM shControl: n=10; E0771-BrM shs*100a9*#43: n=8; P= 0,0606; E0771-BrM shs*100a9*#44: n=7; P=0.1225).

9. Targeting S100A9-dependent signalling pathway to sensitize brain metastases against radiotherapy.

9.1. RAGE but not TLR2 levels are increased upon radiation.

In order to elucidate the autocrine pathway responsible for S100A9-dependent radiation resistance phenotype that we have observed, we evaluated the expression of the different receptors of S100A9, including the receptor for advanced glycation end products (RAGE) and Toll-like receptors 2 (TLR2). We analysed their levels in different assays. Under non-irradiated conditions, we observed that there was no significant difference in the expression of neither *RAGE* nor *TLR2* neither in H2030-BrM cells growing under adherent conditions or H2030-BrM cells that growing inside the brain tissue (RAGE n=3, P=0,2098; TLR2 n=3, P= 0.3564).

In contrast, after irradiation we observed a significant increase in the expression of *RAGE* in H2030-BrM either under normal adherent conditions or when cells were cultured as oncospheres (Figure 17B). In contrast, this trend did not affect *TLR2*, suggesting that cancer cells might become sensitized to extracellular S100A9 levels after receiving radiation by increasing RAGE, which might act as a mechanism to further promote the acquired resistance (Figure 17A).

Figure 18. RAGE but not TLR2 levels are increased upon radiation

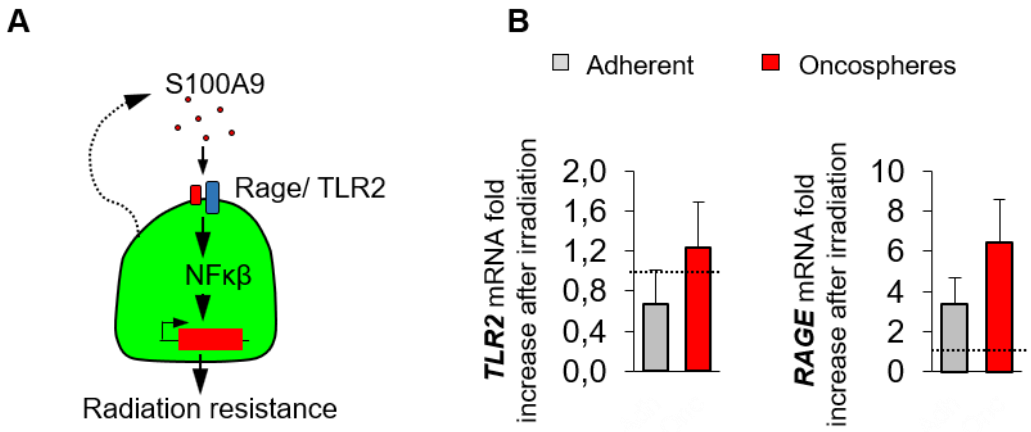

Figure 18. A. Schematic model of the pathway S100A9-TLR2/RAGE-NFκβ. B. Quantification of *TLR2* (right graph) and *RAGE* (left graph) fold increase of

expression comparing H2030-BrM adherent cells with H2030-BrM oncospheres on irradiated condition.

9.2. NFκβ pathway is induced upon radiation

To evaluate the downstream effects of S100A9-dependent pathways in BrM cells, we engineered H2030-BrM cells with a NFκβ pathway reporter (REF). Our previous data suggest that BrM cells cultured in particular conditions (i.e. oncospheres, organotypic cultures) increase the production of S100A9 but it is not until they receive radiation that they are sensitized due to the increase in the RAGE receptor. Consequently, H2030-BrM cells engineered with the NFκβ-mCherry reporter showed increased red fluorescence when plated in brain slices that were treated with radiation (single dose, 10Gy) (Figure 18) (Control n=11; Irradiated n=7; P= 0.0268).

Figure 19. NFκβ pathway is induced upon radiation

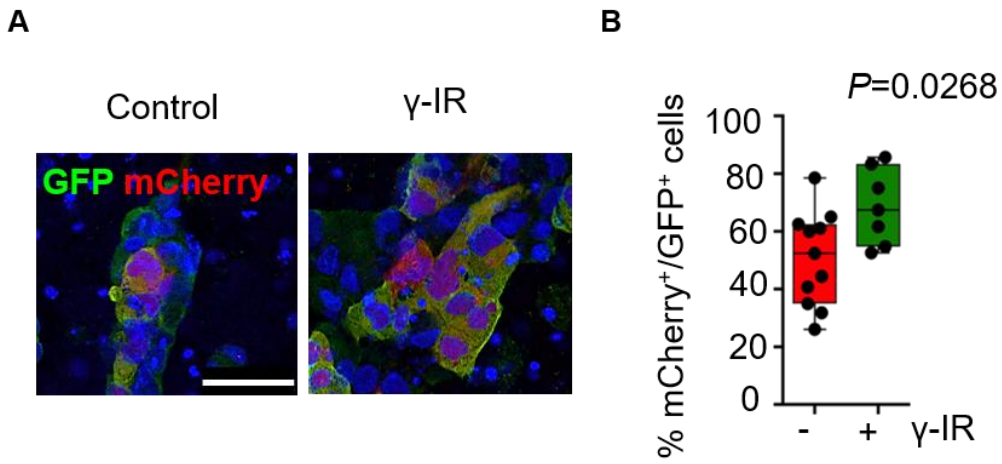

Figure 19. A. Representative images of immunofluorescence of H2030-BrM cells plaited on brain slices. Immunofluorescence images shown levels of expression of mCherry on H2030-BrM Non-irradiated (left image) and irradiated (right image). GFP: green fluorescence protein (green). mCherry (red). B. Quantification of percentage of number of mCherry positive cells per number of GFP positive cells.

9.3. Pharmacologic blockade of S100A9 pathway increases sensitivity to radiation

In order to functionally validate S100A9-RAGE and its downstream signalling activating NFκβ as part of radiation resistance, we tested two different pharmacological inhibitors. FPS-ZM1 is a BBB-permeable RAGE receptor inhibitor which has been shown to be safe in the clinical setting (Sun *et al.*, 2012; Qu *et al.*, 2019). Bay-117082 is an IKK inhibitor which favours NFκβ sequestration and loss of its transcriptional activity (Pierce *et al.*, 1997; Kamthong and Wu, 2001). Given that RAGE is a known activator of NFκβ, we reasoned that inhibiting this pathway should mimic direct RAGE inhibition.

We tested these two inhibitors in organotypic brain cultures treated with radiation to evaluate whether resistance could be impaired (Figure 19A). BrM cells (H2030-BrM) were plated on top of normal brain slices and either FPS-ZM1 (10uM), Bay-117082 (50uM), or vehicle (DMSO) were added to the culture media. 18 hours after plating BrM cells, a single dose of radiation (10Gy) was applied to a group of experimental samples. BLI was acquired 72 hours post-irradiation and BrdU was added to the media 4 hours before fixation. Both bioluminescence (Figure 19B and E) and BrdU staining (Figure 19D and G) demonstrated decreased values when RAGE and Ικκ inhibitors were used combined with radiation (Figure 19C and F) (Non-irradiated + FPS-ZM1, n=14; Irradiated + FPS-ZM1, n=14; BLI values P= 0,027; BrdU+ cells P=0,035; Non-Irradiated + Bay11-7082, n= 12; Irradiated + Bay11-7082, n=12; BLI values P=0,04; BrdU+ cells P=0,014).

These results suggest that targeting S100A9 receptor RAGE and the downstream pathway NFκβ impairs radiation resistance in organotypic brain cultures.

Figure 20. Pharmacologic blockade of S100A9-RAGE-NFκβ pathway.

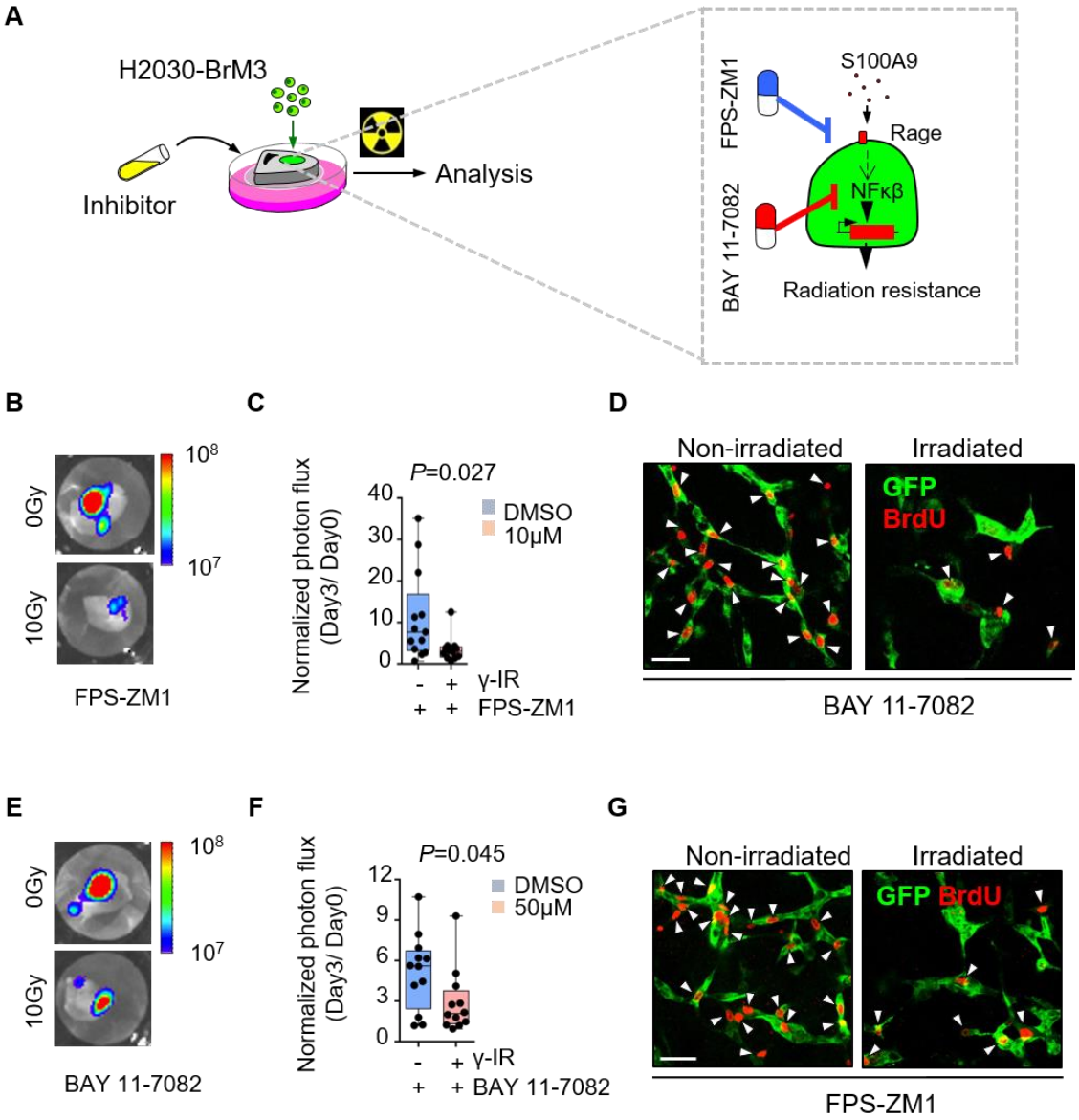

Figure 20 A. Schema of the experimental design including plating BrM cells on the brain slices (left schema), which mimics initial stages, treated with the inhibitor added to the culture media. A schematic model of the S100A9-RAGE-NFκβ pathway and the targets of the inhibitors (right scheme). B and E. Representative images of cultured brain slices for 3 days. BLI is shown in non-irradiated brain slices (top image) and irradiated slices (bottom image). B correspond to results after treatment with FPS-ZM1 while E correspond to brain slices treated with Bay 11-7082. C and F. Quantification of normalized photon flux in organotypic cultures comparing the conditions Non-irradiated plus inhibitor vs Irradiated plus inhibitor, with FPS-ZM1 (C) and Bay 11-7082 (F), respectively (Non-irradiated plus FPS-

ZM1 n=13, 11.20± 3.00; irradiated plus FPS-ZM1 n=12, 3.57 ± 3.06; P= 0.027; Non-irradiated plus Bay 11-7082 n=12, 5.17± 0.82; irradiated plus Bay 11-7082 n=12, 2.90± 0.68; P= 0.045). D. and G. Representative images of immunofluorescence of non-irradiated and irradiated organotypic cultures with H2030-BrM cells treated with FPS-ZM1 (D) or with Bay 11-7082 (G). GFP: green fluorescence protein (green). BrdU: bromodeoxyuridine (red). White arrows point the positive BrdU cells.

10. S100A9 in human brain metastasis

In order to confirm our findings in human samples we stained S100A9 in 26 brain metastasis samples from patients with lung cancer (8 samples, 30.77%) and breast cancer (18 samples, 69.23%). The expression level of S100A9 was scored from 0 (no S100A9 signal) to 3 (highest level) by an expert pathologist. We found that only 15% of the cases (4/26) were completely negative for S100A9 all the other samples were positive to S100A9 (22/26), suggesting that our findings might well be conserved in human, since most patients do not respond to radiotherapy.

10.1. Targeting S100A9-dependent pathway in human brain metastasis

In order to functionally validate the S100A9-RAGE-NFκβ pathway in human brain metastases, we performed patient-derived organotypic cultures (PDoC) from fresh neurosurgeries obtained through a collaboration with Hospital 12 de Octubre. Two lung adenocarcinoma brain metastases (Sample#1 and sample#2) were sectioned with the vibratome alive. Sections were plated on membranes and cultured for 3 days after receiving a single dose of radiation (10 Gy). BrdU was administered 4 hours before fixation. Sample#1 was scored as 0, meaning absence of S100A9, while sample#2 had a score of 1, indicating the presence of S100A9. Interestingly, while sample#1 showed a significant reduction of BrdU incorporation upon radiation treatment, sample#2 was not affected (Figure 20C) (non-irradiated without inhibitor treatment: n=11; irradiated without inhibitor treatment: n=9; P=0.0155), suggesting that resistance to radiation might correlate with the presence of S100A9 in human samples.

Given our previous data regarding the ability of FPS-ZM1 to radiosensitize S100A9-expressing brain metastatic cells, we applied the same strategy to sample#2 and observed that inhibition of RAGE blocked resistance to radiation (Figure 20C) (non-irradiated without inhibitor treatment: n=8; irradiated without inhibitor treatment: n=8; P=0.1440; non-irradiated plus inhibitor: n=8; P=0.6304; irradiated plus inhibitor n=9; P=0.0069),

Consequently, in agreement with our experimental models, the presence of S100A9 in PDoC correlates with resistance to radiation, which could be ameliorated by using the BBB-permeable RAGE inhibitor FPS-ZM1. Although these results are encouraging, additional samples are needed in order to provide more solid evidence in human tissue.

Figure 21. Validation of S100A9 levels in human samples.

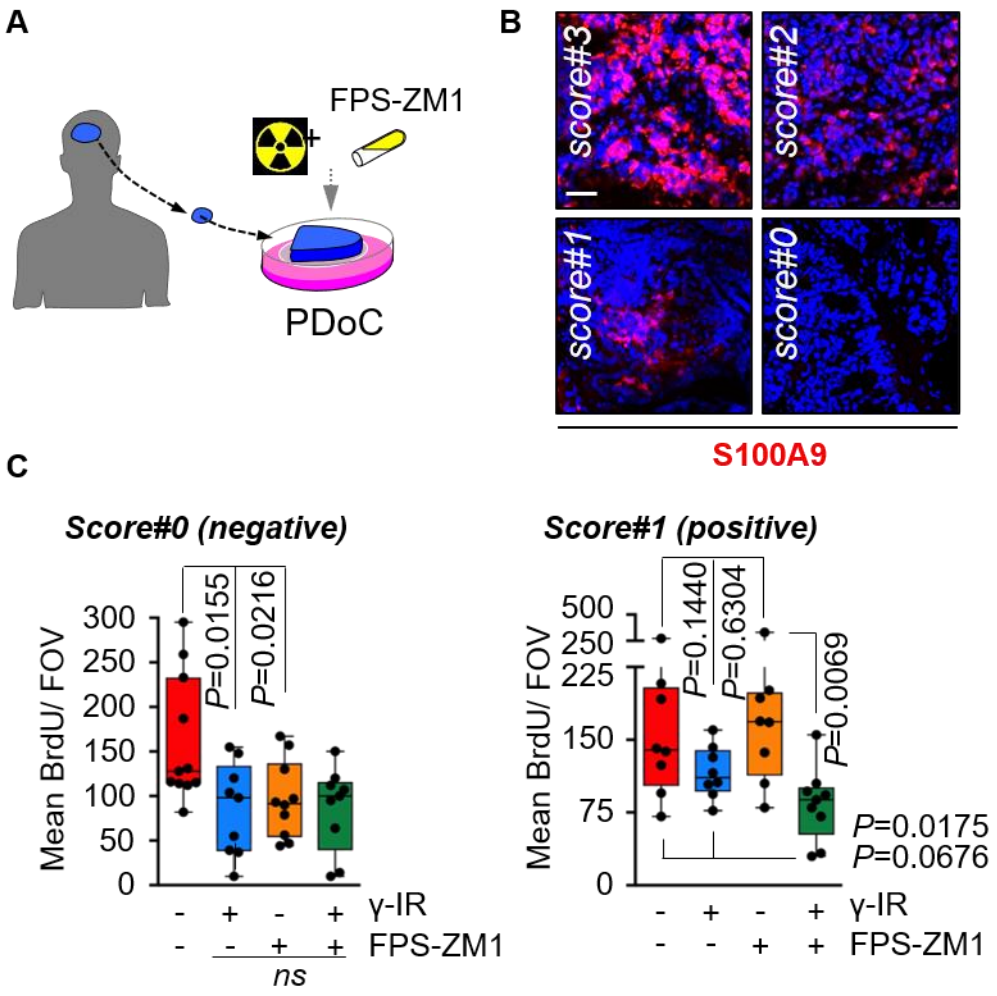

Figure 21. A. Schema of the experimental design of patient derived organotypic cultures (PDoC). B. Representative images of immunofluorescence of four different samples of brain metastasis tissue from four different patients. Dapi: staining the cell nuclei (blue). S100A9 protein expression (red). C. Quantification of mean of BrdU per field of view in organotypic cultures comparing four groups of conditions: non-irradiated without inhibitor treatment (red), irradiated without inhibitor treatment (blue), non-irradiated plus inhibitor (orange), irradiated plus inhibitor (green). On the left we can see graph of sample with S100A9 expression negative (score 0, left graph) (Mean BrdU positive cells/FOV ± SEM: non-irradiated without inhibitor treatment: n=11, 166± 20.63; irradiated without inhibitor treatment: n=9, 47.8± 9.65; P=0.0155; non-irradiated plus inhibitor: n=10, 99± 11.54; P=0.0216; irradiated plus inhibitor n=9, 82.25± 13.58), on the right graph we analysed the results of sample with S100A9 low expression (score1) (Mean BrdU positive cells/FOV ± SEM: non-irradiated without inhibitor treatment: n=8, 155.37± 21.81; irradiated without inhibitor treatment: n=8, 116.38± 8.94; P=0.1440; non-irradiated plus inhibitor: n=8, 172.88± 25.14; P=0.6304; irradiated plus inhibitor n=9, 83.56± 11.89; P=0.0069),

Discussion

Discussion

In the work described here, I have generated a novel, syngeneic, immunocompetent model of breast cancer brain metastasis (E0771-BrM). This model is suitable for *in vivo*, *ex vivo*, and *in vitro* modelling of brain metastasis. Due to a limited number of experimental models that allow studying brain metastasis in an immunocompetent background and the importance of the immune system in cancer including brain tumours, we are confident that this new model will be well-received by other researchers of the field. In fact, we have already distributed this cell line with various national and international laboratories interested in brain metastasis, evidencing the importance of this new model for the field.

With respect to the central question of my thesis, we have demonstrated that despite ubiquitous *in vitro* radiation sensitivity, BrM models are largely radiation-resistant *in vivo*. Although the result was unexpected regarding the sharp contrast in the phenotype between these experimental conditions, several clinical observations have claimed that the benefits of whole brain radiation therapy (WBRT) is limited and consequently, the overall survival of patients does not increase after treatment (Kocher *et al.*, 2011). In conclusion, *in vivo* irradiation of established metastases from lung or breast cancer, using a protocol similar to the current standard of care, has no significant effect on metastatic progression or survival *in vivo* in experimental BrM models. This finding seems independent of the primary source or the metastasis as well as of the acquired immune system.

We were able to recapitulate the radiation resistance observed *in vivo* using *ex vivo* organotypic brain cultures, co-cultures with glial cells or simply by growing cancer cells as oncospheres. With these different culture techniques, we have been able to interrogate in an unbiased way potential mediators involved in radiation resistance in brain metastasis. Given the transient character of the resistance that we have found, we propose that it has a strong dependence on the context and thus might be highly influenced by the microenvironment. In addition, we have demonstrated that *in vitro*/ *ex vivo* approaches are useful to interrogate therapeutic resistance in brain metastasis. In fact, we were able to

observe that the levels of DNA damage induced by gamma irradiation in cancer cells cultures *in vitro* and *ex vivo* under resistance conditions were recovered as fast as *in vivo*, which confirms the existance of a molecular rationale behind the resistance phenotype. We hypothesize that these findings suggest an enhanced ability to repair DNA under these experimental conditions.

However, none of our experimental designs nor the data we have generated were detailed enough for claiming any stronger than this about the molecular mechanisms that could be responsible for this phenotype. Future studies should clarify the molecular mediators of the increased efficiency of DNA repair in brain metastasis.

Our main contribution to the mechanism behind radiation resistance in brain metastasis was the identification of a ten-gene signature. Within this signature we identified S100A9, an inducer of the NFκβ pathway, as a target of particular interest since it was represented in all resistance surrogates. Given that the implication of NFκβ in radiation resistance is well documented and includes primary brain tumours (Bhat *et al.*, 2013) we became interested to functionally validate this finding.

We provided the evidence that S100A9 is indeed mediating radiation resistance of brain metastasis *in vivo* in two models of brain metastasis and validated this finding in human samples.

In view of our findings, we propose a model depicted in Figure 22. In brief, the levels of inflammatory cytokines such as TNFα would dramatically increase within the brain microenvironment following the colonization by cancer cells (Seike *et al.*, 2011; Xing *et al.*, 2015). High levels of TNFα activate TNFα receptor 1 (we found in this work the expression of this receptor in our BrM cells, data not shown) present in brain metastatic cancer cells as well as in other cells of the microenvironment. It is known that activation of the TNFR1 leads to the induction of *S100A9* expression (Bianchi, Giambanco and Donato, 2010). S100A9 is strongly induced in metastases. Once the cancer cells are irradiated, RAGE receptor expression increases. Thus, after irradiating cancer cells in the brain there is an increase in both the ligand (S100A9) and the receptor (RAGE). Therefore, the combination would lead to the increased activation of the S100A9-

RAGE-NFκβ pathway. The NFκβ pathway might further increase the expression of *S100A9* through a positive feedback loop but also drive the expression of other molecules known to be protective against radiation, such as *CEBPB* (Du *et al.*, 2019). As a result of this process, brain metastatic cancer cells would become resistant to radiation.

Looking for options to translate our findings into better opportunities for cancer patients we identified a potential radiosensitizer. FPS-ZM1, a BBB-permeable RAGE antagonist (H. Wang *et al.*, 2018) that has been used in experimental treatments for Alzheimer (Deane *et al.*, 2012; Walker *et al.*, 2015), was able to increase the sensitivity to radiation in brain metastatic cancer cells. Due to our positive results with this inhibitor *ex vivo* in mice and human patients brain metastases we speculate that the use of FPS-ZM1 as a radiosensitizer could be useful for patients with radiation-resistant brain metastasis, thus high for S100A9 levels. However, the *in vivo* validation using experimental brain metastasis models remains to be tested.

Besides the therapeutic promise of inhibiting the S100A9 pathway through RAGE to restore radiation sensitivity, we believe that S100A9 itself could be used as a potential radiation response biomarker. Preliminary results of this thesis with a small retrospective cohort of patients showed a limited patients with low levels of S100A9, which might explain the frequent lack of response in patients with brain metastasis to this treatment modality. Even more, we were able to compare a sample without S100A9 and observed that, as hypothesized, response to radiotherapy was higher compared to another sample rich in S100A9 levels. Therefore, we believe that it is worthwhile to explore the potential of S100A9 as a biomarker of response to radiation in order to avoid the indiscriminate use of radiotherapy to patients that potentially will be bad responders. In fact, brain radiation is associated with significant comorbidities, including cognitive decline, loss of memory, and others, so it would be beneficial to identify those patients who are more likely to benefit from it. Despite the promising results in human samples, it is appropriate to admit that the number of specimens is very limited and a more dedicated efforts to validate these finding in human samples is warranted.

Figure 22. Hypothetical model of the mechanism of brain metastatic cells radiation resistance.

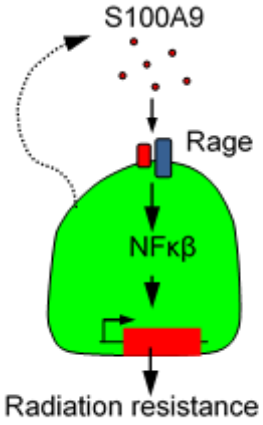

Conclusions

Conclusions

1. Brain metastatic cell lines are sensitive to radiation *in vitro* but resistant *in vivo;*
2. WBRT does not impact the progression of the disease;
3. Brain metastatic cells grown *in vitro* as oncospheres or co-cultures with glial cells increase resistance to radiotherapy;
4. Brain metastatic cells cultured *ex vivo* in organotypic cultures are resistant to radiation;
5. We have identified a transcriptomic signature enriched in various brain metastasis models of radiation resistance;
6. Targeting S100A9 decreases the resistance of brain metastasis to radiation both *ex vivo* and *in vivo*;
7. S100A9-dependent radiation resistance could be blocked by BBB-permeable RAGE inhibitor FPS-ZM1;
8. We provide some evidence that S100A9-dependent radioresistance is mediated by NFκβ;
9. We suggest the possibility that S100A9 could be used as a predictive biomarker to personalize the use of radiotherapy.

References

References

Achrol, A. S. *et al.* (2019) ‘Brain metastases.’, *Nature reviews. Disease primers*. England, 5(1), p. 5. doi: 10.1038/s41572-018-0055-y.

Anderson, E. S. *et al.* (2017) ‘Melanoma brain metastases treated with stereotactic radiosurgery and concurrent pembrolizumab display marked regression; efficacy and safety of combined treatment.’, *Journal for immunotherapy of cancer*. England, 5(1), p. 76. doi: 10.1186/s40425-017-0282-x.

Ansari, J. *et al.* (2009) ‘Role of tyrosine kinase inhibitors in lung cancer.’, *Anti-cancer agents in medicinal chemistry*. Netherlands, 9(5), pp. 569–575. doi: 10.2174/187152009788451879.

Arvanitis, C. D., Ferraro, G. B. and Jain, R. K. (2019) ‘The blood–brain barrier and blood–tumour barrier in brain tumours and metastases’, *Nature Reviews Cancer*. doi: 10.1038/s41568-019-0205-x.

Arvold, N. D. *et al.* (2016) ‘Updates in the management of brain metastases.’, *Neuro-oncology*. England, 18(8), pp. 1043–1065. doi: 10.1093/neuonc/now127.

Badr, C. E. *et al.* (2009) ‘Real-time monitoring of nuclear factor kappaB activity in cultured cells and in animal models.’, *Molecular imaging*. United States, 8(5), pp. 278–290.

Bargagli, E. *et al.* (2011) ‘Calgranulin B (S100A9/MRP14): A key molecule in idiopathic pulmonary fibrosis?’, *Inflammation*, 34, pp. 85–91. doi: 10.1007/s10753-010-9210-7.

Barnholtz-Sloan, J. S. *et al.* (2004) ‘Incidence proportions of brain metastases in patients diagnosed (1973 to 2001) in the Metropolitan Detroit Cancer Surveillance System.’, *Journal of clinical oncology : official journal of the American Society of Clinical Oncology*. United States, 22(14), pp. 2865–2872. doi: 10.1200/JCO.2004.12.149.

Bergenfelz, C. *et al.* (2015) ‘S100A9 expressed in ER−PgR− breast cancers

induces inflammatory cytokines and is associated with an impaired overall survival', *British Journal of Cancer*, 113(8), pp. 1234–1243. doi: 10.1038/bjc.2015.346.

Berghoff, A. S. *et al.* (2016) 'Descriptive statistical analysis of a real life cohort of 2419 patients with brain metastases of solid cancers.', *ESMO open*. England, 1(2), p. e000024. doi: 10.1136/esmoopen-2015-000024.

Bhat, K. P. L. *et al.* (2013) 'Mesenchymal differentiation mediated by NF-kappaB promotes radiation resistance in glioblastoma.', *Cancer cell*. United States, 24(3), pp. 331–346. doi: 10.1016/j.ccr.2013.08.001.

Bianchi, R., Giambanco, I. and Donato, R. (2010) 'S100B/RAGE-dependent activation of microglia via NF-kappaB and AP-1 Co-regulation of COX-2 expression by S100B, IL-1beta and TNF-alpha.', *Neurobiology of aging*. United States, 31(4), pp. 665–677. doi: 10.1016/j.neurobiolaging.2008.05.017.

Bos, P. D. *et al.* (2009) 'Genes that mediate breast cancer metastasis to the brain.', *Nature*. England, 459(7249), pp. 1005–1009. doi: 10.1038/nature08021.

Brastianos, H. C., Cahill, D. P. and Brastianos, P. K. (2015) 'Systemic therapy of brain metastases.', *Current neurology and neuroscience reports*. United States, 15(2), p. 518. doi: 10.1007/s11910-014-0518-9.

Brastianos, P. K. *et al.* (2015) 'Genomic Characterization of Brain Metastases Reveals Branched Evolution and Potential Therapeutic Targets', *Cancer Discovery*, 5(11), pp. 1164 LP – 1177. doi: 10.1158/2159-8290.CD-15-0369.

Brown, P. D. *et al.* (2016) 'Effect of Radiosurgery Alone vs Radiosurgery With Whole Brain Radiation Therapy on Cognitive Function in Patients With 1 to 3 Brain Metastases: A Randomized Clinical Trial', *JAMA*, 316(4), pp. 401–409. doi: 10.1001/jama.2016.9839.

Celià-Terrassa, T. and Kang, Y. (2016) 'Distinctive properties of metastasis-initiating cells.', *Genes & development*, 30(8), pp. 892–908. doi: 10.1101/gad.277681.116.

Chang, K.-A., Kim, H. J. and Suh, Y.-H. (2012) 'The role of S100a9 in the pathogenesis of Alzheimer's disease: the therapeutic effects of S100a9 knockdown or knockout.', *Neuro-degenerative diseases*. Switzerland, 10(1–4), pp. 27–29. doi: 10.1159/000333781.

Chen, Q. *et al.* (2016) 'Carcinoma-astrocyte gap junctions promote brain metastasis by cGAMP transfer.', *Nature*. England, 533(7604), pp. 493–498. doi: 10.1038/nature18268.

Chen, W. *et al.* (2018) 'Organotropism: new insights into molecular mechanisms of breast cancer metastasis', *npj Precision Oncology*, 2(1), p. 4. doi: 10.1038/s41698-018-0047-0.

Cho, Y. J. *et al.* (2019) 'Clinical analysis of patients with skeletal metastasis of lung cancer.', *BMC cancer*, 19(1), p. 303. doi: 10.1186/s12885-019-5534-3.

Contreras-Zarate, M. J. *et al.* (2019) 'Estradiol induces BDNF/TrkB signaling in triple-negative breast cancer to promote brain metastases.', *Oncogene*. England. doi: 10.1038/s41388-019-0756-z.

Davies, M. A. *et al.* (2017) 'Dabrafenib plus trametinib in patients with BRAF(V600)-mutant melanoma brain metastases (COMBI-MB): a multicentre, multicohort, open-label, phase 2 trial.', *The Lancet. Oncology*. England, 18(7), pp. 863–873. doi: 10.1016/S1470-2045(17)30429-1.

Deane, R. *et al.* (2012) 'A multimodal RAGE-specific inhibitor reduces amyloid beta-mediated brain disorder in a mouse model of Alzheimer disease.', *The Journal of clinical investigation*. United States, 122(4), pp. 1377–1392. doi: 10.1172/JCI58642.

Du, Q. *et al.* (2019) 'PGC1alpha/CEBPB/CPT1A axis promotes radiation resistance of nasopharyngeal carcinoma through activating fatty acid oxidation.', *Cancer science*. England, 110(6), pp. 2050–2062. doi: 10.1111/cas.14011.

Dummer, R. *et al.* (2014) 'Vemurafenib in patients with BRAF(V600) mutation-positive melanoma with symptomatic brain metastases: final results of an open-label pilot study.', *European journal of cancer (Oxford, England : 1990)*. England,

50(3), pp. 611–621. doi: 10.1016/j.ejca.2013.11.002.

Er, E. E. *et al.* (2018) 'Pericyte-like spreading by disseminated cancer cells activates YAP and MRTF for metastatic colonization.', *Nature cell biology*. England, 20(8), pp. 966–978. doi: 10.1038/s41556-018-0138-8.

Ferlay, J. *et al.* (2015) 'Cancer incidence and mortality worldwide: sources, methods and major patterns in GLOBOCAN 2012.', *International journal of cancer*. United States, 136(5), pp. E359-86. doi: 10.1002/ijc.29210.

Fox, B. D. *et al.* (2011) 'Epidemiology of metastatic brain tumors.', *Neurosurgery clinics of North America*. United States, 22(1), pp. 1–6, v. doi: 10.1016/j.nec.2010.08.007.

Freedman, R. A. *et al.* (2016) 'Translational Breast Cancer Research Consortium (TBCRC) 022: A Phase II Trial of Neratinib for Patients With Human Epidermal Growth Factor Receptor 2-Positive Breast Cancer and Brain Metastases.', *Journal of clinical oncology : official journal of the American Society of Clinical Oncology*. United States, 34(9), pp. 945–952. doi: 10.1200/JCO.2015.63.0343.

Freedman, R. A. *et al.* (2017) 'TBCRC 022: Phase II trial of neratinib + capecitabine for patients (Pts) with human epidermal growth factor receptor 2 (HER2+) breast cancer brain metastases (BCBM).', *Journal of Clinical Oncology*. American Society of Clinical Oncology, 35(15_suppl), p. 1005. doi: 10.1200/JCO.2017.35.15_suppl.1005.

Gebhardt, C. *et al.* (2006) 'S100A8 and S100A9 in inflammation and cancer.', *Biochemical pharmacology*. England, 72(11), pp. 1622–1631. doi: 10.1016/j.bcp.2006.05.017.

Goldberg, S. B. *et al.* (2016) 'Pembrolizumab for patients with melanoma or non-small-cell lung cancer and untreated brain metastases: early analysis of a non-randomised, open-label, phase 2 trial.', *The Lancet. Oncology*. England, 17(7), pp. 976–983. doi: 10.1016/S1470-2045(16)30053-5.

Grommes, C. *et al.* (2011) '"Pulsatile" high-dose weekly erlotinib for CNS metastases from EGFR mutant non-small cell lung cancer.', *Neuro-oncology*.

England, 13(12), pp. 1364–1369. doi: 10.1093/neuonc/nor121.

Gruden, M. A. *et al.* (2016) 'The misfolded pro-inflammatory protein S100A9 disrupts memory via neurochemical remodelling instigating an Alzheimer's disease-like cognitive deficit', *Behavioural Brain Research*, 306, pp. 106–116. doi: https://doi.org/10.1016/j.bbr.2016.03.016.

Hall, W. A. *et al.* (2000) 'Long-term survival with metastatic cancer to the brain.', *Medical oncology (Northwood, London, England)*. United States, 17(4), pp. 279–286.

Hanahan, D. and Weinberg, R. A. (2000) 'The hallmarks of cancer.', *Cell*. United States, 100(1), pp. 57–70. doi: 10.1016/s0092-8674(00)81683-9.

Harbeck, N. *et al.* (2019) 'Breast cancer', *Nature Reviews Disease Primers*, 5(1), p. 66. doi: 10.1038/s41572-019-0111-2.

Hartgerink, D. *et al.* (2018) 'Stereotactic Radiosurgery in the Management of Patients With Brain Metastases of Non-Small Cell Lung Cancer: Indications, Decision Tools and Future Directions ', *Frontiers in Oncology* , p. 154. Available at: https://www.frontiersin.org/article/10.3389/fonc.2018.00154.

Horvath, I. *et al.* (2016) 'Pro-inflammatory S100A9 Protein as a Robust Biomarker Differentiating Early Stages of Cognitive Impairment in Alzheimer's Disease', *ACS Chemical Neuroscience*. American Chemical Society, 7(1), pp. 34–39. doi: 10.1021/acschemneuro.5b00265.

Jilaveanu, L. B. *et al.* (2015) 'PLEKHA5 as a Biomarker and Potential Mediator of Melanoma Brain Metastasis', *Clinical Cancer Research*, 21(9), pp. 2138 LP – 2147. doi: 10.1158/1078-0432.CCR-14-0861.

Johnstone, C. N. *et al.* (2015) 'Functional and molecular characterisation of EO771.LMB tumours, a new C57BL/6-mouse-derived model of spontaneously metastatic mammary cancer.', *Disease models & mechanisms*. England, 8(3), pp. 237–251. doi: 10.1242/dmm.017830.

Jonasson, L. *et al.* (2017) 'Stress-induced release of the S100A8/A9 alarmin is

elevated in coronary artery disease patients with impaired cortisol response', *Scientific Reports*, 7(1), p. 17545. doi: 10.1038/s41598-017-17586-6.

Jovanovic, V. *et al.* (2018) 'A155 MOLECULAR LANDSCAPE OF ULCERATIVE COLITIS AND CROHN'S DISEASE IS CONSERVED ', *Journal of the Canadian Association of Gastroenterology*, 1(suppl_1), pp. 267–268. doi: 10.1093/jcag/gwy008.156.

Kaidar-Person, O., Bar-Sela, G. and Person, B. (2011) 'The two major epidemics of the twenty-first century: obesity and cancer.', *Obesity surgery*. United States, 21(11), pp. 1792–1797. doi: 10.1007/s11695-011-0490-2.

Kamthong, P. J. and Wu, M. (2001) 'Inhibitor of nuclear factor-kappaB induction by cAMP antagonizes interleukin-1-induced human macrophage-colony-stimulating-factor expression.', *The Biochemical journal*, 356(Pt 2), pp. 525–530. doi: 10.1042/0264-6021:3560525.

Khanna, C. and Hunter, K. (2005) 'Modeling metastasis in vivo.', *Carcinogenesis*. England, 26(3), pp. 513–523. doi: 10.1093/carcin/bgh261.

Klein, C. A. (2009) 'Parallel progression of primary tumours and metastases.', *Nature reviews. Cancer*. England, pp. 302–312. doi: 10.1038/nrc2627.

Kocher, M. *et al.* (2011) 'Adjuvant whole-brain radiotherapy versus observation after radiosurgery or surgical resection of one to three cerebral metastases: results of the EORTC 22952-26001 study.', *Journal of clinical oncology : official journal of the American Society of Clinical Oncology*, 29(2), pp. 134–141. doi: 10.1200/JCO.2010.30.1655.

Krause, M. *et al.* (2017) 'Cancer stem cells: Radioresistance, prediction of radiotherapy outcome and specific targets for combined treatments.', *Advanced drug delivery reviews*. Netherlands, 109, pp. 63–73. doi: 10.1016/j.addr.2016.02.002.

Lambert, A. W., Pattabiraman, D. R. and Weinberg, R. A. (2017) 'Emerging Biological Principles of Metastasis.', *Cell*. United States, 168(4), pp. 670–691. doi: 10.1016/j.cell.2016.11.037.

Leanderson, T., Liberg, D. and Ivars, F. (2015) 'S100A9 as a Pharmacological Target Molecule in Inflammation and Cancer.', *Endocrine, metabolic & immune disorders drug targets*. United Arab Emirates, 15(2), pp. 97–104. doi: 10.2174/1871530315666150316123854.

Leder, K. *et al.* (2014) 'Mathematical modeling of PDGF-driven glioblastoma reveals optimized radiation dosing schedules.', *Cell*. United States, 156(3), pp. 603–616. doi: 10.1016/j.cell.2013.12.029.

van Lent, P. L. E. M. *et al.* (2008) 'Myeloid-related proteins S100A8/S100A9 regulate joint inflammation and cartilage destruction during antigen-induced arthritis', *Annals of the Rheumatic Diseases*, 67(12), pp. 1750 LP – 1758. doi: 10.1136/ard.2007.077800.

Li, B. *et al.* (2013) 'Elevated PLGF contributes to small-cell lung cancer brain metastasis.', *Oncogene*. England, 32(24), pp. 2952–2962. doi: 10.1038/onc.2012.313.

Lim, S. Y. *et al.* (2016) 'Tumor-infiltrating monocytes/macrophages promote tumor invasion and migration by upregulating S100A8 and S100A9 expression in cancer cells', *Oncogene*, 35(44), pp. 5735–5745. doi: 10.1038/onc.2016.107.

Liu, Q. *et al.* (2017) 'Factors involved in cancer metastasis: a better understanding to "seed and soil" hypothesis', *Molecular Cancer*, 16(1), p. 176. doi: 10.1186/s12943-017-0742-4.

Liu, Y. and Cao, X. (2016) 'Characteristics and Significance of the Pre-metastatic Niche', *Cancer Cell*, 30(5), pp. 668–681. doi: https://doi.org/10.1016/j.ccell.2016.09.011.

Long, G. V *et al.* (2012) 'Dabrafenib in patients with Val600Glu or Val600Lys BRAF-mutant melanoma metastatic to the brain (BREAK-MB): a multicentre, open-label, phase 2 trial.', *The Lancet. Oncology*. England, 13(11), pp. 1087–1095. doi: 10.1016/S1470-2045(12)70431-X.

Lorenz, E. *et al.* (2008) 'Different expression ratio of S100A8/A9 and S100A12 in acute and chronic lung diseases', *Respiratory Medicine*, 102(4), pp. 567–573.

doi: https://doi.org/10.1016/j.rmed.2007.11.011.

Marchan, E. M. *et al.* (2018) 'Postoperative Cavity Stereotactic Radiosurgery for Brain Metastases.', *Frontiers in oncology*, 8, p. 342. doi: 10.3389/fonc.2018.00342.

Markowitz, J. and Carson, W. E. 3rd (2013) 'Review of S100A9 biology and its role in cancer.', *Biochimica et biophysica acta*. Netherlands, 1835(1), pp. 100–109. doi: 10.1016/j.bbcan.2012.10.003.

Martin, A. M. *et al.* (2017) 'Brain Metastases in Newly Diagnosed Breast Cancer: A Population-Based Study.', *JAMA oncology*. United States, 3(8), pp. 1069–1077. doi: 10.1001/jamaoncol.2017.0001.

Martinez-Aranda, A. *et al.* (2013) 'Development of a preclinical therapeutic model of human brain metastasis with chemoradiotherapy.', *International journal of molecular sciences*. Switzerland, 14(4), pp. 8306–8327. doi: 10.3390/ijms14048306.

Martínez-Aranda, A. *et al.* (2015) 'FN14 and GRP94 expression are prognostic/predictive biomarkers of brain metastasis outcome that open up new therapeutic strategies.', *Oncotarget*, 6(42), pp. 44254–44273. doi: 10.18632/oncotarget.5471.

Massague, J., Batlle, E. and Gomis, R. R. (2017) 'Understanding the molecular mechanisms driving metastasis.', *Molecular oncology*. United States, pp. 3–4. doi: 10.1002/1878-0261.12024.

McArthur, G. A. *et al.* (2017) 'Vemurafenib in metastatic melanoma patients with brain metastases: an open-label, single-arm, phase 2, multicentre study.', *Annals of oncology : official journal of the European Society for Medical Oncology*. England, 28(3), pp. 634–641. doi: 10.1093/annonc/mdw641.

McTyre, E. R. *et al.* (2017) 'Predictors of neurologic and nonneurologic death in patients with brain metastasis initially treated with upfront stereotactic radiosurgery without whole-brain radiation therapy.', *Neuro-oncology*. England, 19(4), pp. 558–566. doi: 10.1093/neuonc/now184.

Melero, I. *et al.* (2015) 'Evolving synergistic combinations of targeted immunotherapies to combat cancer', *Nature Reviews Cancer*, 15(8), pp. 457–472. doi: 10.1038/nrc3973.

Mulvenna, P. *et al.* (2016) 'Dexamethasone and supportive care with or without whole brain radiotherapy in treating patients with non-small cell lung cancer with brain metastases unsuitable for resection or stereotactic radiotherapy (QUARTZ): results from a phase 3, non-inferiority, ', *Lancet (London, England)*. England, 388(10055), pp. 2004–2014. doi: 10.1016/S0140-6736(16)30825-X.

Nacken, W. *et al.* (2003) 'S100A9/S100A8: Myeloid representatives of the S100 protein family as prominent players in innate immunity.', *Microscopy research and technique*. United States, 60(6), pp. 569–580. doi: 10.1002/jemt.10299.

Nardin, C. *et al.* (2018) 'Tolerance and outcomes of stereotactic radiosurgery combined with anti-programmed cell death-1 (pembrolizumab) for melanoma brain metastases.', *Melanoma research*. England, 28(2), pp. 111–119. doi: 10.1097/CMR.0000000000000413.

Nayak, L., Lee, E. Q. and Wen, P. Y. (2012) 'Epidemiology of brain metastases.', *Current oncology reports*. United States, 14(1), pp. 48–54. doi: 10.1007/s11912-011-0203-y.

Neal, M. T. *et al.* (2014) 'Predictors of survival, neurologic death, local failure, and distant failure after gamma knife radiosurgery for melanoma brain metastases.', *World neurosurgery*. United States, 82(6), pp. 1250–1255. doi: 10.1016/j.wneu.2013.02.025.

Nedjadi, T. *et al.* (2018) 'S100A8 and S100A9 proteins form part of a paracrine feedback loop between pancreatic cancer cells and monocytes', *BMC Cancer*, 18(1), p. 1255. doi: 10.1186/s12885-018-5161-4.

Nguyen, D. X. *et al.* (2009) 'WNT/TCF signaling through LEF1 and HOXB9 mediates lung adenocarcinoma metastasis.', *Cell*. United States, 138(1), pp. 51–62. doi: 10.1016/j.cell.2009.04.030.

Nguyen, D. X., Bos, P. D. and Massague, J. (2009) 'Metastasis: from

dissemination to organ-specific colonization.', *Nature reviews. Cancer*. England, 9(4), pp. 274–284. doi: 10.1038/nrc2622.

Nieder, C. *et al.* (2011) 'Presentation, patterns of care, and survival in patients with brain metastases: what has changed in the last 20 years?', *Cancer*. United States, 117(11), pp. 2505–2512. doi: 10.1002/cncr.25707.

Nys, G. *et al.* (2019) 'Targeted proteomics reveals serum amyloid A variants and alarmins S100A8-S100A9 as key plasma biomarkers of rheumatoid arthritis', *Talanta*, 204, pp. 507–517. doi: https://doi.org/10.1016/j.talanta.2019.06.044.

Obenauf, A. C. and Massagué, J. (2015) 'Surviving at a Distance: Organ-Specific Metastasis.', *Trends in cancer*, 1(1), pp. 76–91. doi: 10.1016/j.trecan.2015.07.009.

Patchell, R. A. (1995) 'Metastatic brain tumors.', *Neurologic clinics*. United States, 13(4), pp. 915–925.

Pavlidis, P. *et al.* (2016) 'Early change in faecal calprotectin predicts primary non-response to anti-TNFα therapy in Crohn's disease', *Scandinavian Journal of Gastroenterology*. Taylor & Francis, 51(12), pp. 1447–1452. doi: 10.1080/00365521.2016.1205128.

Peinado, H. *et al.* (2017) 'Pre-metastatic niches: organ-specific homes for metastases', *Nature Reviews Cancer*, 17. doi: 10.1038/nrc.2017.6.

Pierce, J. W. *et al.* (1997) 'Novel inhibitors of cytokine-induced IkappaBalpha phosphorylation and endothelial cell adhesion molecule expression show anti-inflammatory effects in vivo.', *The Journal of biological chemistry*. United States, 272(34), pp. 21096–21103. doi: 10.1074/jbc.272.34.21096.

Priego, N. *et al.* (2018) 'STAT3 labels a subpopulation of reactive astrocytes required for brain metastasis.', *Nature medicine*. United States, 24(7), p. 1481. doi: 10.1038/s41591-018-0108-5.

Psaila, B. and Lyden, D. (2009) 'The metastatic niche: adapting the foreign soil.', *Nature reviews. Cancer*, pp. 285–293. doi: 10.1038/nrc2621.

Qu, Y. *et al.* (2019) 'Tumor microenvironment-driven non-cell-autonomous resistance to antineoplastic treatment.', *Molecular cancer*. England, 18(1), p. 69. doi: 10.1186/s12943-019-0992-4.

Quail, D. F. and Joyce, J. A. (2017) 'The Microenvironmental Landscape of Brain Tumors.', *Cancer cell*. United States, 31(3), pp. 326–341. doi: 10.1016/j.ccell.2017.02.009.

Riva, M. *et al.* (2012) 'Induction of nuclear factor-κB responses by the S100A9 protein is Toll-like receptor-4-dependent.', *Immunology*, 137(2), pp. 172–182. doi: 10.1111/j.1365-2567.2012.03619.x.

Rogakou, E. P. *et al.* (1998) 'DNA double-stranded breaks induce histone H2AX phosphorylation on serine 139.', *The Journal of biological chemistry*. United States, 273(10), pp. 5858–5868. doi: 10.1074/jbc.273.10.5858.

Rosenberg, S. A. (2014) 'Entering the mainstream of cancer treatment', *Nature Reviews Clinical Oncology*, 11(11), pp. 630–632. doi: 10.1038/nrclinonc.2014.174.

Rycaj, K. and Tang, D. G. (2014) 'Cancer stem cells and radioresistance.', *International journal of radiation biology*, 90(8), pp. 615–621. doi: 10.3109/09553002.2014.892227.

Saha, A. *et al.* (2013) 'Demographic and clinical profile of patients with brain metastases: A retrospective study.', *Asian journal of neurosurgery*, 8(3), pp. 157–161. doi: 10.4103/1793-5482.121688.

Sak, A. and Stuschke, M. (2010) 'Use of gammaH2AX and other biomarkers of double-strand breaks during radiotherapy.', *Seminars in radiation oncology*. United States, 20(4), pp. 223–231. doi: 10.1016/j.semradonc.2010.05.004.

Schildge, S. *et al.* (2013) 'Isolation and culture of mouse cortical astrocytes.', *Journal of visualized experiments : JoVE*. United States, (71). doi: 10.3791/50079.

Seike, T. *et al.* (2011) 'Interaction between lung cancer cells and astrocytes via

specific inflammatory cytokines in the microenvironment of brain metastasis', *Clinical & Experimental Metastasis*, 28(1), pp. 13–25. doi: 10.1007/s10585-010-9354-8.

Sevenich, L. *et al.* (2014) 'Analysis of tumour- and stroma-supplied proteolytic networks reveals a brain-metastasis-promoting role for cathepsin S.', *Nature cell biology*, 16(9), pp. 876–888. doi: 10.1038/ncb3011.

Seyfried, T. N. and Huysentruyt, L. C. (2013) 'On the origin of cancer metastasis.', *Critical reviews in oncogenesis*, 18(1–2), pp. 43–73. doi: 10.1615/critrevoncog.v18.i1-2.40.

Sharp, A. *et al.* (2016) 'Development of molecularly targeted agents and immunotherapies in small cell lung cancer', *European Journal of Cancer*, 60, pp. 26–39. doi: https://doi.org/10.1016/j.ejca.2016.03.004.

Smart, D. *et al.* (2015) 'Analysis of radiation therapy in a model of triple-negative breast cancer brain metastasis.', *Clinical & experimental metastasis*. Netherlands, 32(7), pp. 717–727. doi: 10.1007/s10585-015-9739-9.

Smith, S. L. *et al.* (2017) 'The predictive value of serum S100A9 and response to etanercept is not confirmed in a large UK rheumatoid arthritis cohort', *Rheumatology*, 56(6), pp. 1019–1024. doi: 10.1093/rheumatology/kew387.

Soffietti, R. *et al.* (2017) 'Diagnosis and treatment of brain metastases from solid tumors: guidelines from the European Association of Neuro-Oncology (EANO).', *Neuro-oncology*. England, 19(2), pp. 162–174. doi: 10.1093/neuonc/now241.

Sperduto, P. W. *et al.* (2010) 'Diagnosis-specific prognostic factors, indexes, and treatment outcomes for patients with newly diagnosed brain metastases: a multi-institutional analysis of 4,259 patients.', *International journal of radiation oncology, biology, physics*. United States, 77(3), pp. 655–661. doi: 10.1016/j.ijrobp.2009.08.025.

Srikrishna, G. (2012) 'S100A8 and S100A9: new insights into their roles in malignancy.', *Journal of innate immunity*. Switzerland, 4(1), pp. 31–40. doi: 10.1159/000330095.

Steeg, P. S., Camphausen, K. A. and Smith, Q. R. (2011) ‘Brain metastases as preventive and therapeutic targets.’, *Nature reviews. Cancer*. England, 11(5), pp. 352–363. doi: 10.1038/nrc3053.

Sun, Y. *et al.* (2012) ‘Treatment-induced damage to the tumor microenvironment promotes prostate cancer therapy resistance through WNT16B.’, *Nature medicine*. United States, 18(9), pp. 1359–1368. doi: 10.1038/nm.2890.

Tabouret, E. *et al.* (2012) ‘Recent trends in epidemiology of brain metastases: an overview.’, *Anticancer research*. Greece, 32(11), pp. 4655–4662.

Taggart, D. *et al.* (2018) ‘Anti-PD-1/anti-CTLA-4 efficacy in melanoma brain metastases depends on extracranial disease and augmentation of CD8(+) T cell trafficking.’, *Proceedings of the National Academy of Sciences of the United States of America*. United States, 115(7), pp. E1540–E1549. doi: 10.1073/pnas.1714089115.

Tardif, M. R. *et al.* (2015) ‘Secretion of S100A8, S100A9, and S100A12 by Neutrophils Involves Reactive Oxygen Species and Potassium Efflux.’, *Journal of immunology research*, 2015, p. 296149. doi: 10.1155/2015/296149.

Thallinger, C. *et al.* (2018) ‘Review of cancer treatment with immune checkpoint inhibitors’, *Wiener klinische Wochenschrift*, 130(3), pp. 85–91. doi: 10.1007/s00508-017-1285-9.

Tolaney, S. M. *et al.* (2017) ‘Abemaciclib for the treatment of brain metastases (BM) secondary to hormone receptor positive (HR+), HER2 negative breast cancer.’, *Journal of Clinical Oncology*, 35(15_suppl), p. 1019. doi: 10.1200/JCO.2017.35.15_suppl.1019.

Toyokawa, G. *et al.* (2015) ‘Insights into brain metastasis in patients with ALK+ lung cancer: is the brain truly a sanctuary?’, *Cancer metastasis reviews*. Netherlands, 34(4), pp. 797–805. doi: 10.1007/s10555-015-9592-y.

Twyman-Saint Victor, C. *et al.* (2015) ‘Radiation and dual checkpoint blockade activate non-redundant immune mechanisms in cancer.’, *Nature*. England, 520(7547), pp. 373–377. doi: 10.1038/nature14292.

Valiente, M. *et al.* (2014) ‘Serpins promote cancer cell survival and vascular co-option in brain metastasis.’, *Cell*. United States, 156(5), pp. 1002–1016. doi: 10.1016/j.cell.2014.01.040.

Valiente, M. *et al.* (2018) ‘The Evolving Landscape of Brain Metastasis.’, *Trends in cancer*. United States, 4(3), pp. 176–196. doi: 10.1016/j.trecan.2018.01.003.

Walker, D. *et al.* (2015) ‘Receptor for advanced glycation endproduct modulators: a new therapeutic target in Alzheimer’s disease.’, *Expert opinion on investigational drugs*, 24(3), pp. 393–399. doi: 10.1517/13543784.2015.1001490.

Wang, C. *et al.* (2014) ‘The role of pro-inflammatory S100A9 in Alzheimer’s disease amyloid-neuroinflammatory cascade’, *Acta Neuropathologica*, 127(4), pp. 507–522. doi: 10.1007/s00401-013-1208-4.

Wang, H. *et al.* (2018) ‘Targeted inhibition of RAGE reduces amyloid-beta influx across the blood-brain barrier and improves cognitive deficits in db/db mice.’, *Neuropharmacology*. England, 131, pp. 143–153. doi: 10.1016/j.neuropharm.2017.12.026.

Wang, S. *et al.* (2018) ‘S100A8/A9 in Inflammation.’, *Frontiers in immunology*, 9, p. 1298. doi: 10.3389/fimmu.2018.01298.

Wasilewski, D. *et al.* (2017) ‘Reactive Astrocytes in Brain Metastasis.’, *Frontiers in oncology*. Switzerland, 7, p. 298. doi: 10.3389/fonc.2017.00298.

Wells, A. *et al.* (2013) ‘The dormancy dilemma: quiescence versus balanced proliferation.’, *Cancer research*, 73(13), pp. 3811–3816. doi: 10.1158/0008-5472.CAN-13-0356.

Welsh, J. W. *et al.* (2013) ‘Phase II trial of erlotinib plus concurrent whole-brain radiation therapy for patients with brain metastases from non-small-cell lung cancer.’, *Journal of clinical oncology : official journal of the American Society of Clinical Oncology*. United States, 31(7), pp. 895–902. doi: 10.1200/JCO.2011.40.1174.

Wingrove, E. *et al.* (2019) ‘Transcriptomic Hallmarks of Tumor Plasticity and Stromal Interactions in Brain Metastasis.’, *Cell reports*. United States, 27(4), pp. 1277-1292.e7. doi: 10.1016/j.celrep.2019.03.085.

Wrage, M. *et al.* (2015) ‘Identification of HERC5 and its potential role in NSCLC progression.’, *International journal of cancer*. United States, 136(10), pp. 2264–2272. doi: 10.1002/ijc.29298.

Xing, F. *et al.* (2015) ‘miR-509 suppresses brain metastasis of breast cancer cells by modulating RhoC and TNF-α’, *Oncogene*, 34(37), pp. 4890–4900. doi: 10.1038/onc.2014.412.

Yamanaka, R. (2009) ‘Medical management of brain metastases from lung cancer (Review).’, *Oncology reports*. Greece, 22(6), pp. 1269–1276.

Yuzhalin, A. E. and Yu, D. (2019) ‘Brain Metastasis Organotropism.’, *Cold Spring Harbor perspectives in medicine*. United States. doi: 10.1101/cshperspect.a037242.

Appendix

Appendix

1. Publications

- Priego, N. *et al.* (2018) 'STAT3 labels a subpopulation of reactive astrocytes required for brain metastasis.', *Nature medicine*. United States, 24(7), p. 1481. doi: 10.1038/s41591-018-0108-5.

- Wingrove, E. *et al.* (2019) 'Transcriptomic Hallmarks of Tumor Plasticity and Stromal Interactions in Brain Metastasis.', *Cell reports*. United States, 27(4), pp. 1277-1292.e7. doi: 10.1016/j.celrep.2019.03.085.

- Monteiro, C. et al. (in prep) 'S100A9 mediates radiation resistance of brain metastasis'

2. Poster presentations

- Monteiro C. et al., "Increased production of S100A9 *in situ* mediates resistance of brain metastasis to whole brain radiation therapy", CNIO Labday, Madrid, 18th December 2017

- Monteiro C. et al., "In vivo radiation resistance of brain metastasis: new models to interrogate the underlying biology", EACR-AACR-SIC 2nd Special Conference, Florence, 24th-27th of June 2017

- Monteiro C. et al.," Epigenetic regulation of brain metastasis by linker histone H1.2"**,** CNIO Frontiers meeting – Primary and secondary brain tumours, Madrid, 19th-22nd of February 2017

- Monteiro C. et al., "Radiation resistance in brain metastasis: new models to interrogate the underlying biology", CNIO Labday, Madrid, 1st December 2016

3. Oral communications

- Cátia Monteiro, “S100A9-dependent radiation resistance in brain metastasis”, CNIO Progress reports, Madrid, 27th of June 2018
- Cátia Monteiro et al. “S100A9 mediates resistance of brain metastasis to radiation therapy”, 1st PhD Research Symposium in Health Sciences and Biomedicine, Madrid, 18th of May 2018
- Cátia Monteiro, “Radiation resistance in brain metastasis: new models to interrogate the underlying biology”. CNIO Progress reports, Madrid, 6th of July 2016

4. Awards

- 2018, EMBO Short-term Fellowship
- 2017, Best Poster award, CNIO frontiers meeting – Primary and secondary brain tumours, Madrid
- 2015, PhD student grant (SFRH/BD/100089/2014), Portuguese Foundation for science and technology (FCT), Portugal

List of figures

List of figures

List of tables

List of Tables